

Does Sarcolipin Ablation Alter Deflazacort Treatment Effects in *mdx* Mice?

by
Catherine A Bellissimo

A thesis
presented to the University of Waterloo
in fulfillment of the
thesis requirement for the degree of
Master of Science
in
Kinesiology

Waterloo, Ontario, Canada, 2017
© Catherine Bellissimo 2017

Author's Declaration

I hereby declare that I am the sole author of this thesis. This is a true copy of the thesis, including any required final revisions, as accepted by my examiners.

I understand that my thesis may be made electronically available to the public.

Catherine A. Bellissimo

Abstract

Duchenne Muscular Dystrophy (DMD) and the murine model *mdx* are degenerative diseases that are characterized by the absence of the protein dystrophin causing membrane instability, calcium (Ca^{2+}) influx, and progressive muscle wasting. The sarco(endo)plasmic reticulum Ca^{2+} -ATPase (SERCA) is the enzyme responsible for maintaining low cytosolic Ca^{2+} and is dysfunctional in *mdx* mice, contributing to elevations in cytosolic Ca^{2+} . Sarcolipin (SLN) is an endogenous protein regulator of SERCA that reduces SERCA activity by lowering the apparent Ca^{2+} affinity of SERCA. SLN is highly upregulated in *mdx* muscle, yet when ablated from *mdx* mice a worsened phenotype is observed, possibly due to blunted calcineurin/NFAT signaling. Glucocorticoid steroids are the primary therapy for DMD patients and combat the dystrophic phenotype in *mdx* mice. Glucocorticoid steroids have been shown to stimulate calcineurin signaling, which results in the upregulation of utrophin, the homologue of dystrophin. Glucocorticoids also increase the expression of SLN, which may function to regulate calcineurin activity. The aim of this study was to determine whether SLN plays a role in the positive treatment effects of glucocorticoid steroids in *mdx* mice. It was hypothesized that glucocorticoid treatment would increase SLN expression, stimulate calcineurin activity and increase utrophin expression in muscles from *mdx* mice but not in muscles from *mdx* mice lacking SLN (i.e. *mdx/Sln*^{-/-}). Here, four week old *mdx* and *mdx/Sln*^{-/-} mice were injected with either the glucocorticoid, deflazacort (DFZ), or vehicle (VEH) alone for 7 days. Following treatment, soleus (SOL) and diaphragm (DIA) muscles were collected for biochemical and histological analyses. Protein content of SLN, utrophin, calcineurin, SERCA isoforms and nuclear factor activation T cell (NFAT), a transcription factor dephosphorylated by calcineurin, was determined using western blotting. Immunofluorescent/histological techniques were used

to assess centralized nuclei, collagen infiltration, myosin heavy chain isoform, cross sectional area (CSA), and fibre size variability, using the variance coefficient of minimal Feret's diameter. Activation of the calcineurin/NFAT signaling pathway was also assessed using co-localization of NFATc1 and DAPI, which stains nuclear DNA. DFZ treatment improved several markers of the dystrophic phenotype in both the SOL and DIA, including centrally nucleated fibres and collagen infiltration. There were some muscle-specific differences in fibre type distribution between genotypes and treatments but these were mostly minor differences in hybrid fibres. CSA was not affected in the majority of fibre types by DFZ or genotype. Unexpectedly, variability in fibre size was not improved by DFZ treatment but was actually increased in DFZ treated *mdx/Sln*^{-/-} DIA compared with VEH. DFZ increased NFATc1 and DAPI co-localization in both *mdx* and *mdx/Sln*^{-/-} mice in the SOL only. However, calcineurin content and utrophin in both SOL and DIA were not different between any groups. SERCA1a and SERCA2a content in SOL and DIA were not different between DFZ and VEH treated mice, but SERCA1a was lower in the DIA of *mdx/Sln*^{-/-} mice compared to *mdx* mice. DFZ treatment increased SLN content in *mdx* SOL but not in DIA. In summary, 7 days of DFZ treatment improved some histological features of DMD in both *mdx* and *mdx/Sln*^{-/-} mice in the SOL, which was associated with increased NFATc1 nuclear translocation, suggesting increased activation of the calcineurin/NFAT pathway. Despite histological improvements in the DIA with DFZ treatment, the calcineurin/NFAT pathway appeared not to be active in that tissue relative to VEH. Finally, contrary to the main hypothesis, DFZ effects were similar in *mdx* and *mdx/Sln*^{-/-} mice, suggesting that SLN does not play a role in mediating the positive effects of DFZ.

Acknowledgements

First, I would like to acknowledge and thank my supervisor, Russ Tupling, for being so open and welcoming to undergraduate students in the program. You have always given people the benefit of the doubt and given opportunity for anyone who had any interest in research. Russ, you helped shape my career when you offered me the chance to volunteer in the lab without much of a second thought. You have always been patient, kind and overwhelmingly supportive. You have created an environment in the lab that I was proud to call home for 5 years. I look forward to the challenge of a PhD and hopefully this will be just the beginning.

I definitely need to thank all of my lab mates past and present; Val Fajardo, Dan Gamu, Paige Chambers, Emma Juracic, Chris Vigna, Ian Smith, Khanh Tran, Riley Sonnenburg, Frenk Kwon, Brad “the wonder boy” Rietz, Gabbi Lugod and several others I am missing. You guys have been indispensable in my time at the lab; being a teacher, a spare set of hands, someone to make me laugh or a necessary distraction. You guys have been my family for so long that deciding to leave was one of the hardest decisions.

To the other members of the kin-physiol; Kayleigh, Katie, Tina (Erin), Kirsten, Jan and the many others, you all have made my time in the lab a memorable experience. I will miss coming in and seeing everyone around the lunch table or grabbing beers at bomber.

To Eric Bombardier, without you I would have been this undergrad who just washed dishes and ultimately stopped coming. You have constantly challenged me to read more, think more and reign me in when I do too much. You have always been my biggest supporter but also my largest critic. You never once worried about taking it easy on me because you knew I could handle it. You and your family (Robina, Kiera and Kayla) have been welcoming and supportive from day one. You definitely have shaped me as a researcher and as a person. You will always be forcing me to grow and I thank you for that. Without you the CTX project would never have been written... oh wait that's coming soon.

To my family, Mom, Dad and Matt, you three have always been my biggest cheerleaders in life and at school. In my time at Waterloo you all were just a phone call away making sure I was okay, well fed and not breaking down over a chemistry midterm. I know this track I am on is long and winding but I hope you are all proud. To Caylen, I threw you into my world of science experiments, grad students and nerdiness to the extreme, and you did not back down. You have been an incredible source of strength (not just for moving me city to city), support and a shoulder to lean on.

As I take these next steps in my PhD, I am completely humbled that I know I have such a great team of supporters every step of the way. Thank you all so very much.

Dedication

This thesis is dedicated to my family, friends, professors and colleagues. Thank you all for the support, knowledge and guidance.

Table of Contents

Author's Declaration	ii
Abstract.....	iii
Acknowledgements	v
Dedication	vi
List of Figures.....	viii
List of Abbreviations	x
Introduction	1
Duchenne Muscular Dystrophy	1
Calcium Dysregulation and the Progression of DMD	4
Sarcolipin in DMD and Calcineurin/NFAT Signaling	6
Glucocorticoid Steroids in the Treatment of DMD	9
Pathways Involved in Glucocorticoid Treatment of DMD	11
Statement of the Problem	13
Objectives and Hypothesis	14
Methods.....	15
Transgenic Mice	15
Experimental Design	16
Antibodies for Western Blotting and Immunofluorescence	17
Histological & Immunofluorescence Staining	18
Western Blotting Analysis	21
Serum Creatine Kinase	22
Statistical Analyses	23
Results	23
Animal Physical Characteristics and Serum Creatine Kinase Levels	23
Histological Features of DMD in the Soleus & Diaphragm	27
Immunofluorescent Features of DMD in the Soleus & Diaphragm	31
Calcineurin/NFAT Signaling in the Soleus & Diaphragm	35
Calcium Handling Proteins in the Soleus & Diaphragm	45
Discussion	49
Future Directions	60
Conclusion	62
References	64
Appendices	74
Appendix A: Supplementary Material for Thesis	74
Appendix B: Breeding Strategy and Genotyping Protocol for <i>mdx</i> and <i>mdx/Sln^{-/-}</i>	78
Appendix C: Western Blotting Protocols	82

List of Figures

Figure 1.1: Conceptual map of the effect of SLN on calcineurin/NFAT signaling	9
Figure 1.2: Conceptual map of the effect of <i>Sln</i> -ablation on glucorticoid treatment	13
Figure 2.1: Schematic of experimental design and allocation of animals	17
Figure 3.1: Absolute and change in (Δ) body weight of <i>mdx</i> and <i>mdx/Sln</i> ^{-/-} mice treated with VEH or DFZ	24
Figure 3.2: Absolute and relative SOL weight in <i>mdx</i> and <i>mdx/Sln</i> ^{-/-} mice treated with VEH or DFZ	25
Figure 3.3: DIA absolute and relative weight of <i>mdx</i> and <i>mdx/Sln</i> ^{-/-} mice treated with VEH or DFZ	25
Figure 3.4: EDL absolute weight and relative muscle weight in <i>mdx</i> and <i>mdx/Sln</i> ^{-/-} mice treated with VEH or DFZ	26
Figure 3.5: Serum CK levels in <i>mdx</i> and <i>mdx/Sln</i> ^{-/-} mice after treatment protocol	26
Figure 3.6: Centralized nuclei and total fibre number in SOL from <i>mdx</i> and <i>mdx/Sln</i> ^{-/-} mice treated with VEH or DFZ	28
Figure 3.7: Centralized nuclei and total fibre number in DIA from <i>mdx</i> and <i>mdx/Sln</i> ^{-/-} mice treated with VEH or DFZ	29
Figure 3.8: Collagen infiltration in SOL of <i>mdx</i> and <i>mdx/Sln</i> ^{-/-} mice treated with VEH or DFZ	30
Figure 3.9: Collagen infiltration in DIA of <i>mdx</i> and <i>mdx/Sln</i> ^{-/-} mice treated with VEH or DFZ	31
Figure 3.10: Fibre type distribution, CSA and covariance of minimal Feret's diameter in SOL muscles from <i>mdx</i> and <i>mdx/Sln</i> ^{-/-} after treatment with VEH or DFZ	33
Figure 3.11: Fibre type distribution, CSA and covariance of minimal Feret's diameter of DIA from <i>mdx</i> and <i>mdx/Sln</i> ^{-/-} mice after treatment with VEH or DFZ	34
Figure 3.12: Western blot analysis of total NFATc1, phosphorylated NFATc1 and ratio of NFATc1-p to total NFATc1 in SOL of <i>mdx</i> and <i>mdx/Sln</i> ^{-/-} mice after treatment with VEH or DFZ	36
Figure 3.13: NFATc1 localization in SOL sections from <i>mdx</i> and <i>mdx/Sln</i> ^{-/-} mice after treatment with VEH or DFZ	37
Figure 3.14: Western blot analysis of total NFATc1, phosphorylated NFATc1 and ratio of NFATc1-p to total NFATc1 in DIA of <i>mdx</i> and <i>mdx/Sln</i> ^{-/-} mice after treatment with VEH or DFZ	38

Figure 3.15: NFATc1 localization in DIA sections from <i>mdx</i> and <i>mdx/Sln^{-/-}</i> mice after VEH or VEH treatment	39
Figure 3.16: Western blot analysis of calcineurin content in SOL from <i>mdx</i> and <i>mdx/Sln^{-/-}</i> after treatment with VEH or DFZ	40
Figure 3.17: Western blot analysis of calcineurin content of DIA muscles from <i>mdx</i> and <i>mdx/Sln^{-/-}</i> mice after VEH or DFZ treatment	41
Figure 3.18: Western blot analysis of utrophin content of SOL from <i>mdx</i> and <i>mdx/Sln^{-/-}</i> mice after VEH or DFZ	42
Figure 3.19: Immunofluorescent detection of utrophin in SOL of <i>mdx</i> and <i>mdx/Sln^{-/-}</i> mice after treatment	43
Figure 3.20: Western blotting of utrophin content in DIA in <i>mdx</i> and <i>mdx/Sln^{-/-}</i> mice after treatment with VEH or DFZ	44
Figure 3.21: Normalized fluorescent intensity of utrophin staining from DIA of <i>mdx</i> and <i>mdx/Sln^{-/-}</i> mice	45
Figure 3.22: Western blotting of SERCA1a and SERCA2a in SOL of <i>mdx</i> and <i>mdx/Sln^{-/-}</i> mice after VEH or DFZ treatment	46
Figure 3.23: Western blot analysis of SERCA1a and SERCA2a content in DIA of <i>mdx</i> and <i>mdx/Sln^{-/-}</i> mice after treatment protocol	47
Figure 3.24: Western blot analysis of SLN content in SOL of <i>mdx</i> mice treated with VEH or DFZ	48
Figure 3.25: Western blot analysis of SLN content in DIA of <i>mdx</i> after treatment with VEH or DFZ	48
Figure S1.1: Body weight monitoring during injection protocol	74
Figure S1.2: Distribution of all fibre types in SOL of <i>mdx</i> and <i>mdx/Sln^{-/-}</i> after treatment protocol	75
Figure S1.3: Distribution of all fibre types in DIA of <i>mdx</i> and <i>mdx/Sln^{-/-}</i> after treatment protocol	76
Figure S1.4: Full western blot of SLN content in SOL and DIA from <i>mdx</i> and <i>mdx/Sln^{-/-}</i> mice after DFZ or VEH treatment	77

List of Abbreviations

ATP – Adenosine Triphosphate

Ca^{2+} - Calcium

$[\text{Ca}^{2+}]_i$ – Intracellular calcium concentrations

CK – Creatine kinase

CSA – Cross sectional area

CsA- Cyclosporine A

DAPI - 4',6-diamidino-2-phenylindole

DFZ – Deflazacort

DIA - Diaphragm

DMD – Duchenne Muscular Dystrophy

DNA – Deoxyribonucleic acid

EDL – Extensor digitorum longus

H&E – Haematoxylin and eosin staining

Hsp70 – Heat Shock Protein 70

mdx – mouse model for Duchenne Muscular Dystrophy

mdx/Sln^{-/-} - mouse model for Duchenne Muscular Dystrophy with SLN genetically ablated

mdx/utrophin^{-/-} - mouse model for Duchenne Muscular Dystrophy lacking utrophin protein

MEF2- Myocyte Enhancer Factor 2

MHC – Myosin Heavy Chain

MLN - Myoregulin

NFAT – Nuclear Factor of Activated T-Cells

NFAT-p- Phosphorylated Nuclear Factor of Activated T-Cells

PLN – Phospholamban

Pln^{OE} - mouse model with phospholamban genetically overexpressed in type I muscle fibres

SERCA – Sarco(endo)plasmic reticulum Calcium ATPase

SERCA1a – SERCA isoform found predominantly in fast muscle

SERCA2a – SERCA isoform found predominantly in slow muscle

SLN – Sarcolipin

Sln^{-/-} - mouse model with sarcolipin genetically removed

SOL – Soleus

SR – Sarcoplasmic Reticulum

STIM1- Stromal interaction molecule 1

VEH- Vehicle

WT – Wild-type mice

Introduction

Calcium ions (Ca^{2+}) are vital in governing physiological processes throughout the body, including skeletal muscle, where it acts as an important signaling and regulatory molecule that governs excitation-contraction, thermogenesis, second messenger signaling, activation of transcription factors and apoptosis [1]. The regulation of cytosolic Ca^{2+} is critical in the proper function of skeletal muscle and loss of Ca^{2+} homeostasis either through impairments in Ca^{2+} release or uptake have severe implications for muscle health and function. Ca^{2+} reuptake into the sarcoplasmic reticulum (SR) is facilitated by the sarco(endo)plasmic reticulum Ca^{2+} ATPase (SERCA) and impairments in this enzyme have already been documented in a number of muscle diseases, including Duchenne Muscular Dystrophy (DMD) [2]. The gold standard therapy for DMD, glucocorticoid steroids, have been shown to alter Ca^{2+} handling and promote Ca^{2+} sensitive adaptation pathways, namely the calcineurin/NFAT pathway [3]. Ablation of regulators of SERCA is associated with improved Ca^{2+} handling yet paradoxically have a worsened disease phenotypes, through the blunting of the calcineurin/NFAT pathway [2, 4]. This thesis examines the treatment of *mdx* mice with glucocorticoids if its positive effects are associated with SLN expression.

Duchenne Muscular Dystrophy

Muscular dystrophies are a classification of genetic disorders that affect primarily skeletal muscle. Duchenne muscular dystrophy (DMD), an X-linked myopathy, is the most severe and prevalent of the dystrophies, affecting 1 in 3500 live male births [5]. Symptoms are exhibited during childhood and include weakness in limb muscles, scoliosis and impairments in ambulation, with onset typically occurring at age 5, leading to wheelchair use by age 12 [5,

6]. As a result of the impairments in skeletal muscle, DMD patients suffer from respiratory weakness leading to assisted ventilation and respiratory failure [7]. Previously, this was the most common cause of death in DMD patients, but due to improvements in respiratory care patients are living longer allowing for other developments in the disease [8]. In fact, cardiomyopathies have emerged as the leading cause of death in DMD patients, contributing to approximately 20% of DMD patient deaths [8, 9].

DMD is an inherited genetic disease that is a result of an out-of-frame deletion or missense mutation in the Duchenne gene at Xp21 [5, 10]. This mutation results in the complete lack of the protein dystrophin. Dystrophin is a large (427kDa) structural protein that provides a physical link from the extracellular matrix to the cytoskeleton of muscle fibres [6, 10, 11]. Dystrophin is an integral component of the dystroglycan complex (DGC), where it connects to γ -actin through its N-terminus binding domain, and to the β -dystroglycan subunit via its C-terminus. The β -subunit interacts with the α -dystroglycan subunit, which binds to laminin in the extracellular matrix (reviewed in [12, 13]).

Due to the interaction dystrophin has with the DCG and other associated proteins, dystrophin provide stability to muscle fibres during muscle contraction and relaxation [14]. In addition, dystrophin provides a communication pathway from inside the myofibre to the extracellular matrix and vice versa [15]. Therefore, the loss of dystrophin results in both structural instability and impairment in signal transduction (reviewed in [13]).

In DMD and the commonly used murine model, *mdx*, there is a complete lack of functional dystrophin [16]. In addition, there is a 80-90% down regulation of dystrophin associated proteins, such as α and β - dystroglycan which contribute to the pathology of the

disease [13]. The pathology of *mdx* mice and DMD patients possess a number of similar markers such as elevated plasma creatine kinase, variability in fibre size, necrosis, macrophage invasion, centralized myonuclei, and replacements of muscle tissue with adipose and/or connective tissue [17-21]. However, compared with DMD patients, *mdx* mice have a much less severe disease phenotype and relatively normal life spans [18, 19], which has led some researchers to utilize other genetic models, most importantly the *mdx/utrophin*^{-/-} mice [22, 23]. Nevertheless, the *mdx* model still provides researchers with the ability to understand the underlying mechanisms and progression of the disease.

One major reason for the relatively mild disease phenotype of *mdx* mouse mice is an endogenous upregulation of the protein utrophin [23, 24]. Utrophin, previously known as dystrophin related protein, is typically expressed at the neuromuscular junctions in healthy muscle where it provides vital scaffolding in the post synaptic apparatus [25-27] and is expressed beyond the junction in developing muscle [28, 29]. Utrophin does have a similar function to dystrophin [30], but expression patterns differ between these proteins where dystrophin is expressed in both oxidative and glycolytic muscles while utrophin is expressed more so in oxidative muscles compared to glycolytic muscles [26, 31]. In human DMD patients and *mdx* mice, utrophin extends beyond the neuromuscular junction when examined with immunofluorescent staining [27, 28, 32-34]. This upregulation was thought to be a compensatory mechanism to stabilize the sarcolemmal membrane in order to minimize contraction induced damage [35]. The ability of utrophin to compensate in stabilizing the sarcolemmal membrane then poses as an interesting therapeutic target for DMD [36].

Like human DMD, *mdx* mice undergo phases of muscle degeneration and regeneration, but unlike humans, *mdx* mice have an improved regenerative capability and a less severe

phenotype in the majority of skeletal muscles [23, 37]. The degeneration in human DMD progresses very quickly; causing wheelchair dependence in mid-teens and death by age 30 if untreated [38]. *Mdx* mice on the other hand, exhibit four distinct stages of disease progression. From just after birth to approximately 3 weeks of age, *mdx* mice present very similarly to wildtype (WT) littermates, with no differences in fibre size, fibre type distribution or muscle damage [34, 39]. At 3-4 weeks of age, *mdx* mice undergo a substantial degenerative phase [34, 40, 41], followed by a phase of regeneration until 7 weeks old [17, 20, 42]. After this time period, *mdx* mice exhibit a plateau phase, until 4 to 6 months of age where degeneration is matched by regeneration [14, 43]. Following this plateau, *mdx* mice exhibit degeneration, marked by progressive loss of body weight, extensive fibrosis of limb and respiratory muscles, decreases in type IIB fibre proportions and ultimately death at approximately 2 years of age [43-45]. Therefore, 3-7 weeks of age in *mdx* mice is an appropriate time frame to examine the underlying mechanism of disease progression and how pharmacological interventions affect relevant outcomes, while being more correlative to human DMD.

Calcium Dysregulation and the Progression of DMD

The impairments in functional capability of those with DMD are attributed to progressive muscle weakness and muscle degeneration, caused by extreme membrane instability due to the lack of dystrophin. This membrane instability results in an influx of extracellular calcium ions (Ca^{2+}) and increased ion permeability [11, 46-48]. Contraction induced micro-tears in the sarcolemmal membrane lead to the insertion of “leak channels”, which reinforces this Ca^{2+} overload within the cytosol [46, 49, 50]. This influx of Ca^{2+} results in higher intracellular Ca^{2+} concentrations ($[\text{Ca}^{2+}]_i$) that have cytotoxic effects. Ca^{2+} activated proteolytic enzymes, namely calpains and caspases, are increased in DMD and *mdx* mice

which contributes to the degeneration of limb and respiratory muscles [49-53]. The leak channels become constantly active by Ca^{2+} activated proteolysis which further promotes myofibril degeneration, increases fibrosis and the progression of the disease phenotype [47, 54].

In theory, if calcium reuptake into the SR was able to match this increased influx of Ca^{2+} then the Ca^{2+} associated degeneration may be limited, but if Ca^{2+} reuptake into the SR is impaired, then increases in cytosolic Ca^{2+} would occur. Ca^{2+} reuptake is facilitated by the sarco(endo)plasmic reticulum Ca^{2+} ATPase (SERCA). SERCAs are 110kDa integral membrane proteins that pump Ca^{2+} from the cytosol into the SR at the expense of adenosine triphosphate (ATP) and are critical in the relaxation of muscle and maintaining cytosolic Ca^{2+} levels [55-57]. Adult skeletal muscle has two predominate SERCA isoforms, SERCA1a and SERCA2a, which are thought to be dependent on fibre type. SERCA1a is primarily expressed in fast-twitch muscles and SERCA2a is expressed in slow-twitch muscle [58], however there is evidence to show that both SERCA isoforms are expressed within the same fibre type. In human vastus lateralis both SERCA1a and SERCA2a are present in type I or type IIA fibres [59].

In *mdx* mice, SERCA is functionally altered as a result of oxidative damage [60, 61], causing sustained elevations in cytosolic Ca^{2+} and further contributing to the progression of the disease [2, 62, 63]. Improvements in the dystrophic phenotype have been observed when SERCA content is overexpressed [64, 65] or when oxidative damage of SERCA is prevented, through the increase of the chaperone protein Hsp72 [66, 67]. Thus, altering SERCA activity or content in DMD can normalize cytosolic Ca^{2+} and thus alter the disease phenotype.

Sarcolipin in DMD and Calcineurin/NFAT Signaling

One possible way to alter SERCA activity is through targeting key regulators of SERCA, such as sarcolipin (SLN) and phospholamban (PLN). SLN regulates SERCA through its physical interaction with the pump [68-71]. SLN is a small, 31 amino acid (6 kDa) protein, comprised of a transmembrane, cytoplasmic and luminal domain [72, 73], that inhibits SERCA activity by reducing the apparent affinity of SERCA for Ca^{2+} [72, 74-76]. Interestingly, in many myopathies, including *mdx* mice, an upregulation of SLN content is observed [2, 77-80], which is associated with decreased SERCA activity and thus may contribute to elevations in cytosolic Ca^{2+} , and the activation of Ca^{2+} sensitive pathways. Therefore, one might expect that reducing or deleting SLN may improve SERCA function and decrease cytosolic Ca^{2+} content, especially as *Sln*-null (*Sln*^{-/-}) mice show improved Ca^{2+} transport [75, 76].

In order to test this hypothesis, our lab bred *mdx* mice with *Sln*^{-/-} mice, creating a progeny of dystrophic mice that completely lack SLN [81]. These mice allowed us to test whether improving SERCA function by removing SLN could improve the dystrophic phenotype in soleus and diaphragm muscles. Compared with *mdx* mice, improvements in Ca^{2+} apparent affinity were observed but maximal SERCA activity was not different in *mdx/Sln*^{-/-} mice [4]. Despite this improvement in calcium handling, *mdx/Sln*^{-/-} mice had a worse pathology than *mdx* mice, marked by increases in centralized nuclei, increased collagen infiltration and elevations in serum creatine kinase (CK). Since *mdx/Sln*^{-/-} mice also had decreased utrophin expression, reduced myofibre size and increased percentages of fast glycolytic fibres, which could be indicative of blunted calcineurin/NFAT signaling, it was hypothesized that SLN upregulation may be a compensatory mechanism to increase calcineurin signaling in *mdx* mice.

Calcineurin, a Ca^{2+} sensitive serine-threonine phosphatase is comprised of catalytic subunit A and a regulatory B subunit. When stimulated by sustained low amplitude elevation in Ca^{2+} , calmodulin binds to the calcineurin heterodimers and increases the affinity calcineurin has for Ca^{2+} [82-84]. Thus, small elevations in Ca^{2+} can greatly increase calcineurin activity [85]. This association dislodges the auto-inhibitory domain of calcineurin A, allowing the active site of the catalytic subunit to be opened and calcineurin to dephosphorylate downstream targets [86-88]. One of these downstream targets is the family of nuclear factor activating T-Cells (NFAT), which includes NFATc1-c5 [89], but of these, only NFATc1-c4 is responsive to calcineurin [90-93].

Once dephosphorylated by calcineurin, NFATs translocate to the nucleus where they act as transcription factors and promote gene expression [86, 94]. Different isoforms of NFATs promote specific gene expression. For example NFATc1 is key in promoting an oxidative phenotype of muscle through the transcription of myosin heavy chain I, troponin I and myoglobin [92, 95-100]. Interestingly, there is a NFAT binding site in the utrophin A (an isoform of utrophin) promoter [101]. Thus when NFATc1 is translocated and an oxidative phenotype is promoted, utrophin expression is also expressed [31]. The calcineurin/NFAT pathway is sensitive to Ca^{2+} levels and can improve the dystrophic phenotype through utrophin expression [101, 102].

The potential of SLN upregulation in stimulating calcineurin activity to bring about positive adaptations such as utrophin expression is promising. Work performed in our lab reinforces the concept that SLN upregulation may serve as compensatory mechanism in disease. In mice that overexpress the SLN homologue phospholamban (PLN) in slow-twitch muscle (Pln^{OE}), a centronuclear myopathy-like phenotype is observed [77]. The loss of SLN

from *Pln*^{OE} mice results in further exacerbation of the disease phenotype through blunting of the calcineurin/NFAT pathway [103]. These mice lacking SLN showed a delayed fast-to-slow fibre type transition, decreases in NFATc1 translocation, and decreases in stabilin-2 content (phosphatidylserine receptor required for myoblast fusion specific regulated by NFATc1) [104]. Furthermore, *Sln*^{-/-} mice fail to show the same adaptive responses to functional overload of the plantaris and tetonomy (unloading) of the soleus muscle compared with WT controls. In the overloaded plantaris muscle, *Sln*^{-/-} mice showed impairments in calcineurin signaling with impaired fast-to-slow fibre transition, no translocation of NFAT into the nucleus or change in stabilin-2 compared to sham controls. In the tetonomized soleus, there was no translocation of NFAT to the nucleus and no change in stabilin-2, again indicating an impairment of the calcineurin/NFAT pathway [104].

Furthermore, mice overexpressing SLN show increased calcineurin activity and increased NFAT nuclear translocation resulting in an increased oxidative capacity [105]. Utrophin expression correlates with oxidative capacity and is regulated by calcineurin-NFAT signaling [31]. Collectively, these results highlight the role SLN plays in activating the calcineurin/NFAT pathway and thus it is plausible that the upregulation of SLN in *mdx* mice is a compensatory mechanism to activate the calcineurin/NFAT pathway to promote utrophin expression (see Figure 1.1).

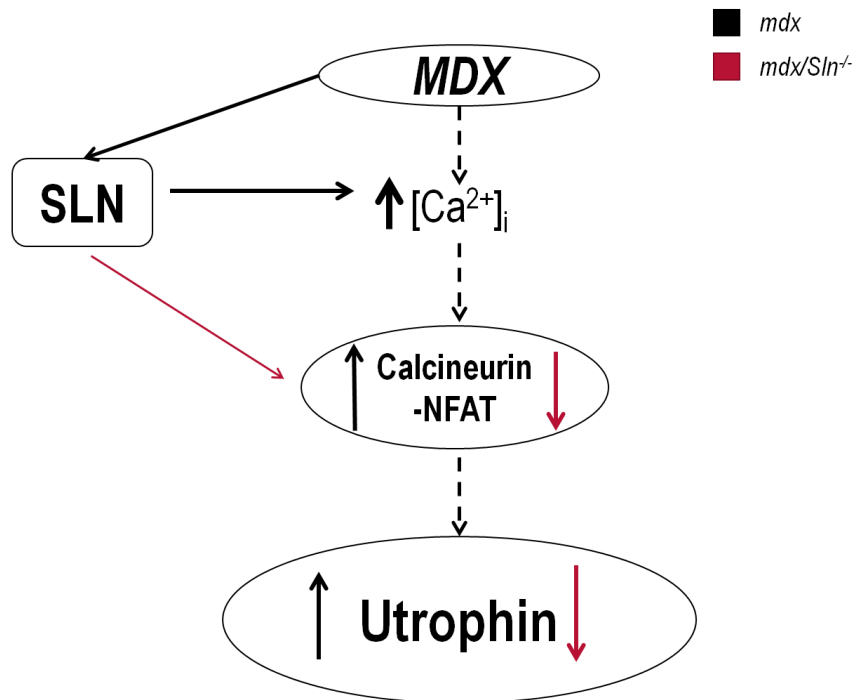


Figure 1.1: Conceptual map of the effect of SLN on calcineurin/NFAT signaling. Black solid arrows represent *mdx* mice which have an intrinsic upregulation of SLN content which is associated with increased calcineurin/NFAT signaling that can increase utrophin content. Red solid arrow represents *mdx/Sln^{-/-}* mice which have blunted calcineurin/NFAT signaling that results in decreased utrophin content.

Glucocorticoid Steroids in the Treatment of DMD

Currently, DMD patients undergo several drug and ventilation therapies in order to delay wheelchair dependence, improve quality of life and lengthen the life span of patients [8, 106]. There is no cure for DMD, and until such a time that genetic therapy can be utilized to remove the mutation that causes the loss of functional dystrophin in DMD patients, other treatments must be used to combat disease progression. Research utilizing the CRISPR-9/Cas9 technology appears promising in mouse models of the disease, by restoring dystrophin expression through the deletion of multiple exons in the DMD gene [107-109]. While these genetic therapies are being tested for viability in humans, the current “gold standard” in the

treatment of DMD is with glucocorticoid steroids, namely prednisone and its oxazoline derivative, deflazacort (DFZ) [110].

Glucocorticoid steroids are a subclass of corticoid steroids that are endogenously expressed in the body. They are secreted by the adrenal cortex in order to maintain metabolic homeostasis in the body [111]. Glucocorticoids mobilize glucose as well as amino acids and fat stores [112]. Endogenous and synthetic glucocorticoids are capable of diffusing across the plasma membrane due to their lipophilic nature in order to interact with their intracellular receptors. The inactive receptor is found in the cytosol bound in a complex containing heat shock proteins 90 (hsp90), hsp70, hsp56, hsp40, p23, and several immunophilins [113, 114]. Once within the cell, glucocorticoids bind to their receptors, which then dissociates from its complex. The receptor and ligand then translocate to the nucleus where it acts as a transcription factor either through binding directly to DNA or through protein-protein interactions [115].

In healthy populations and some diseases, glucocorticoids have a catabolic effect on the body, with muscle loss typically being a consequence of glucocorticoid use. Elevations in endogenous glucocorticoids, such as cortisol, are typically associated with states of muscle atrophy and decreased protein synthesis. However, glucocorticoids, namely the synthetically derived prednisone and its derivative DFZ, produce paradoxical improvements in DMD patients. Several studies saw improvements in muscle strength and prolonged ambulation with prednisone or DFZ treatment [116-119]. These benefits were first observed by Drachman et al., (1974) where 14 DMD patients treated with prednisone for 28 months showed somewhat positive effects. The group concluded that prednisone improved muscle strength, prolonged the functional status of the patient for another two years and that this warranted further study in a larger population [116]. These positive effects of glucocorticoids were corroborated by several

other groups both in human DMD [120-122] and *mdx* mice [123, 124], but the underlying mechanisms remained unknown for some time.

The selection and dosage of DFZ for this study was based on the study performed by St. Pierre et al. (2004), which has examined the underlying mechanism of glucocorticoid treatment that will be described below. DFZ is the oxazoline derivative of prednisone, the primary prescribed drug for the treatment of DMD. DFZ has been gaining momentum as a treatment for DMD, as it is reported to have similar benefits to the dystrophic phenotypes with less severe side effects compared to prednisone [125-128]. In addition, it has been reported that DFZ may have other beneficial effects to delay the progression of DMD through laminin expression and myogenic repair in *mdx* mice [124]. Although this dosage is higher than what is used in humans [125, 128], it was capable of promoting utrophin transcription in the *mdx* model [3].

Pathways Involved in Glucocorticoid Treatment of DMD

Glucocorticoid treatments have been shown to increase utrophin expression in *mdx* mice, muscle fibres and myotubes [3, 32, 129], but it was not clear as to how. One potential pathway is the calcineurin/NFAT cascade because the utrophin A promoter contains an NFAT binding site, thus any activation of this pathway could lead to utrophin transcription [101]. Indeed, expression of a constitutively active calcineurin in mice leads to chronic stimulation of the calcineurin/NFAT pathway, resulting in upregulation of utrophin protein [101, 130]. When these mice are crossbred with *mdx* mice, the upregulation of utrophin still persists and the dystrophic phenotype is mitigated [101, 130, 131]. Blocking this pathway, either through inhibition of calmodulin [132] or through pharmacological inhibition of calcineurin with

cyclosporine A (CsA) [3, 31, 133], results in reduced utrophin expression and an exacerbation of the phenotype.

Given that activation of calcineurin mitigates the dystrophic phenotype through increasing utrophin content, it was hypothesized that glucocorticoids act through this pathway to increase utrophin expression [3]. *Mdx* mice treated with DFZ showed improvements in the dystrophic phenotype through decreases in centralized nuclei and fibre size variability, but this was completely lost in *mdx* mice treated with both DFZ and CsA. In this same study, DFZ treated dystrophic myotubes showed increased translocation of NFATc1 and calcineurin activity [3]. This study provided the first evidence that glucocorticoids increase utrophin expression through activating the calcineurin/NFAT pathway thereby improving the dystrophic phenotype.

From this evidence, it stands to reason that altering Ca^{2+} levels to activate calcineurin may be a viable approach to increase utrophin expression and mitigate DMD. Interestingly, glucocorticoids have been observed to increase SLN content in rat diaphragm. Gayan-Ramirez et al. (2000) utilized triamcinolone (a fluorinated glucocorticoid) through intramuscular injections for five days and observed a significant increase in SLN mRNA in diaphragm. The researchers speculated that an increase in SLN expression might be a compensatory mechanism to combat atrophy of the muscle [80]. As described above, given that SLN reduces the pumping of Ca^{2+} by SERCA, elevations in SLN could result in increased cytosolic Ca^{2+} , which would then activate Ca^{2+} sensitive pathways, like the calcineurin/NFAT pathway. Therefore, it is possible that increased SLN expression with glucocorticoids might be important or even required for activating calcineurin signaling and promoting utrophin transcription (see Figure 1.2).

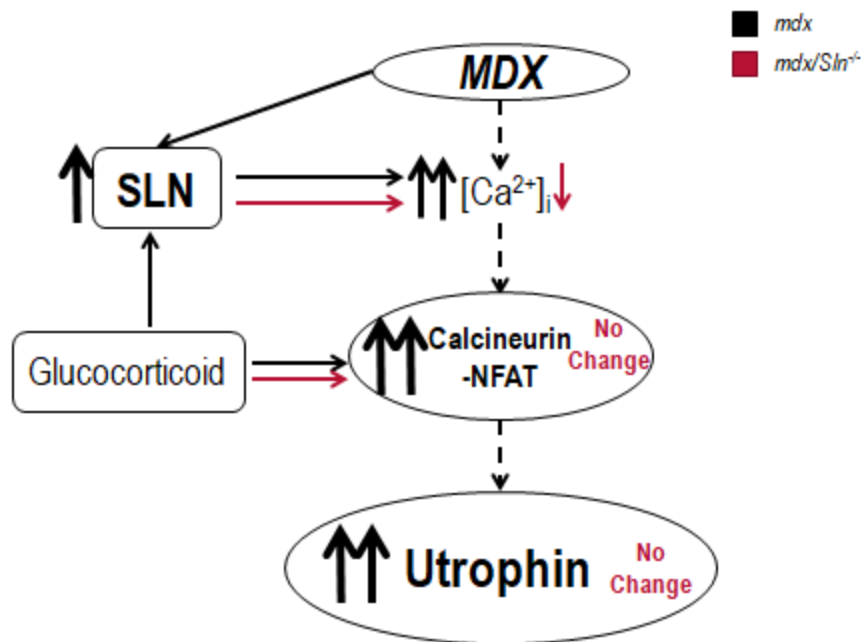


Figure 1.2: Conceptual map of the effect of *Sln*-ablation on glucocorticoid treatment. Black solid arrows represent *mdx* mice, where DFZ treatment further increases SLN content which is associated with increased cytosolic Ca^{2+} and calcineurin/NFAT activity resulting in increased utrophin content, which correlates to improved dystrophic phenotype. Red solid arrows represent *mdx/Sln^{-/-}* mice where DFZ treatment does not alter calcineurin/NFAT activity or utrophin content, preventing the positive effects of glucocorticoids.

Statement of the Problem

Glucocorticoid treatment improves dystrophic pathology through calcineurin stimulation and increased utrophin expression. Given that SLN overexpression can stimulate calcineurin and both DMD and glucocorticoid steroids increase SLN content, the purpose of this study was to examine the role of SLN in the therapeutic effects of glucocorticoids in DMD using *mdx* and *mdx/Sln^{-/-}* mice. Given that glucocorticoids have been shown to mitigate the progression of the disease phenotype and improve ambulation in *mdx* mice and DMD patients [38, 117, 126, 128, 134, 135], but cause muscle atrophy in healthy populations [112, 136-139],

healthy wild type (WT) animals were excluded from the study as they would likely produce confounding effects that would not be relevant to the main goal of this thesis. Analyses were restricted to soleus (SOL) and diaphragm (DIA) muscles based on two characteristics: 1) the presence of SLN and 2) the severity of muscle damage. The soleus and diaphragm both express SLN protein at a basal state [59, 140, 141] which becomes upregulated in numerous disease states including *mdx* mice. DMD affects limb muscles such as the SOL but the DIA muscle is more clinically relevant as DIA of *mdx* mice presents a similar phenotype to human DMD [142].

Objectives and Hypotheses

Objectives

The objectives for this thesis are as follows:

- i) To compare the effects of DFZ treatment on muscle fibre type distribution, fibre size, centralized nuclei, fibrosis and serum creatine kinase between *mdx* and *mdx/Sln^{-/-}* mice.
- ii) To compare the effects of DFZ treatment on calcineurin/NFAT signaling between *mdx* and *mdx/Sln^{-/-}* mice.
- iii) To compare the effects of DFZ treatment on protein expression of SERCA isoforms and the SERCA regulator, SLN between *mdx* and *mdx/Sln^{-/-}* mice.

Hypotheses

The hypotheses in relation to these objectives listed above:

- i) DFZ treatment will reduce pathology in both SOL and DIA including decreases in fibrosis, centralized nuclei, fibre size variability and serum CK in *mdx* mice but not *mdx/Sln^{-/-}* mice.
- ii) DFZ treatment will increase body weight, and both SOL and DIA weight and fibre CSA in *mdx* mice but not *mdx/Sln^{-/-}* mice.
- iii) DFZ treatment will increase the proportion of slower (type I and IIA) fibres and SERCA2a expression and decrease the proportion of faster (type IIX and IIB) fibres and SERCA1a expression in *mdx* mice but not *mdx/Sln^{-/-}* mice.
- iv) DFZ treatment will increase SLN content, calcineurin signaling (i.e. decrease p-NFAT/NFAT and increase NFAT/DAPI co-localization) and utrophin expression in SOL and DIA in *mdx* mice but not *mdx/Sln^{-/-}* mice.

Methods

Transgenic Animals

The generation of the *mdx/Sln^{+/+}* (*mdx*) and *mdx/Sln^{-/-}* colonies was established within our laboratory as previously described [81]. Two separate colonies were formed: 1) *mdx* and WT littermates and 2) *mdx/Sln^{-/-}* and *Sln^{-/-}* littermates, which indicates that not all experimental animals are littermates and are cousins at best. Genetic background has been kept consistent between colonies, where experimental animals are equal parts C57BL/10ScSn/J: C57BL6/J, (50:50) in both *mdx* and *mdx/Sln^{-/-}*. This was done to reduce the number of culled animals and is consistent with the guidelines outlined by the Canadian Council of Animal Care and the University of Waterloo Animal Care Committee. Appendix B contains the breeding strategy

utilized in this thesis to create *mdx* and *mdx/Sln^{-/-}* animals. All animals were housed on a standard 12:12-hour light-dark cycle and in an environmentally controlled room. Mice had *ad libitum* access to food and water. To determine genotype, littermate animals were ear notched and DNA samples were digested and purified. DNA was amplified through polymerase chain reaction (PCR) to identify whether male animals were wild type or *mdx*. Further details on genotyping can be found in Appendix B. All experiments were reviewed and approved by the University of Waterloo Animal Care Committee in accordance with Canadian Council on Animal Care guidelines.

Experimental Design

Starting at 4 weeks of age, *mdx* and *mdx/Sln^{-/-}* pups (n=20 for each genotype; N=40) were injected subcutaneously every day for 7 days with either DFZ (Sigma Aldrich) dissolved in sterile saline at a dosage of 1mg/kg body weight (n=10) or saline alone (sham injected, n=10). Body weight was monitored throughout the treatment period. Figure 2.1 specifically outlines the number of animals in each experimental group.

Mice were sacrificed 24 hours following the last injection and the intact SOL and DIA muscles were excised and either homogenized or mounted for histology and immunofluorescence staining. The mounted tissue was embedded in optimal cutting temperature compound (OCT) (VWR) (n=10 for each group) and frozen in isopentane chilled in liquid nitrogen. Muscle homogenates were prepared by first removing all connective tissue and then homogenizing the muscle using a manual glass on glass homogenizer at a 10:1 dilution in cold PMSF buffer (250 mM sucrose, 5 mM HEPES, 10 mM NaN₃, and 0.2 mM

phenylmethanesulfonyl fluoride, pH 7.5). The homogenate was then aliquoted and frozen in liquid nitrogen and stored at -80°C for further analysis.

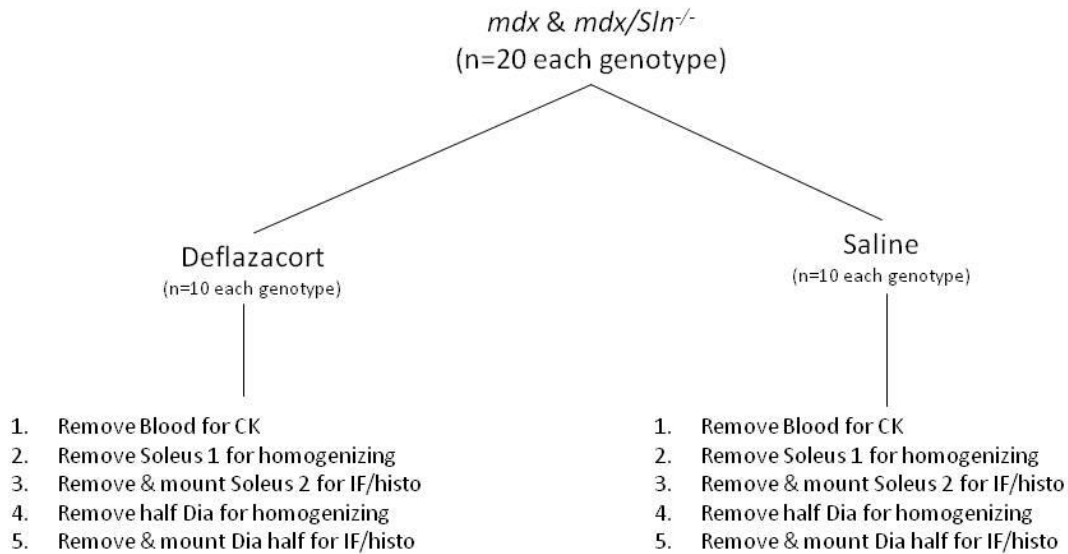


Figure 2.1: Schematic of experimental design and allocation of animals.

Antibodies for Western Blotting and Immunofluorescence

Primary antibodies for SERCA isoforms, NFATc1, phosphorylated NFATc1 (p-NFATc1), calcineurin, α -actin and SLN were utilized in Western blotting. SERCA1a (A52) was generously donated by Dr. David MacLennan (University of Toronto). SERCA2a (2A7-A1), phosphorylated-NFATc1 (PA5-38301) and total NFATc1 (MA3-024) were obtained from Pierce. Calcineurin antibody was obtained from Millipore (07-1491) and the primary antibody against actin (A4700) was obtained from Sigma Aldrich. The utrophin antibody (610896) was obtained from BD Biosciences. The primary antibody for SLN was generated by Lampire Biological Laboratories. Secondary antibodies for Western blotting, specifically goat anti-mouse IgG (peroxidase conjugated; sc-2005) and goat anti rabbit IgG (peroxidase conjugated,

sc-2030), were obtained from Santa Cruz Biotechnology (Dallas, TX). For immunofluorescence staining, primary antibodies for dystrophin (MANDYS1), MHCI (BA-F8), MHCIIa (SC-71), MHCIIb (BF-F3), NFATc1 (MA3-024) and utrophin (MANCHO10) were obtained from Developmental Studies Hybridoma Bank. Secondary antibodies, Alexa Fluor 555 anti-mouse IgG2a, Alexa Fluor 350 anti-mouse IgG2b, Alexa Fluor 488 anti-mouse IgG1 and Alexa Fluor 555 anti-mouse IgM were obtained from Molecular Probes Thermo Fisher.

Histological and Immunofluorescence Staining

SOL and DIA were collected from all groups and cut into 10µm thick serial cross sections with a cryostat (Thermo Electric) maintained at -20°C. Histological staining included haematoxylin and eosin (H&E) and Van Gieson in order to examine muscle health and fibrosis, respectively as described previously [143]. Centralized nuclei counts, representing regenerating muscle fibres were determined from H&E stained sections. Images were collected using the Nikon microscope linked to a Pixel Linked digital camera and quantified with Image Pro PLUS analysis and Image J software.

Immunofluorescence analysis of myosin heavy chain (MHC) expression was performed previously as described by Bloemberg and Quadrilatero [144]. Briefly, slides were blocked in 10% Goat Serum (Sigma-Aldrich) for one hour at room temperature and then incubated against primary antibodies for myosin heavy chain I, IIA, and IIB (see Antibodies section for complete list). Sections were then washed with phosphate buffered saline (PBS) three times for five minutes and incubated with appropriate fluorescently tagged secondary antibodies for one hour

at room temperature. Sections were again washed following the above procedure and mounted with Prolong Gold anti-fade reagent (Molecular Probes) with No.1 coverslips (VWR). Images were taken with Axio Observer Z1 fluorescent microscope equipped with standard red, green, blue filters, an Axiocam HRm camera and AxioVision Software (Carl Zeiss). These images were used to quantify total myofibre number, muscle fibre type distribution, cross sectional area (CSA) and minimal Feret's diameter. Minimal Feret's diameter is a common and reliable measure of muscular dystrophy, whereby the minimum distance of parallel tangents of opposite borders of a myofibre are examined, representing heterogeneity of muscle fibre size [17]. The quantification of fibre type distribution and cross sectional area was performed utilizing ImageJ software. Analysis of minimal Feret's diameter was done using ImageJ software and coefficient of variance was determined using Microsoft excel.

To assess NFATc1 nuclear localization (as a marker of calcineurin signaling), immunofluorescent detection of NFATc1 and 4',6-diamidino-2-phenylindole, DAPI, a marker of nuclear DNA was performed and their co-localization was assessed. This technique utilized Pearson's correlation coefficient to assess whether NFATc1 had translocated to the nucleus. Pearson's correlation coefficient is a measure of linear correlation between two variables, in this case DAPI and NFATc1. A value of +1 indicates a positive correlation, 0 indicates no correlation and -1 represents a negative correlation. In this technique, 20-40 centralized myonuclei (20 for SOL, 40 for DIA) were highlighted at random and NFATc1 colocalization. To quantify colocalization of DAPI and NFATc1, muscle sections of both SOL and DIA were fixed in 4% paraformaldehyde for 10 minutes and then washed in 1X PBS for 5 minutes three times. Following washing, slides were permeabilized with 0.5% Triton X-100 for 30 minutes. Sections were again washed for 5 minutes three times and then blocked in 5% goat serum-PBS

for one hour. Sections were then incubated overnight at room temperature against primary antibodies for NFATc1 (1:50) and α -dystroglycan (1:100) (see Antibodies list for complete information). α -dystroglycan is used to visualize individual fibres, in place of traditional dystrophin, to specifically measure NFAT levels from myonuclei. After incubation, slides were washed in 1X PBS and then incubated against fluorescently tagged secondary antibodies IgG1 and IgM at a dilution of 1:500 for 1 hour. Slides were again washed in 1X PBS and then incubated in 0.3 μ M DAPI solution for 2 minutes. Slides were then washed in PBS before coverslips were adhered to the slides. Images were taken the next day using the confocal Zeiss LSM 800 and colocalization was analyzed using ZEN digital imaging software.

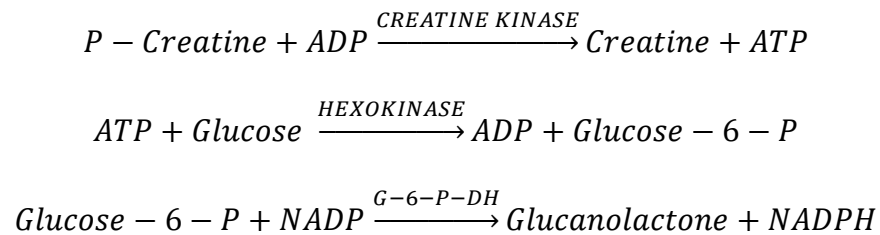
Utrophin expression was also assessed by immunofluorescence by quantifying maximal sarcolemmal utrophin fluorescence intensity, adapting a technique from a study performed by Banks et al. who measured sarcolemmal dystrophin [145]. This technique not only provides a measure of utrophin content but also displays actual localization of utrophin. Briefly, sections were blocked in 5% goat serum-PBS for one hour and then incubated with primary antibodies for utrophin (1:100) and α -dystroglycan (1:100) for another hour. Slides were then washed in 1X PBS for 5 minutes three times and then incubated against IgG1 and IgM fluorescently tagged secondary antibodies for one hour. Images were taken the next day using the confocal Zeiss LSM 800 and analysis was performed using ImageJ computer software (NIH). To quantify utrophin, a line was drawn across the sarcolemma of two adjacent fibres and the maximal fluorescent intensity of the line was identified and normalized to the vehicle *mdx* mice for comparison.

Western Blot Analysis

Western blot analysis were used to determine relative protein levels of SERCA isoforms (SERCA1a and SERCA2a), SLN, calcineurin, utrophin, NFATc1 and p-NFATc1 in SOL and DIA from DFZ and saline injected *mdx/Sln^{-/-}* and *mdx* mice. For detection of SERCA isoforms, calcineurin, NFATc1 and p-NFATc1, samples were separated using standard SDS-PAGE (7.5% total acrylamide) and transferred on to 0.2µm PVDF membranes. Detection of utrophin utilized a 6% total acrylamide gel that was transferred onto a 0.2µm PVDF membrane. For SLN, samples were separated with Tricine-based SDS-PAGE (13% gel) and transferred onto 0.2 µm nitrocellulose membrane. Membranes were probed with their corresponding antibodies for calcineurin (1: 1000), utrophin (1:500), NFATc1 (1: 5000), p-NFATc1 (1:5000), actin (1: 10 000) and SLN (1: 50). Membranes were then washed and probed with secondary goat anti mouse IgG (SERCA isoforms, 1:20 000; calcineurin, 1: 5000; utrophin, 1:2000; p-NFATc1, 1:2000; actin, 1: 20 000) or goat anti rabbit (NFATc1, 1:2000; SLN, 1:2000). Antigen-antibody complexes were detected by either SuperSignal West FemtoTM substrate (Pierce; Thermo Fisher Scientific Inc., Grand Island, NY) for utrophin, SLN and p-NFATc1 or Luminata ForteTM (Millipore, Billerica, MA) for SERCA1a, SERCA2a, calcineurin, and NFATc1. Quantification of optical densities was performed using GeneTools (Syngene, MD) and normalized to total protein content from ponceau staining. Pan actin was used as a loading control for SERCA1a due to the limited protein load which made ponceau staining unreliable in detecting total protein. The ratio of p-NFATc1 to total NFATc1 was quantified and used as a marker of calcineurin signaling, with a lower ratio indicating higher calcineurin signaling and greater nuclear NFATc1 localization. See appendix for further Western blotting details.

Serum Creatine Kinase

Serum creatine kinase (CK), a common measure to assess muscle damage, was measured in sham-injected and DFZ-injected animals of both genotypes (*mdx* & *mdx/Sln*^{-/-}). Briefly, twelve *mdx* mice (six n=6 vehicle & n=6 DFZ) & twelve *mdx/Sln*^{-/-} mice (n=6 vehicle & n=6 DFZ) were sacrificed via cervical dislocation, the thoracic cavity was opened and the heart was removed. Blood then pooled was collected into a syringe, allowed to clot on ice for 10 minutes and was then spun down at 5000 g for 10 min at 4°C. The plasma was decanted and stored at -80°C until analysis. Serum CK activity was measured using a kinetic fluorometric assay as described previously [146]. This assay works based on the rate of production of NADPH from the following reactions.



The production of NADPH was measured on a fluorometer at 340nm for 5 minutes. To do this, 5µL of serum was added to 1mL of solution mixture (Imidazole 25mM, MgCl₂ 2.5mM, N-acetyl cysteine 5mM, glucose 5mM, NADP 500µM, AMP 1mM, ADP 500µM, glucose-6-phosphate dehydrogenase (G-6-P-DH) 0.4U/mL, hexokinase 0.63U/mL), was allowed to equilibrate for 5 minutes. Creatine phosphate (15mM final concentration) was then added and 200µL of the solution was loaded into a black 96well plate and read in triplicate. The rate of NADPH production was then converted into a concentration of creatine kinase by dividing the rate of NADPH production by the NADH standard multiplied by the concentration of NADH.

Statistical Analyses

The data are presented as mean \pm standard error (SEM). Statistical significance was set at $p \leq 0.05$. Unless otherwise stated, all collected data were compared using a Two-Way ANOVA with treatment (VEH or DFZ) and genotype (*mdx* or *mdx/Sln^{-/-}*) as factors. Post-hoc testing was done using a Neuman-Keul test to compare specific means, when appropriate. Trends in data were only labeled as such when $p=0.05-0.1$. Planned comparisons with two-tailed t-test (one-tailed when specified) were utilized only when the literature or data within this thesis provided sufficient evidence to warrant further statistical examination.

Results

Physical Characteristics and Serum Creatine Kinase Levels

Beginning at 4 weeks of age, *mdx* and *mdx/Sln^{-/-}* pups were injected with either VEH (saline) or DFZ, for 7 days. At time of sacrifice (5 weeks of age), *mdx* mice on average were lighter than *mdx/Sln^{-/-}* mice (Figure 3.1A, $p=0.0078$ *mdx* < *mdx/Sln^{-/-}*). In addition, there was a trend where DFZ treated animals weighed less than VEH treated animal ($p=0.0698$; VEH>DFZ). Despite an initial difference in weight (see appendix S1.1), Figure 3.1B shows that weight gain during the course of treatment was similar between *mdx* and *mdx/Sln^{-/-}* mice ($p>0.05$).

The absolute weight of the SOL, DIA and EDL muscles was measured and then normalized to body weight. For SOL, there was no effect of treatment (Figure 3.2, $p>0.05$) but there was a main effect of genotype for both absolute (Figure 3.2A, $p=0.002$) and relative (Figure 3.2B $p=0.0072$) muscle mass, which were greater in *mdx/Sln^{-/-}* compared to *mdx*.

Similar results were found for DIA, as there were no treatment effects (Figure 3.3, $p>0.05$) but there was a main effect of genotype with greater absolute (Figure 3.3A, $p=0.0006$) and relative (Figure 3.3B, $p=0.0002$) muscle weights in *mdx/Sln*^{-/-} compared with *mdx*. There were no differences in either absolute or relative EDL muscle weights between any groups (Figure 3.4; $p>0.05$).

Serum CK, a marker of muscle breakdown or damage, was higher in *mdx/Sln*^{-/-} mice compared with *mdx* mice (main effect of genotype; Figure 3.5 $p=0.0272$, *mdx*<*mdx/Sln*^{-/-}). Surprisingly, CK levels were elevated in DFZ treated groups compared with VEH (main effect of treatment; Figure 3.5 $p=0.0164$, VEH<DFZ).

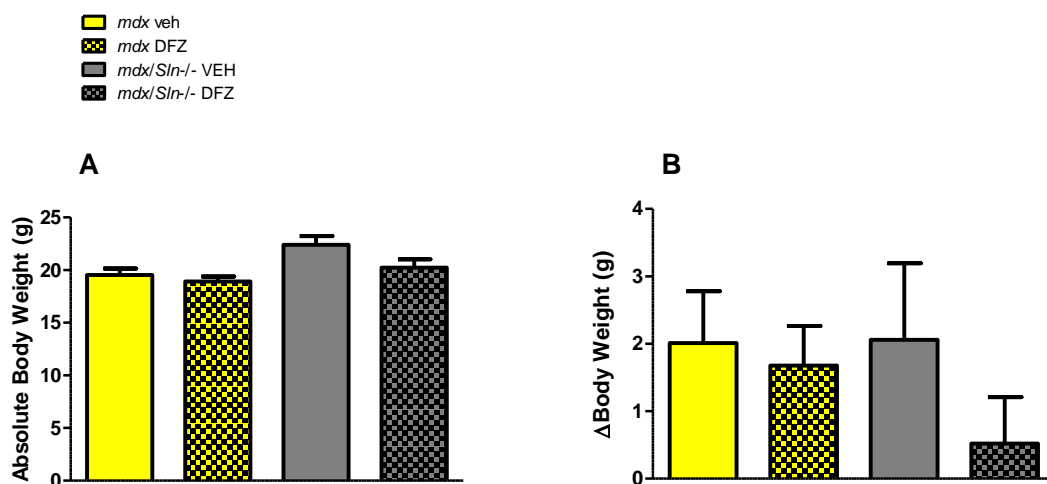


Figure 3.1: Absolute and change in (Δ) body weight of *mdx* and *mdx/Sln*^{-/-} mice treated with VEH or DFZ. (A) Body weight (g) of *mdx* and *mdx/Sln*^{-/-} mice at time of sacrifice shows significant main effect of genotype ($p=0.0078$, *mdx* < *mdx/Sln*^{-/-}) and a trending main effect of treatment ($p=0.0698$, VEH>DFZ). **(B)** Change in body weight from start of treatment to time of sacrifice (g) of *mdx* and *mdx/Sln*^{-/-} mice. All values are presented as mean \pm standard error. (n=8-10 per group)

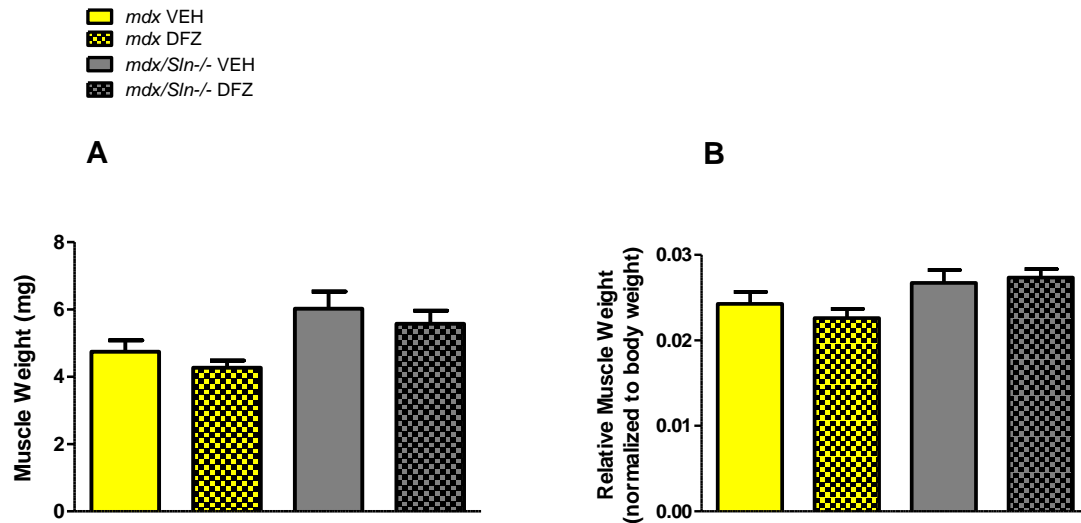


Figure 3.2: Absolute and relative SOL weight in *mdx* and *mdx/Sln^{-/-}* mice treated with VEH or DFZ. (A) Absolute muscle weight (mg) of SOL post treatment with VEH or DFZ. There is a significant main effect of genotype effect ($p=0.002$, $mdx < mdx/Sln^{-/-}$). (B) SOL weight (g) normalized to body weight (g) post treatment shows a significant main effect of genotype ($p=0.0072$, $mdx < mdx/Sln^{-/-}$). All values are presented as mean \pm standard error. (n=8-10 per group)

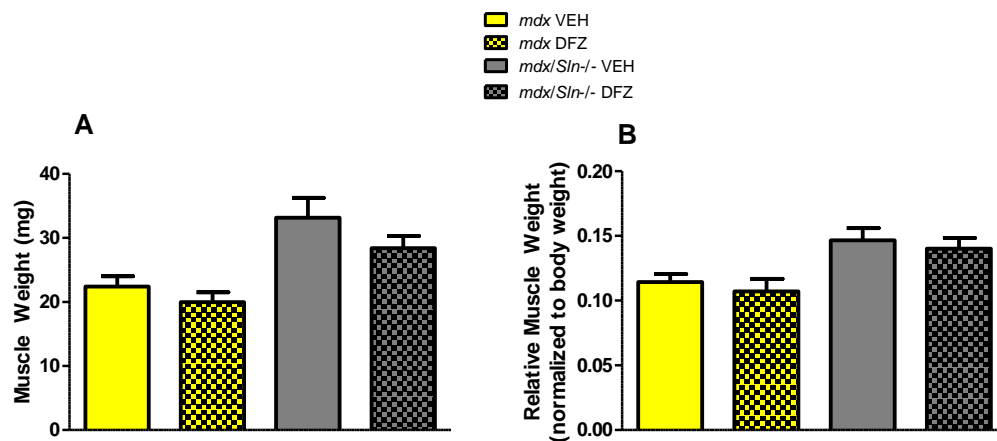


Figure 3.3: DIA absolute and relative weight of *mdx* and *mdx/Sln^{-/-}* mice treated with VEH or DFZ. (A) Absolute DIA weight (mg) and (B) relative DIA weight post treatment in *mdx* and *mdx/Sln^{-/-}* mice. There is a significant main effect of genotype for both absolute and relative DIA weight ($p=0.006$ & $p=0.002$ respectively, $mdx < mdx/Sln^{-/-}$). All values are presented as mean \pm standard error. (n=8-10 per group)

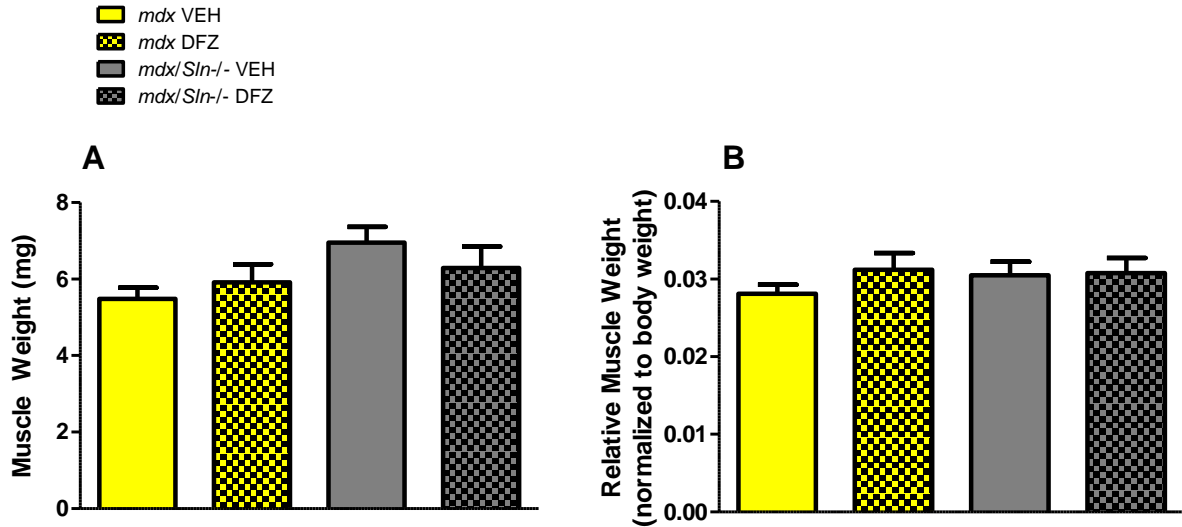


Figure 3.4: EDL absolute weight and relative muscle weight in *mdx* and *mdx/Sln^{-/-}* mice treated with VEH or DFZ. (A) Absolute weight of EDL (mg) and (B) relative EDL weight post treatment in *mdx* and *mdx/Sln^{-/-}* mice. All values are mean \pm standard error. (n=8-10 per group)

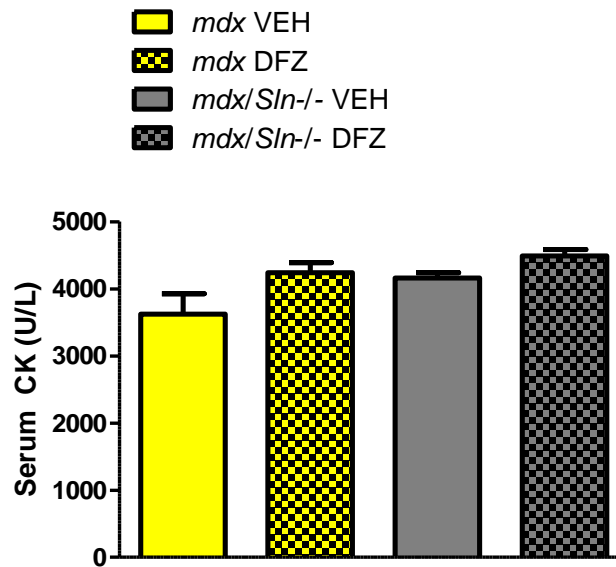


Figure 3.5: Serum CK levels in *mdx* and *mdx/Sln^{-/-}* mice after treatment protocol. Significant main effects of genotype ($p=0.0272$, $mdx < mdx/Sln^{-/-}$) and treatment ($p=0.0164$, $VEH < DFZ$) were observed. All values are mean \pm standard error. (n=6-9 per group)

Histological Features of DMD in the Soleus and Diaphragm

When examining the SOL muscle, there was a trend for a main effect of treatment, where DFZ treated groups showed improvements in centralized nuclei (Figure 3.6B; $p=0.076$ VEH>DFZ). There were no differences ($p>0.05$) in centralized nuclei between *mdx* and *mdx/Sln^{-/-}* mice. Total fibre number was not different between any of the groups (Figure 3.6C; $p>0.05$).

In DIA, DFZ treatment decreased the presence of centrally nucleated fibres in both *mdx* and *mdx/Sln^{-/-}* mice compared to VEH (Figure 3.7A/B; main effect $p=0.015$, VEH>DFZ). A main effect of genotype was also observed, where *mdx/Sln^{-/-}* mice had an increased presence of centralized nuclei ($p=0.0002$, *mdx*<*mdx/Sln^{-/-}*). Total fibre number was not affected by treatment or genotype (Figure 3.7C; $p>0.05$).

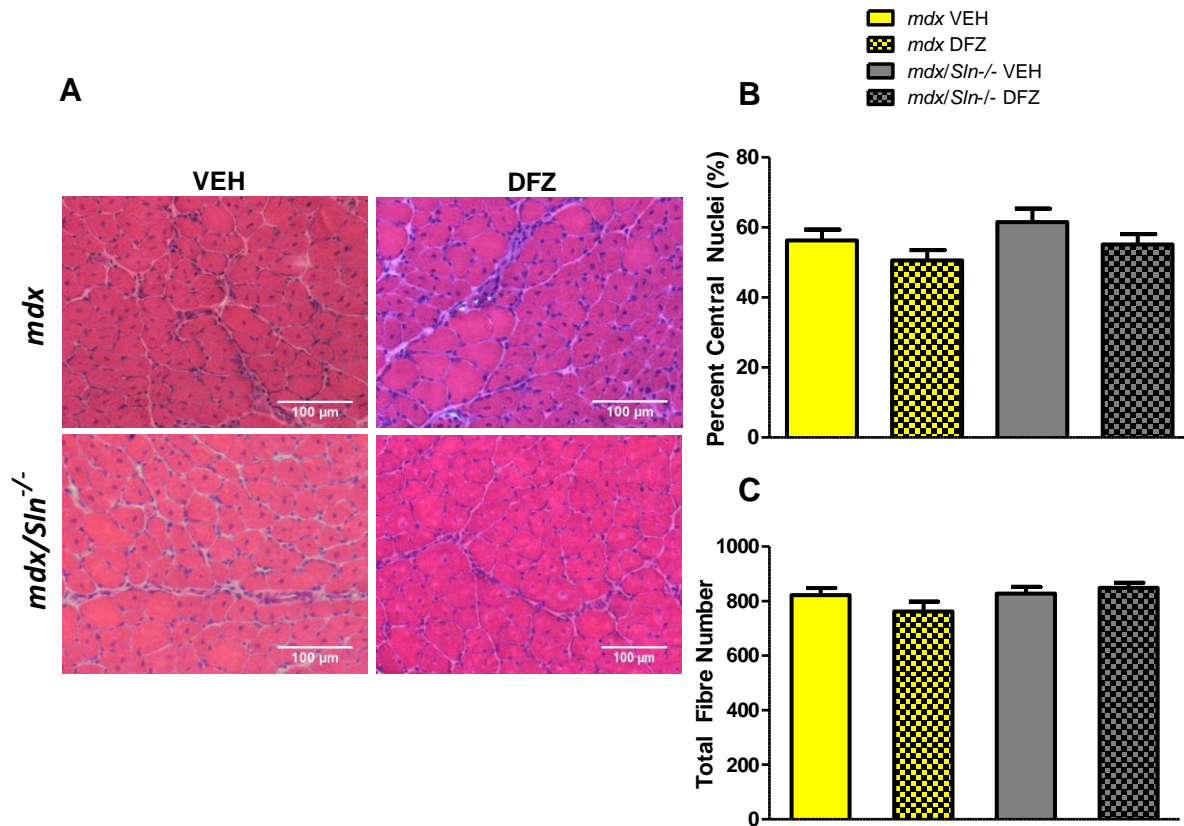


Figure 3.6: Centralized nuclei and total fibre number in SOL from *mdx* and *mdx/Sln*^{-/-} mice treated with VEH or DFZ. (A) Representative images of H&E staining used for quantification of (B) centrally nucleated fibres where a trend for a main effect of treatment were observed ($p=0.076$, VEH>DFZ) and (C) total fibre number. All values are presented as mean \pm standard error ($n=8-10$ per group). Scale bar depicts 100 μ m.

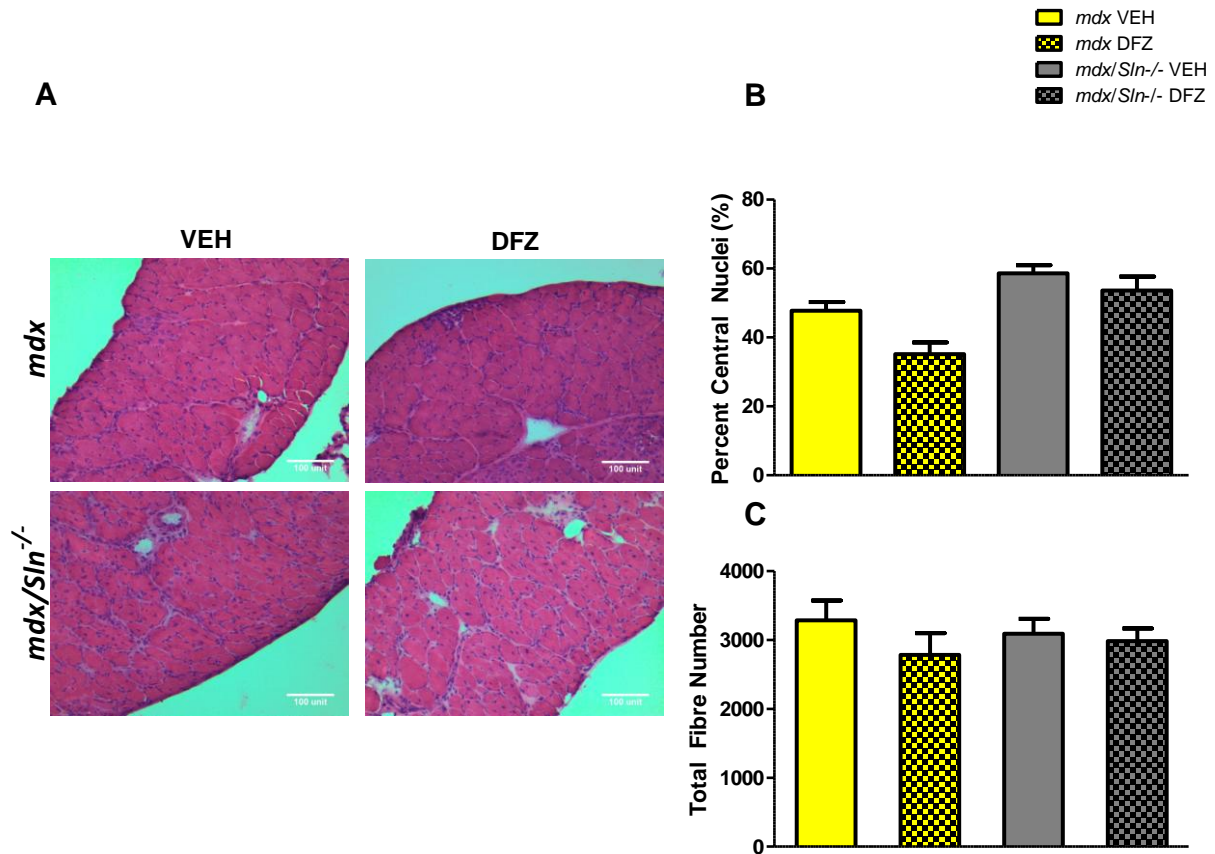


Figure 3.7: Centralized nuclei and total fibre number in DIA from *mdx* and *mdx/Sln^{-/-}* mice treated with VEH or DFZ. (A) Representative images of diaphragm from H&E staining used for quantification of (B) centrally nucleated fibres where main effects of genotype ($p=0.0002$, $mdx < mdx/Sln^{-/-}$) and treatment ($p=0.015$ VEH>DFZ) were observed and (C) total fibre number. All values are presented as mean \pm standard error ($n=6-8$ per group). Scale bar depicts 100 μ m.

Figure 3.8 shows that DFZ significantly decreases the infiltration of collagen in SOL of both *mdx* and *mdx/Sln^{-/-}* mice compared with VEH (main effect, $p=0.0221$; VEH>DFZ). Collagen infiltration in SOL was not different between genotypes ($p>0.05$). DFZ treatment also decreased collagen infiltration in DIA in both *mdx* and *mdx/Sln^{-/-}* mice (Figure 3.9, main effect $p=0.003$; VEH>DFZ). There is also a trend ($p=0.07$) for a main effect of genotype with DIA from *mdx/Sln^{-/-}* mice having greater collagen infiltration compared to DIA from *mdx* mice.

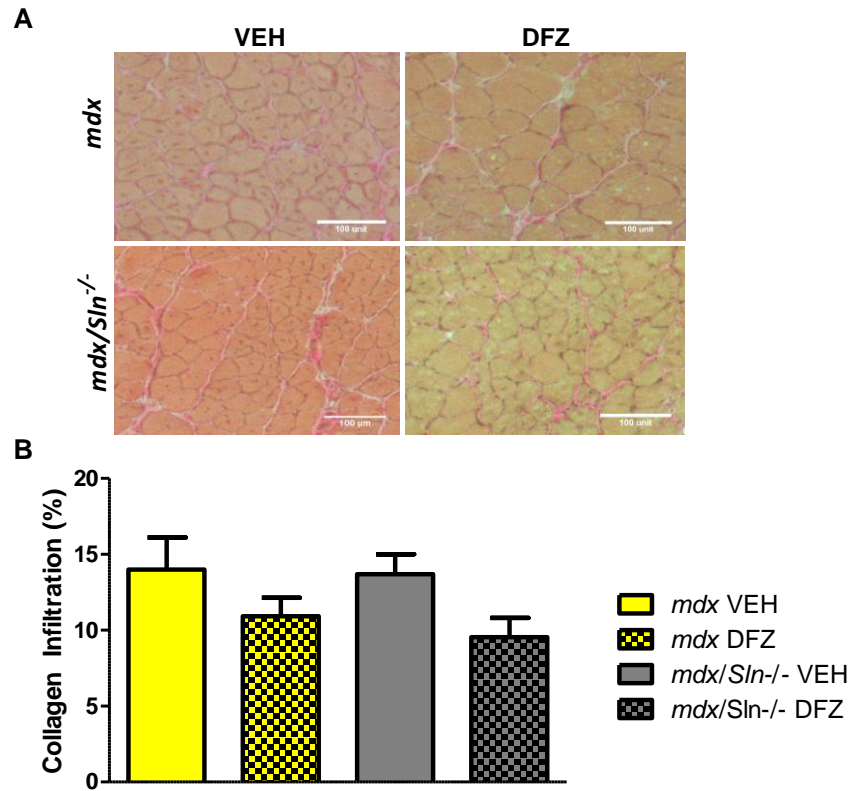


Figure 3.8: Collagen infiltration in SOL of *mdx* and *mdx/Sln^{-/-}* mice treated with VEH or DFZ. (A) Representative Van Gieson staining used for (B) quantification of collagen infiltration in *mdx* and *mdx/Sln^{-/-}* mice post DFZ or VEH treatment. There was a significant main effect of treatment ($p=0.0221$, VEH>DFZ). All values are presented as mean \pm standard error ($n=8-9$ per group). Scale bar depicts 100 μ m.

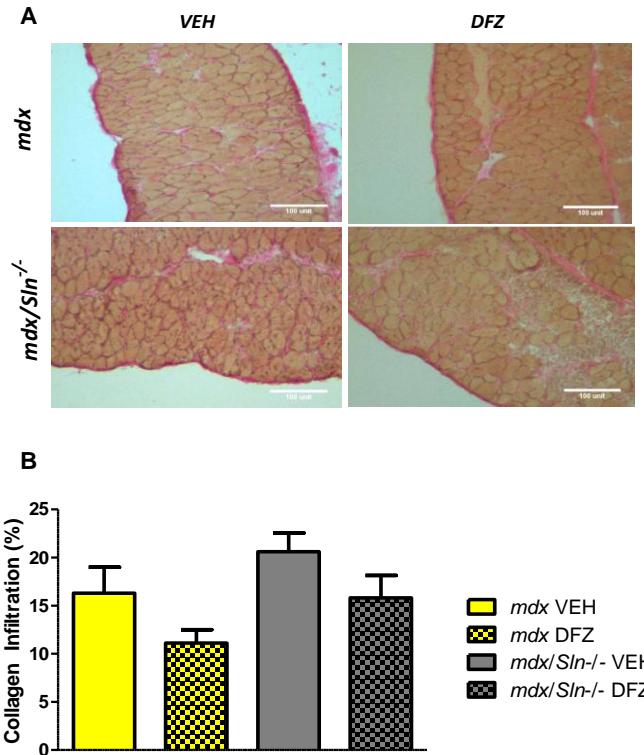


Figure 3.9: Collagen infiltration in DIA of *mdx* and *mdx/Sln^{-/-}* mice after treatment protocol. (A) Representative images of Van gieson staining used for (B) quantification of collagen infiltration in *mdx* and *mdx/Sln^{-/-}* post DFZ or VEH treatment. There was a significant main effect of treatment ($p=0.003$, VEH>DFZ) and a trend for a main effect of genotype ($p=0.07$, *mdx*>*mdx/Sln^{-/-}*). All values are presented as mean \pm standard error ($n=6-8$ per group).

Immunofluorescent Features of DMD in the Soleus and Diaphragm

Immunofluorescent staining was used to quantify fibre type distribution, CSA and coefficient of variation in minimal Feret's diameter in SOL (Figure 3.10 and Figure S1.2) and DIA (Figure 3.11 and Figure S1.3). In SOL, DFZ treatment decreased type IIX fibres proportions in both *mdx* and *mdx/Sln^{-/-}* mice compared to VEH (Figure 3.10B, $p=0.0094$; VEH>DFZ). There was a trend for a main effect of genotype effects for both IIX/IIB hybrid fibres (Figure S1.2, $p=0.069$) and IIB fibres (Figure 3.10B, $p=0.0532$) where *mdx/Sln^{-/-}* mice had increase proportions compared to *mdx*. There were no differences ($p>0.05$) in type I, I/IIA,

IIA and IIA/X fibres between any groups. CSA of type I, IIA, and IIB was also not different ($p>0.05$) between any groups. There was a trend for an interaction effect for CSA of type IIX fibres ($p=0.0765$), whereby DFZ treatment increased CSA in *mdx* mice but decreased CSA in *mdx/Sln^{-/-}* mice compared with VEH (Figure 3.10C); however Newman-keul post-hoc comparisons showed no difference between groups ($p>0.05$). There was also a trend for an interaction effect in fibre size variability in the SOL, as measured by the coefficient of variation of minimal Feret's diameter (Figure 3.10D, $p=0.0903$). Compared with VEH, the DFZ treatment increased variability in *mdx* mice and decreased variability in *mdx/Sln^{-/-}* mice. However, post hoc comparisons revealed no significant differences between groups ($p>0.05$).

In the DIA, proportions of type I, IIA and IIB fibres were not altered by DFZ ($p>0.05$) or genotype ($p>0.05$). DFZ treatment increased IIX fibres in both *mdx* and *mdx/Sln^{-/-}* mice treated with DFZ (main effect, $p=0.0246$, $VEH<DFZ$). There was a main effect of genotype where *mdx/Sln^{-/-}* mice had increased proportions of type I/IIA fibres ($p=0.0349$) and IIA/IIX fibres ($p=0.007$) compared with *mdx* mice (Figure S1.3). There was a main effect of treatment where IIA/IIX fibres were increased after DFZ treatment compared to VEH (Figure S1.3, $p=0.0295$).

There were no difference in CSA of any fibre type in DIA between any groups ($p>0.05$). *Mdx/Sln^{-/-}* mice had increased fibre size variability compared to *mdx* mice ($p=0.0065$), but there were no treatment effects ($p>0.05$) in DIA.

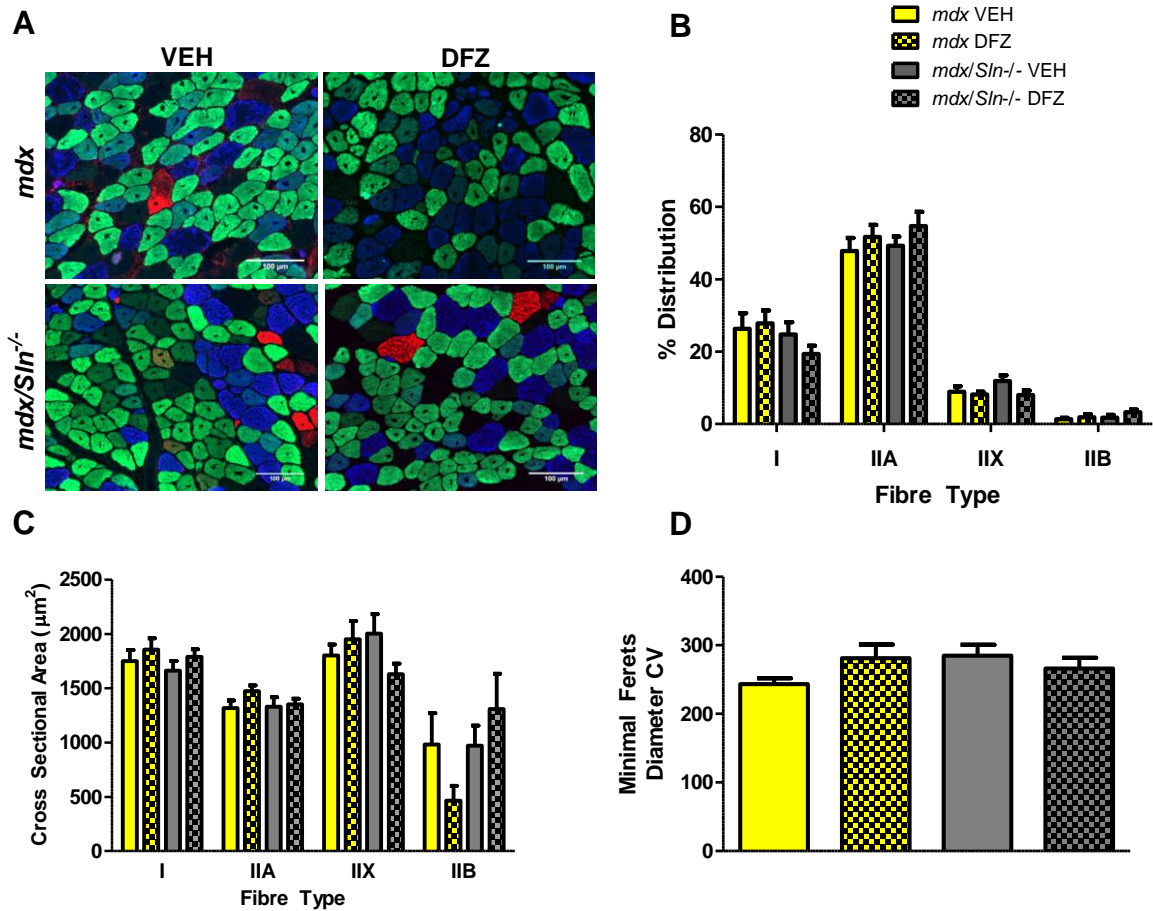


Figure 3.10: Fibre type distribution, CSA and covariance of minimal Feret's diameter in SOL muscles from *mdx* and *mdx/Sln^{-/-}* after treatment with VEH or DFZ. (A) Representative immunofluorescent images of SOL sections show type I fibres in blue, type IIA fibres in green, type IIX fibres in black and IIB fibres in red. Scale bar depicts 100µm. Quantification of (B) fibre type distribution, (C) CSA and (D) covariance of minimal Feret's diameter. A significant treatment effect ($p=0.0094$ VEH<DFZ) was observed in the distribution of IIX fibres and a trend for a genotype effect in IIB fibres ($p=0.0532$, $mdx<mdx/Sln^{-/-}$). A trend for an interaction effect in the CSA of IIX fibres ($p=0.0765$) and in covariance of minimal Feret's diameter ($p=0.0903$) was observed. All values are mean \pm standard error (n=8-9 per group).

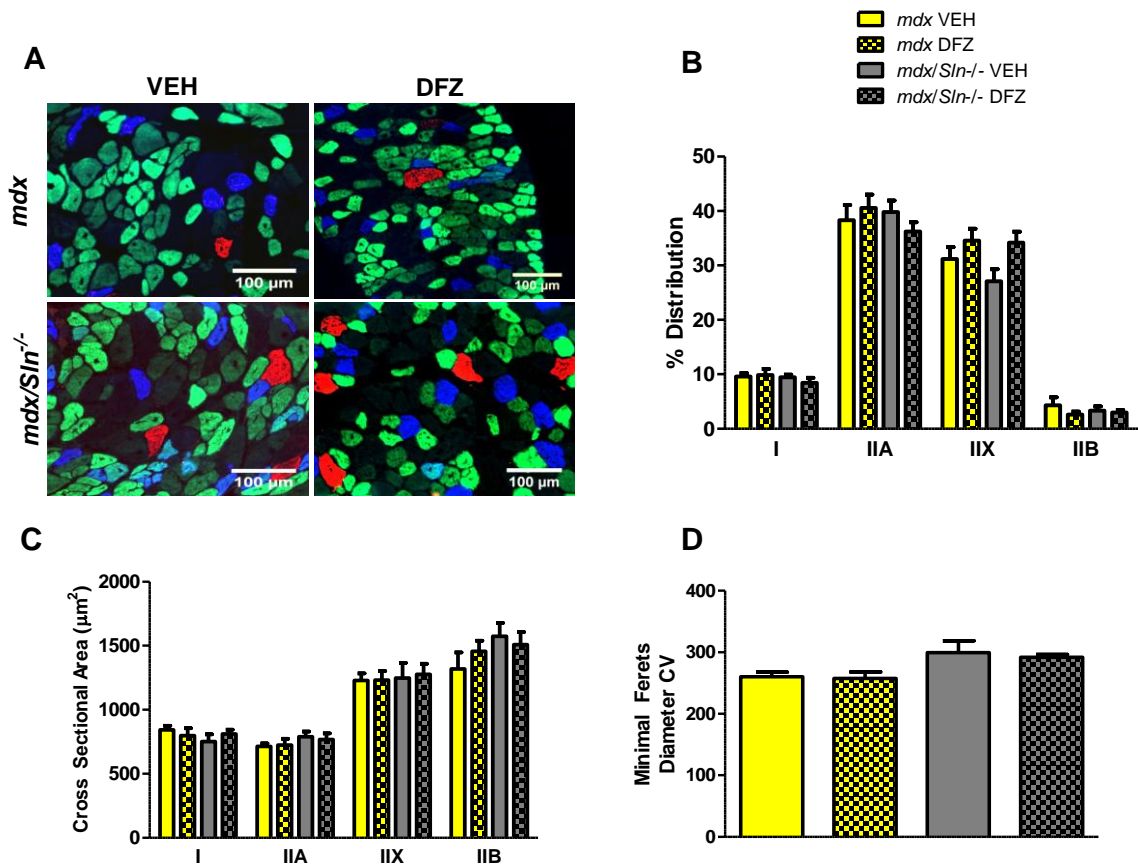


Figure 3.11: Fibre type distribution, CSA and covariance of minimal Feret's diameter of DIA from *mdx* and *mdx/Sln^{-/-}* mice after treatment with VEH or DFZ. (A) Representative immunofluorescent images of myosin heavy chain distribution show type I fibres in blue, type IIA fibres in green, type IIX fibres in black and IIB fibres in red. Scale bar depicts 100µm. Quantification of (B) fibre type distribution, (C) CSA and (D) fibre size variability measured by covariance of minimal Feret's diameter. There was a significant increase in IIX fibres after DFZ treatment ($p=0.0246$, $VEH < DFZ$). *Mdx/Sln^{-/-}* mice have increased covariance of minimal feret's diameter compared to *mdx* mice ($p=0.0065$, $mdx < mdx/Sln^{-/-}$). All values are mean \pm standard error (n=6-8 per group).

Calcineurin/NFAT Signaling in the Soleus and Diaphragm

Western blot analyses of total NFATc1 and NFATc1-p in Sol from DFZ and VEH are shown in Figure 3.12. There were trends for main effects of treatment for both total NFATc1 (Figure 3.12B, $p=0.0836$; VEH < DFZ) and NFATc1-p (Figure 3.12C, $p=0.0791$; VEH < DFZ), indicating that both total and cytosolic NFATc1 pools are increased by DFZ treatment. There was also a trend for a main effect of genotype for total NFATc1 (Figure 3.12B, $p=0.0797$), with content being lower in *mdx* mice compared to *mdx/Sln^{-/-}* mice. No genotype differences were observed in NFATc1-p ($p>0.05$). There were no significant effects of genotype ($p>0.05$) or treatment ($p>0.05$) for NFAT-p to total NFATc1 ratios (Figure 3.12D). Nuclear NFAT localization in SOL was also assessed using immunofluorescent staining of NFATc1 and DAPI (Figure 3.13). This analysis yielded a significant main effect of treatment with higher levels of NFATc1 and DAPI co-localization following DFZ compared with VEH, as measured by Pearson's correlation coefficient (Figure 3.12D, $p=0.018$, VEH < DFZ). There were no genotype differences in NFATc1 and DAPI co-localization ($p>0.05$).

Western blot analyses of total NFATc1 and NFATc1-p in DIA from DFZ and VEH treated mice are shown in Figure 3.14. Total NFATc1 levels were significantly higher in *mdx* mice compared to their *mdx/Sln^{-/-}* counterpart, regardless of treatment (Figure 3.14B, $p=0.0017$). Similar results were found for phosphorylated NFATc1 content but there was only a trend for main effect of genotype (Figure 3.14C; $p=0.0692$, *mdx* > *mdx/Sln^{-/-}*). As a result, the ratio of NFATc1-p to total NFATc1 was significantly higher in *mdx/Sln^{-/-}* compared with *mdx* mice (Figure 3.14D, $p=0.047$), an effect that was independent of treatment. However, when examined using immunofluorescence (Figure 3.15), the co-localization of NFATc1 and DAPI appeared to be very low and there was no genotype or treatment effects ($p>0.05$).

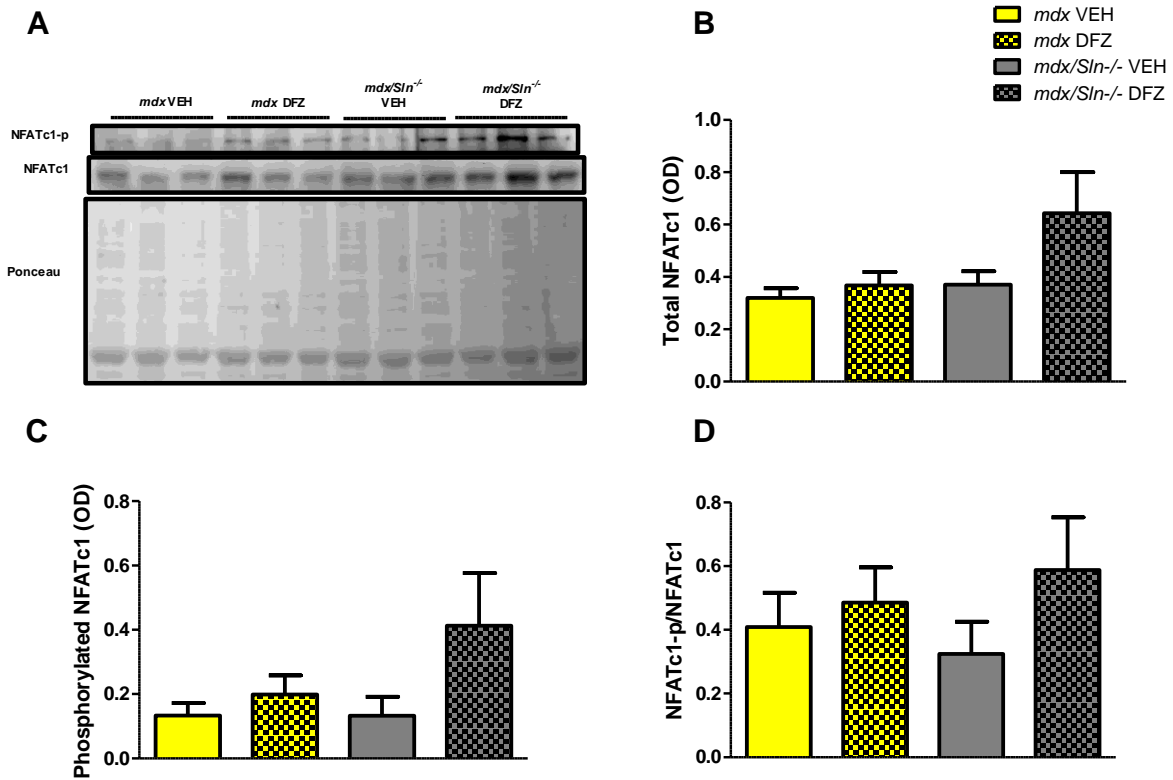


Figure 3.12: Western blot analysis of total NFATc1, phosphorylated NFATc1 and ratio of NFATc1-p to total NFATc1 in SOL of *mdx* and *mdx/Sln*^{-/-} mice after treatment with DFZ or VEH. (A) Representative western blots of (B) total NFATc1 where there were trends for main effects of treatment ($p=0.0836$, VEH<DFZ) and genotype ($p=0.0797$, *mdx*<*mdx/Sln*^{-/-}) and (C) phosphorylated NFATc1 where there was a trending main effect of treatment ($p=0.0791$, VEH<DFZ). (D) The ratio of NFATc1-p to total NFATc1 was calculated as a maker of nuclear NFAT localization. Total NFATc1 and FNATc1-p contents were normalized to total protein from ponceau staining. All values are mean \pm standard error (n=6 per group).

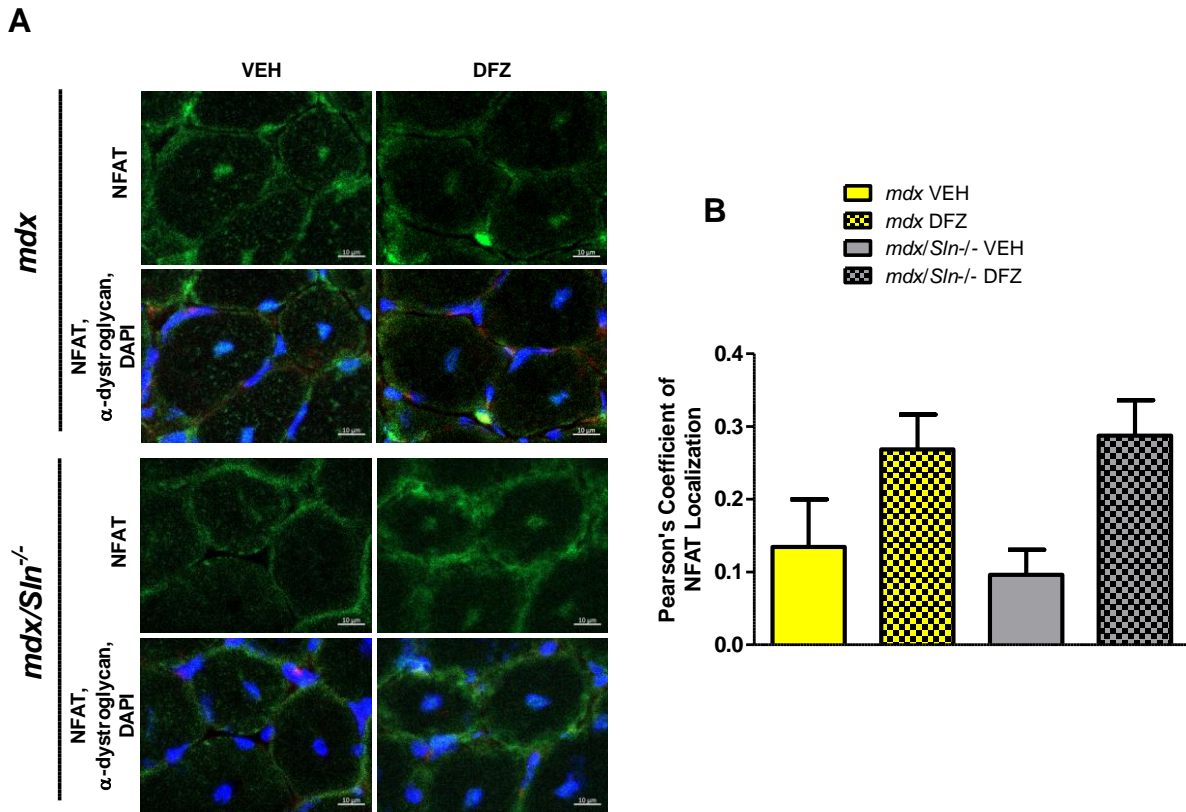


Figure 3.13: NFATc1 localization in SOL sections from *mdx* and *mdx/Sln^{-/-}* mice after treatment with DFZ or VEH. (A) Representative images of NFATc1 localization show NFATc1 in green, α -dystroglycan in red and DAPI in blue. (B) Quantification of Pearson's coefficient of NFATc1 localization. A significant main effect of treatment effect was observed ($p=0.018$, VEH<DFZ). All values are presented as mean \pm standard error ($n=6$ per group). Scale bars depict 10 μ m.

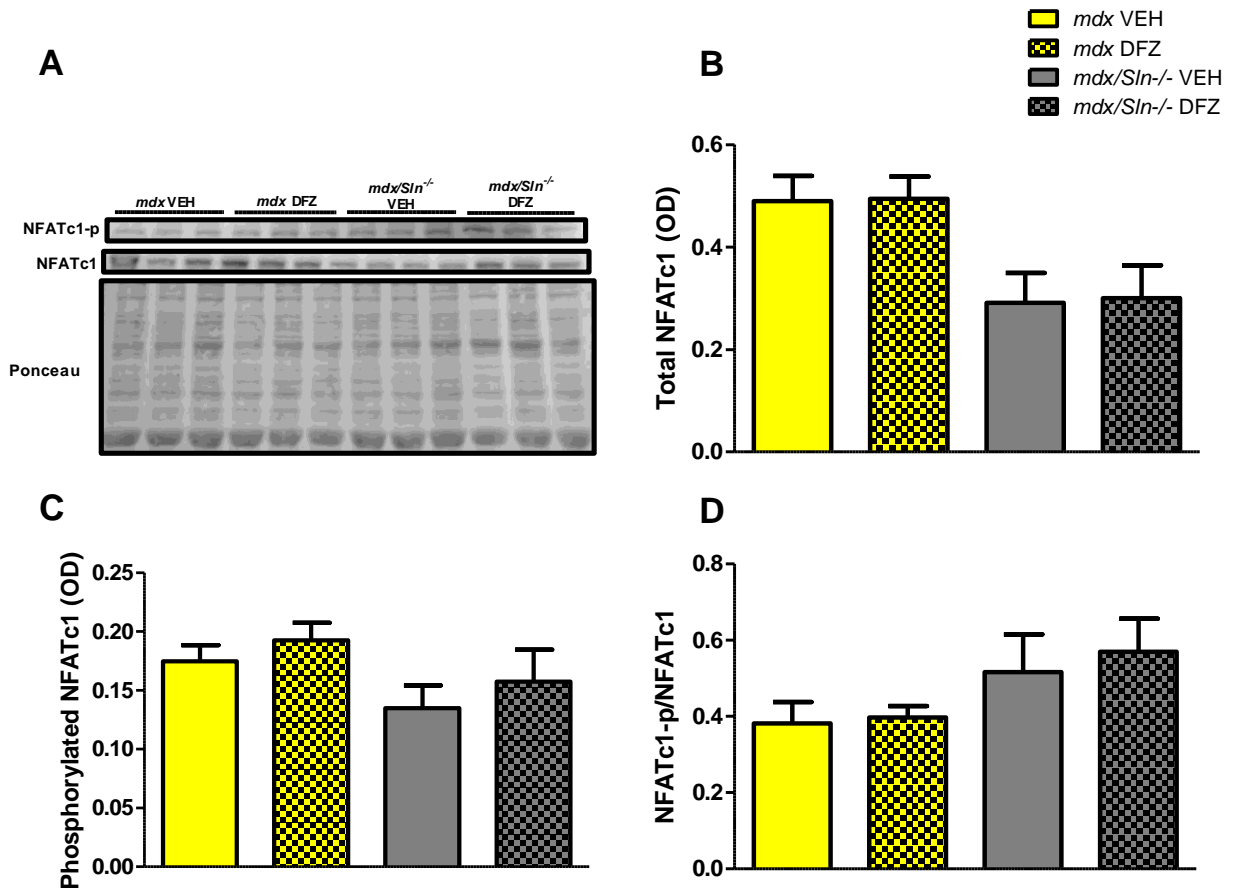


Figure 3.14: Western blotting analysis of total NFATc1, phosphorylated NFATc1 and ratio of NFATc1-p to total NFAT in DIA from *mdx* and *mdx/Sln*^{-/-} mice after DFZ or VEH treatment. (A) Representative western blots of (B) total NFATc1 which was significantly higher in *mdx* mice compared with *mdx/Sln*^{-/-} mice (main effect of genotype, $p=0.0017$) and (C) phosphorylated NFATc1 where there was a trending main effect of genotype ($p=0.0692$, $mdx > mdx/Sln$ ^{-/-}). (D) The ratio of NFATc1-p to total NFATc1 was calculated as a marker of nuclear NFAT localization and there was a significant main effect of genotype ($p=0.047$, $mdx < mdx/Sln$ ^{-/-}). Total NFATc1 and NFATc1-p contents normalized to total protein from ponceau stain. All values are presented as mean \pm standard error ($n=6$ per group).

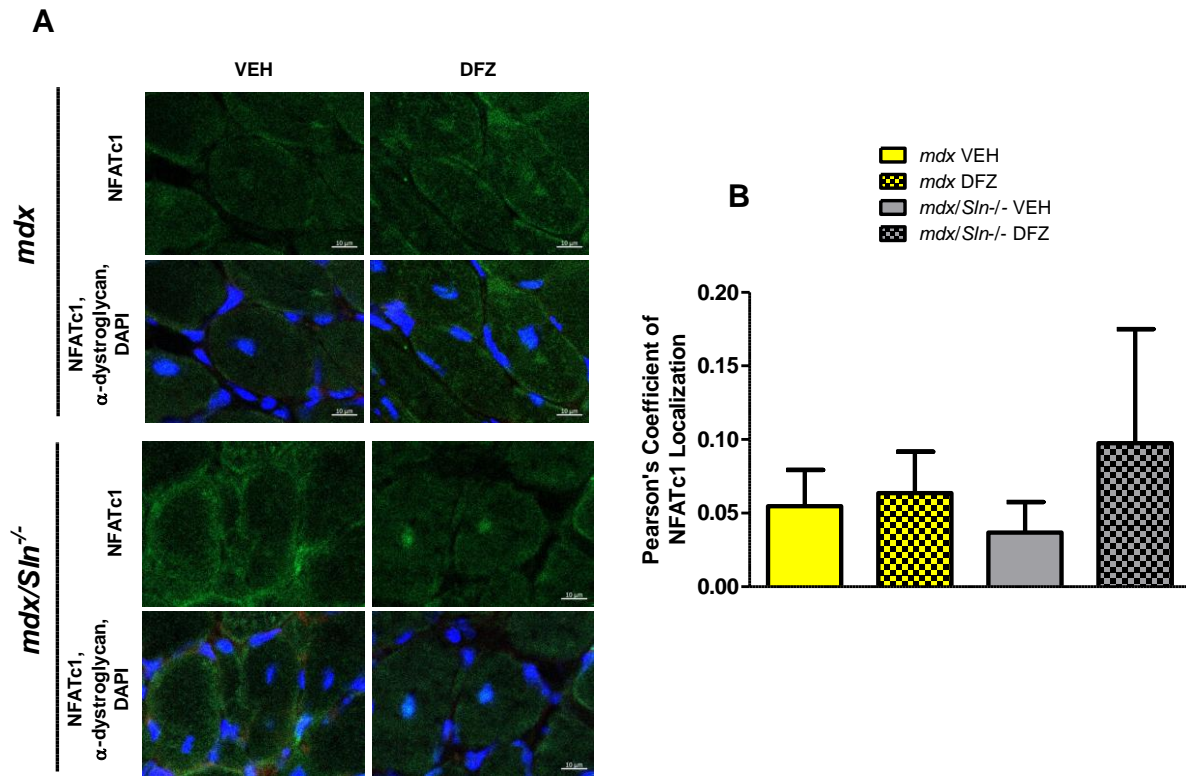


Figure 3.15: NFATc1 localization in DIA sections from *mdx* and *mdx/Sln^{-/-}* mice after DFZ or VEH treatment. (A) Representative images of immunofluorescent detection of NFATc1, where NFATc1 is green, α -dystroglycan in red and DAPI is blue. **(B)** Quantification of Pearson's correlation coefficient of NFATc1 and DAPI localization. All values are presented as mean \pm standard error (n=6 per group). Scale bars depict 10 μ m.

In the SOL, there were no differences in calcineurin content between groups (Figure 3.16, $p > 0.05$). In DIA, there was a trending interaction effect whereby calcineurin content appears to decrease with DFZ treatment in *mdx* mice, while content appears to increase in *mdx/Sln^{-/-}* mice (Figure 3.17, $p = 0.0940$), however post hoc analysis shows no difference between groups. No main effect of genotype or treatment was observed in DIA ($p > 0.05$).

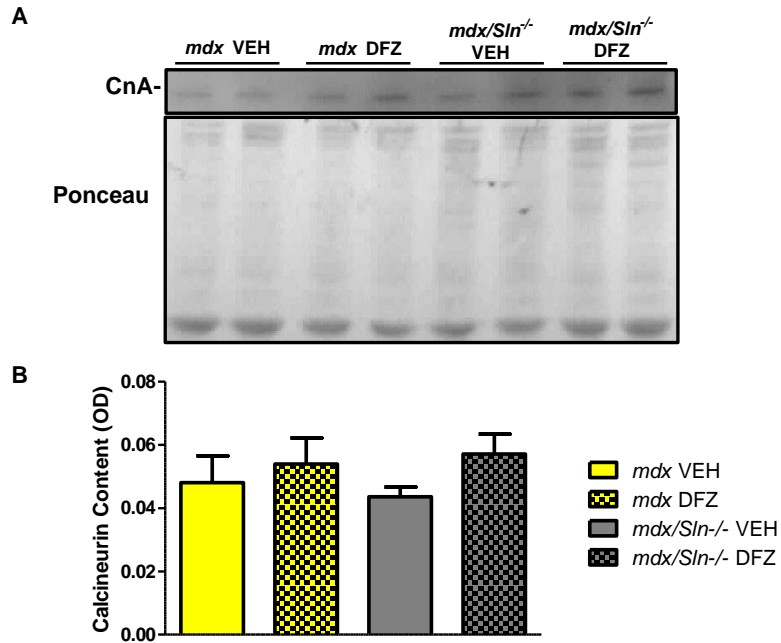


Figure 3.16: Western blot analysis of calcineurin content in SOL from *mdx* and *mdx/Sln*^{-/-} after treatment with VEH or DFZ. (A) Representative western blots of SOL and (B) quantification of calcineurin content which was normalized to total protein from ponceau stain. All values are mean \pm standard error (n=8 per group).

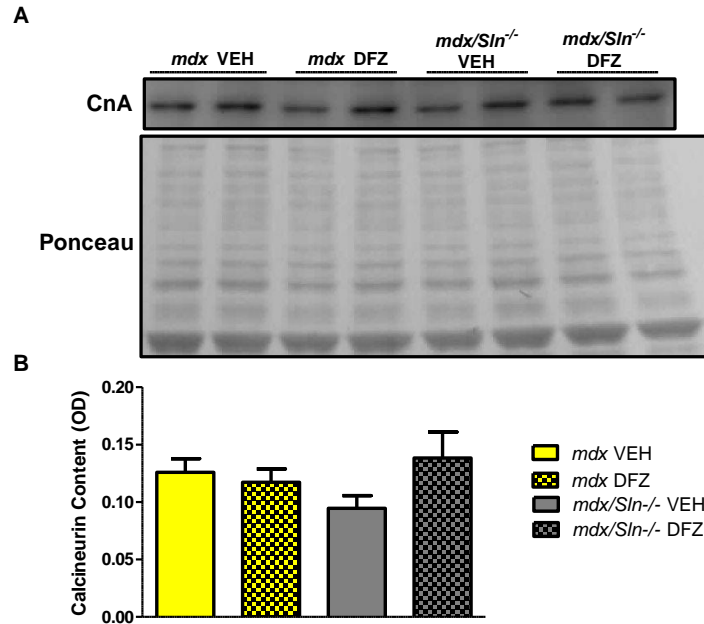


Figure 3.17: Western blot analysis of calcineurin content of DIA muscles from *mdx* and *mdx/Sln*^{-/-} mice after VEH or DFZ treatment. (A) Representative western blotting of (B) calcineurin content from DIA which shows a trend for an interaction effect ($p=0.0940$) where DFZ decreased calcineurin content in *mdx* mice and increases content in *mdx/Sln*^{-/-} mice. Calcineurin content was normalized to total protein from ponceau stain. All values are mean \pm standard error ($n=8$ per group).

Unexpectedly, utrophin content assessed by Western blotting in both SOL and DIA was not different after treatment nor was there any effect of genotype (Figure 3.18B & Figure 3.20, $p>0.05$). Immunofluorescent detection of utrophin also showed there were no differences between groups (Figure 3.19 & Figure 3.21, $p>0.05$) in both SOL and DIA.

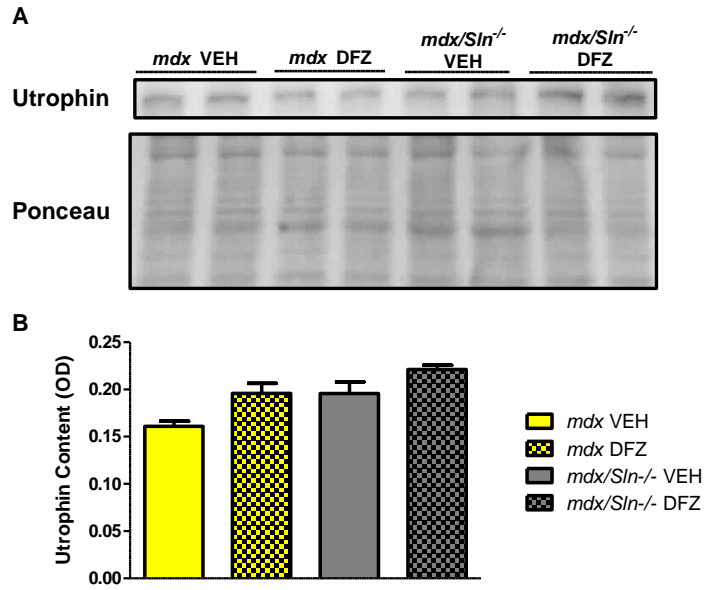


Figure 3.18: Western blot analysis of utrophin content of SOL from *mdx* and *mdx/Sln*^{-/-} mice after VEH or DFZ. (A) Representative western blots of utrophin in SOL of *mdx* and *mdx/Sln*^{-/-} mice after treatment. (B) Quantification of immunoblot of utrophin normalized to total protein from ponceau stain. All values are presented as mean \pm standard error (n=8 per group).

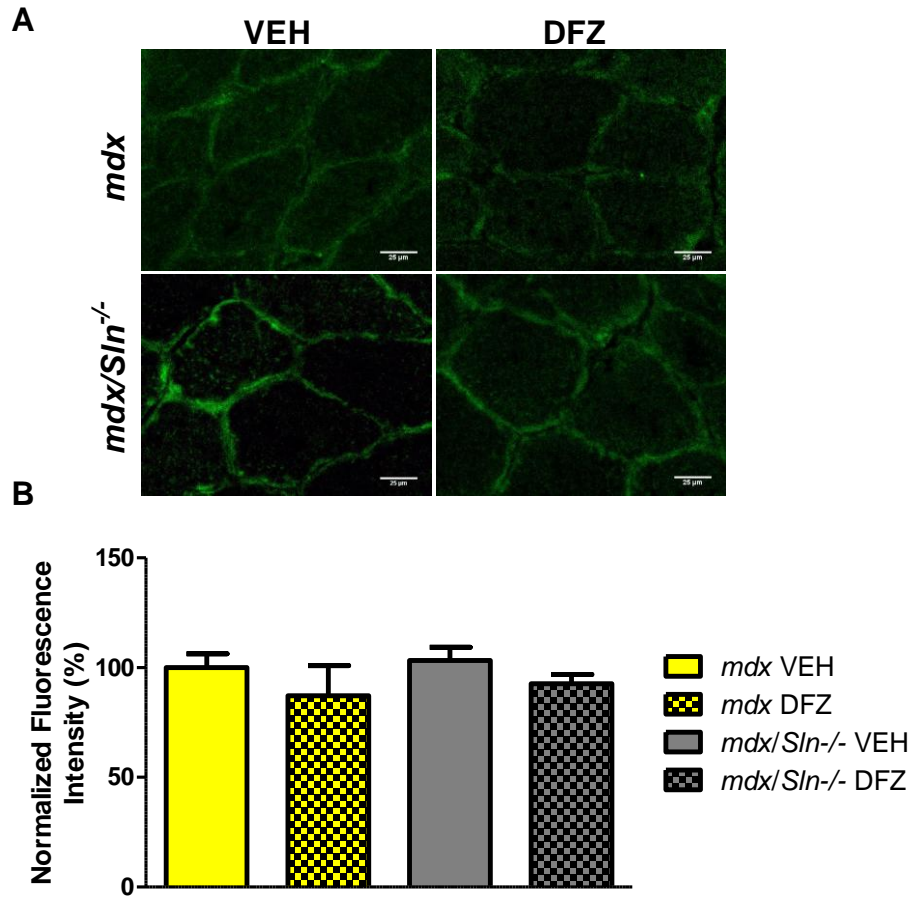


Figure 3.19: Immunofluorescent detection of utrophin in SOL of *mdx* and *mdx/Sln^{-/-}* mice after treatment. (A) Representative images of utrophin and (B) quantification of utrophin normalized to *mdx* VEH SOL. All values are mean \pm standard error (n=6 per group). Scale bars depict 25 μ m.

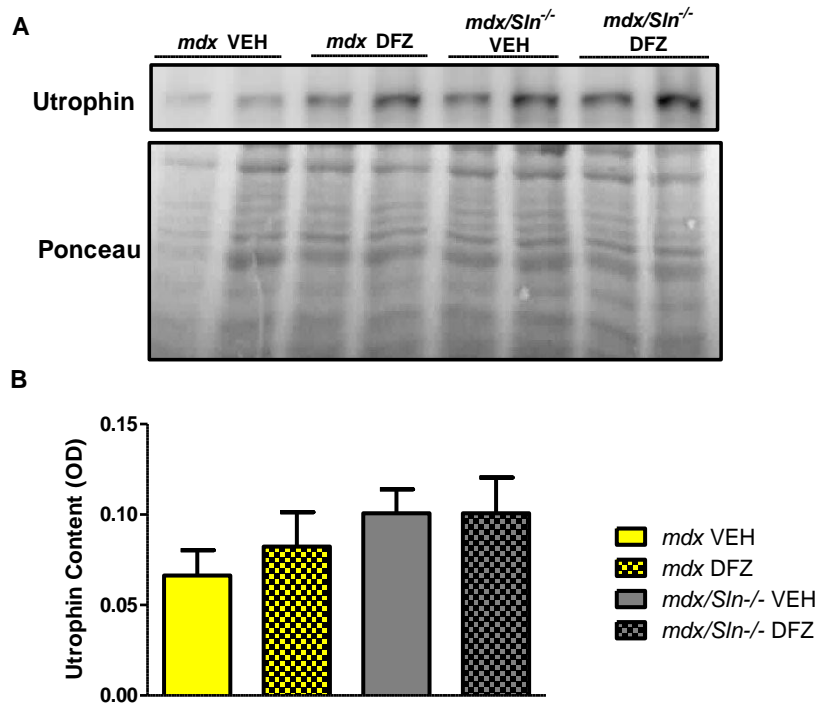


Figure 3.20: Western blotting of utrophin content in DIA in *mdx* and *mdx/Sln*^{-/-} mice after treatment with DFZ and VEH. (A) Western blots for utrophin were (B) quantified for content between treatments and genotypes. All values are mean \pm standard error (n=8 per group).

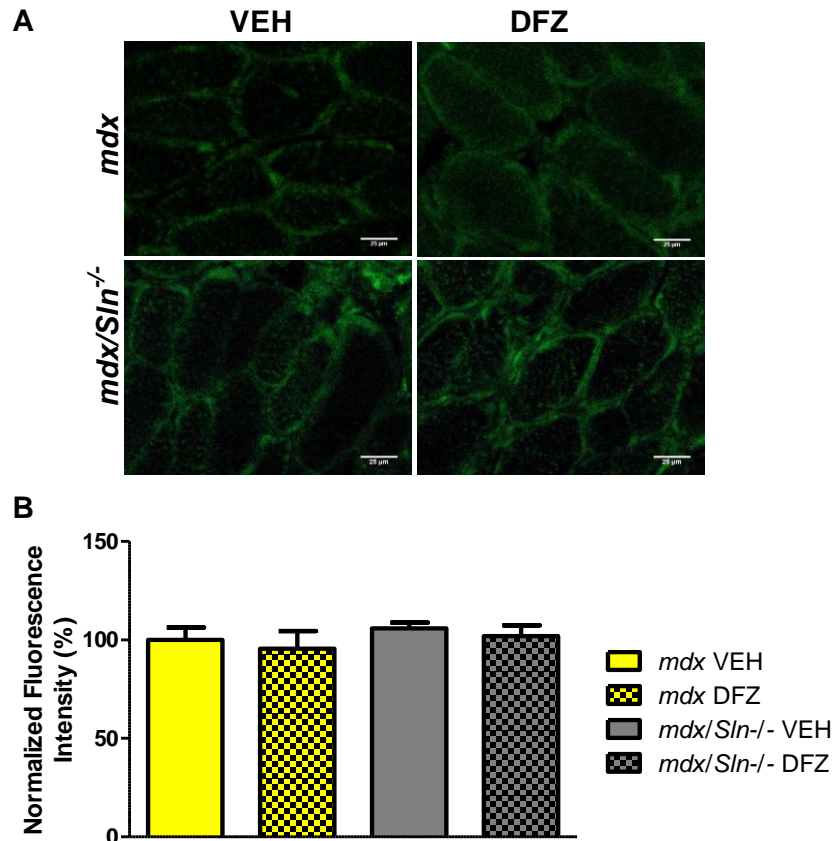


Figure 3.21: Normalized fluorescent intensity of utrophin staining from DIA of *mdx* and *mdx/Sln^{-/-}* mice. (A) Representative immunofluorescent staining of utrophin from DIA sections was (B) quantified and normalized to *mdx* VEH group. Scale bars depict 25µm. All values are mean ± standard error (n=8 per group).

Calcium Handling Proteins in the Soleus and Diaphragm

DFZ or genotype did not change SERCA1a content in the SOL of *mdx* and *mdx/Sln^{-/-}* mice (Figure 3.22C, $p > 0.05$). A trend for a main effect of genotype was observed for SERCA2a content in SOL (Figure 3.23, $p = 0.0544$; $mdx > mdx/Sln^{-/-}$). DFZ did not alter SERCA2a expression in the SOL ($p > 0.05$). In the DIA, SERCA1a and SERCA2a content was not altered by DFZ (Figure 3.24C & D, $p > 0.05$). A significant main effect of genotype was observed in SERCA1a content in DIA (Figure 3.23C, $p = 0.0174$), where *mdx/Sln^{-/-}* mice had

decreased levels of SERCA1a content compared to *mdx* mice. No effect of genotype was observed for SERCA2a content in DIA.

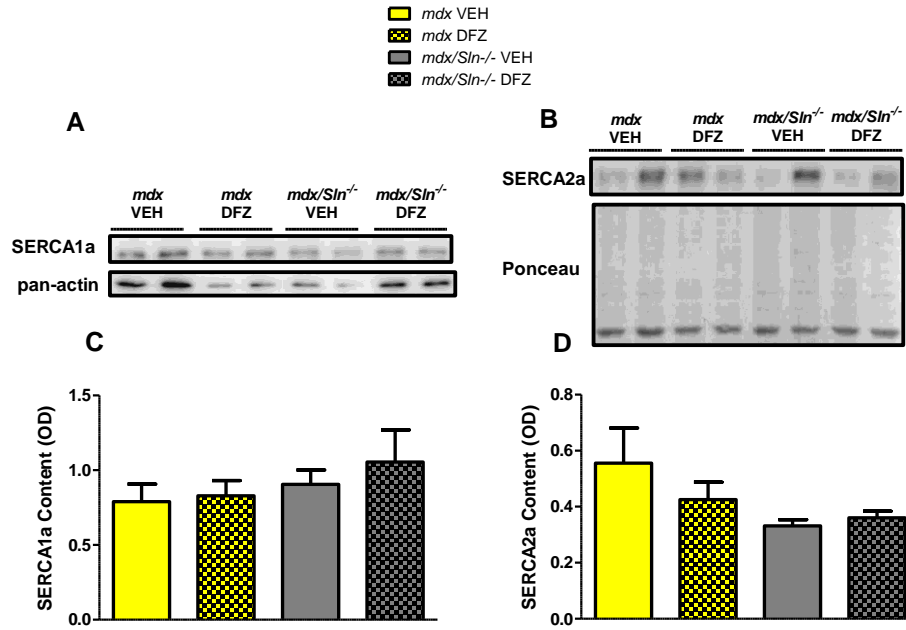


Figure 3.22: Western blotting of SERCA1a and SERCA2a in SOL of *mdx* and *mdx/Sln^{-/-}* mice after VEH or DFZ treatment. Representative western blots of (A) SERCA1a and (B) SERCA2a. Quantification of (C) SERCA1a normalized to actin and (D) quantification of SERCA2a normalized to total protein from ponceau. A trend for a main effect of genotype is observed in SERCA2a content ($p=0.0544$, $mdx > mdx/Sln^{-/-}$). All values are mean \pm standard error ($n=8$ per group).

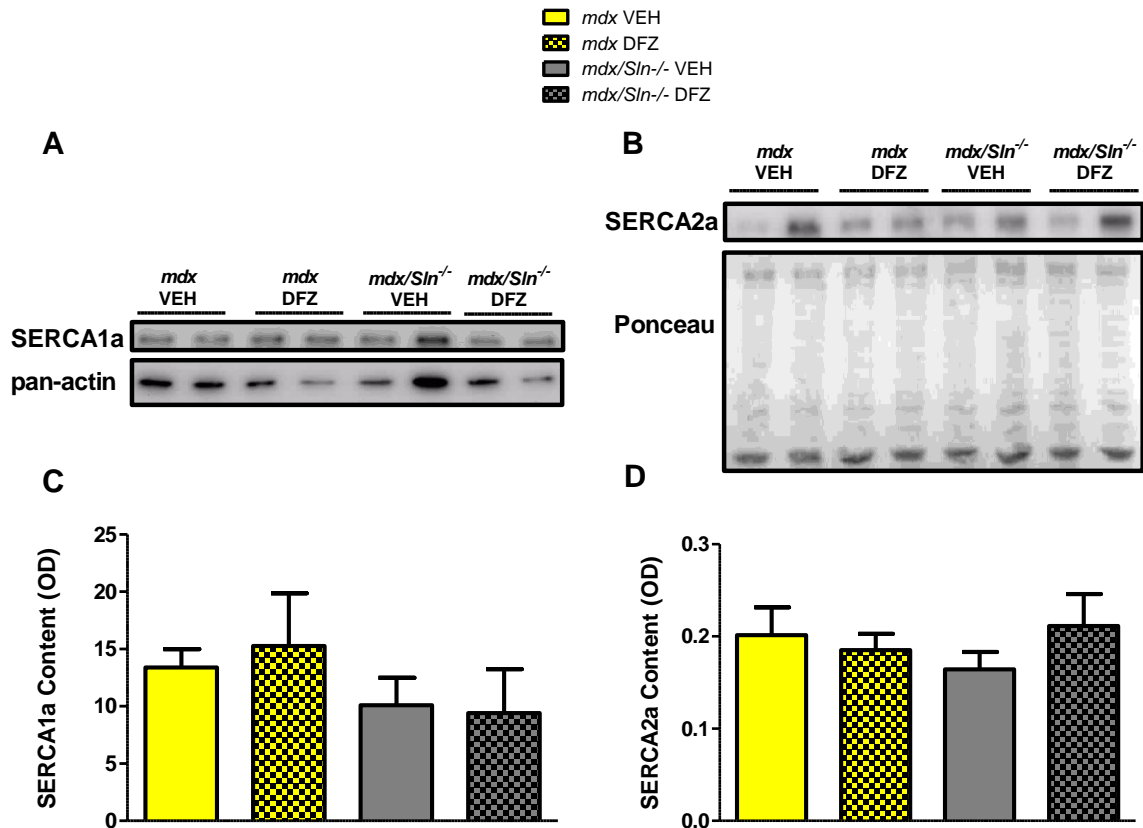


Figure 3.23: Western blot analysis of SERCA1a and SERCA2a content in DIA of *mdx* and *mdx/Sln*^{-/-} mice after treatment protocol. Representative western blots of (A) SERCA1a and (B) SERCA2a. Quantification of (C) SERCA1a content was normalized to actin and (D) SERCA2a content was normalized to total protein from ponceau stain. There is a significant genotype effect on SERCA1a content ($p=0.0174$, $mdx > mdx/Sln^{-/-}$). All values are presented as mean \pm standard error ($n=8$ per group).

In *mdx* mice, DFZ significantly increased SLN content in SOL, when examined with a one tailed paired t-test (Figure 3.24B, $p=0.0479$). A one tailed t-test was used because evidence in the literature has shown glucocorticoid treatments to increase SLN content. However, as shown in Figure 3.25B, there was no change in SLN content in the DIA after the treatment protocol ($p>0.05$). See appendix for full Western blot including samples from *mdx/Sln*^{-/-} mice.

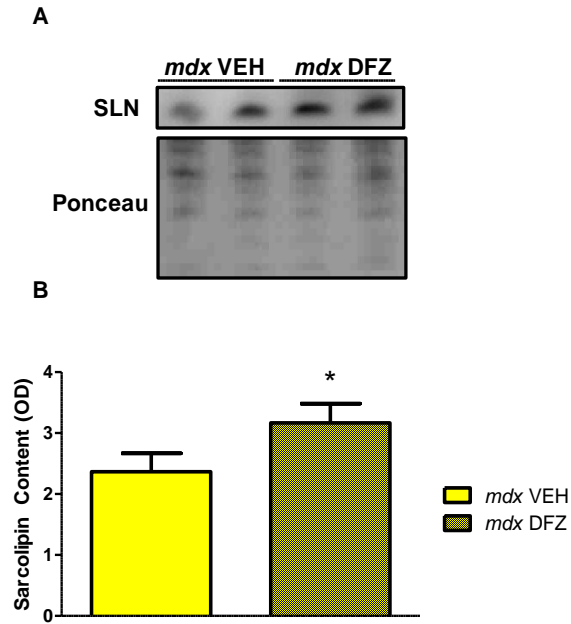


Figure 3.24: Western blot analysis of SLN content in SOL of *mdx* mice treated with VEH or DFZ. (A) A representative western of SLN in SOL. **(B)** Quantification of SLN content is normalized to total protein content from ponceau stain. All values are mean \pm standard error. * indicates a significant increase as examined by a one-tailed paired t-test (n=8 per group).

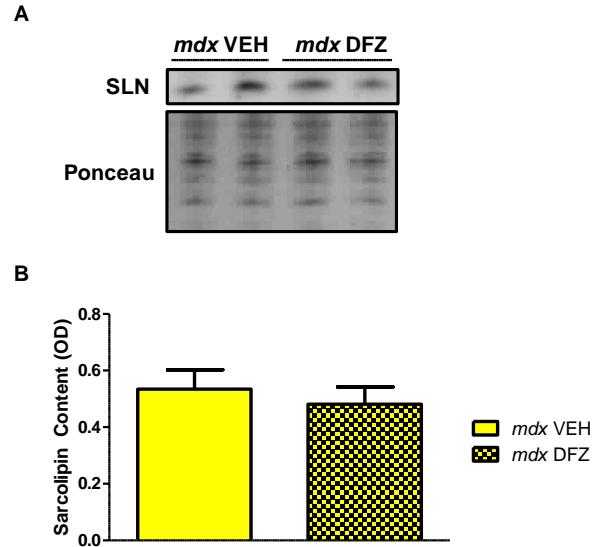


Figure 3.25: Western blot analysis of SLN content in DIA of *mdx* after treatment with VEH or DFZ. (A) Representative western blot of SLN content in *mdx* mice. **(B)** Quantification of SLN content was normalized to total protein from ponceau. All values as mean \pm standard error and were compared with a one-tail paired t-test (n=8 per group).

Discussion

The goal of this research project was to identify if the SERCA regulator, SLN, contributes to the positive effects of glucocorticoid treatment in the mouse model of Duchenne muscular dystrophy. Previous work from our lab has shown that *mdx/Sln*^{-/-} mice exhibit a worsened pathology than *mdx* mice, which was associated with blunted calcineurin/NFAT signaling [81]. Others have shown that glucocorticoids increase SLN content [80] and also activate the calcineurin/NFAT pathway in muscle [3]. Therefore, this thesis tested the hypothesis that ablation of *Sln* would result in blunted therapeutic effects of DFZ in *mdx* mice. As expected and consistent with the hypotheses DFZ improved the dystrophic phenotype of the *mdx* mice in the SOL, which was associated with increased SLN content and evidence for increased calcineurin/NFAT signaling. Despite histological improvements in the DIA, calcineurin/NFAT signaling and SLN content were not altered with DFZ. In contrast to the hypothesis, utrophin content was not altered after DFZ treatment in either SOL or DIA. Unexpectedly, *mdx/Sln*^{-/-} mice also showed histological improvements in SOL and DIA with DFZ suggesting that SLN is not required for those effects.

Western blotting of the ratio of NFATc1-p to total NFATc1 is often used as a marker of calcineurin/NFAT activation and since DFZ has been shown to stimulate this pathway, it was expected that DFZ treatment would decrease this ratio. In contrast to this hypothesis this ratio was unaltered in SOL and DIA of both *mdx* and *mdx/Sln*^{-/-} mice. Although not significant, the visual trend of this ratio increasing in the SOL was opposite to the hypothesis, and thus the colocalization of NFATc1 and DAPI was used as another method to determine NFATc1 localization. A potential reason for the conflicting Western blot data is that the rampant

immune response in DMD results in elevations in NFATc1 content from immune cells instead of muscle [147] and thus the use of colocalization of NFATc1 and DAPI within muscle fibres may provide a more valid marker of calcineurin/NFAT signaling in the myofibre. Using this technique, DFZ significantly increased colocalization of NFATc1 and DAPI in the SOL of *mdx* and *mdx/Slm^{-/-}* mice, but did not affect the DIA. The measurement of the DIA may be an underestimation of colocalization for the number of fibres analyzed. In the SOL 20 fibres are randomly selected and in the DIA only 40 fibres are analyzed. In terms of the total percentage of fibres quantified, the DIA has very little area that is evaluated compared to the SOL. This is the first study to show DFZ activates the calcineurin/NFAT pathway in *mdx* mice, as previous work only showed this in myotubes and measured only utrophin transcripts [3]. Other studies that utilized the *mdx* model have shown no difference in NFAT translocation after treatment with prednisone, the parent drug to DFZ [148]. This technique provides an improved measure of NFAT translocation compared to conventional Western blotting of total and phosphorylated NFAT and is in alignment with the study performed by St. Pierre et al. Future studies should quantify increased proportions of fibres in larger muscles, such as the DIA, to accurately determine the effect of DFZ in the DIA.

The alterations of the activation of this pathway between muscles could be a result of differential calcineurin signaling between muscles. The DIA is known to have increased calcineurin activity compared to limb muscles [149]. This difference in calcineurin signaling could be a result of a number of factors including cytosolic Ca²⁺ levels, calcineurin activity, SLN content and SERCA activity.

Glucocorticoids have been shown to increase cytosolic Ca²⁺ levels [150] and thus both genotypes may be susceptible to this first initial increase that would activate calcineurin and

downstream NFAT translocation. Furthermore, calcineurin signaling may also be altered if calcineurin content is changed. Here, calcineurin content in SOL was unaltered, while there was a trend for an interaction effect in the DIA, where *mdx/Sln*^{-/-} mice had increase calcineurin content with DFZ and *mdx* mice had a decrease in content. An increase in calcineurin content in the *mdx/Sln*^{-/-} DIA may compensate to increase calcineurin activity so that it is no different than the *mdx* mice. However, no differences in NFATc1 and DAPI localization were observed was similar in DFZ and VEH treated mice so differences in calcineurin signaling in these muscles cannot be explained by differences in calcineurin content. An upregulation of SLN was anticipated as glucocorticoids have been shown to increase SLN content in WT DIA [80] but in this experiment only the SOL experienced increased SLN content after DFZ. The extent of SLN upregulation could be limited in the DIA, due to higher basal expression of SLN in the DIA compared to SOL, as well as an overall upregulation of SLN in *mdx* mice [2]. With Western blotting the difference in basal expression was simple to see with the amount of protein necessary for detections. Only 5µg of protein had to be loaded to detect SLN in the DIA, while 12.5µg of protein had to be loaded in the SOL. With this increased basal content of SLN, there may be a limit to which SLN can be upregulated that is reached in the DIA but not yet in the SOL, and thus DFZ was able to stimulate SLN upregulation in the SOL.

In theory, the increased SLN content in *mdx* SOL may have increased $[Ca^{2+}]_i$ which could explain the apparent activation of calcineurin as indicated by an increase in colocalization of NFATc1 and DAPI. However, since SLN content is not altered and calcineurin signaling is increased in *mdx/Sln*^{-/-} mice it seems that SLN content is not required for the effects of DFZ on calcineurin signaling. It is possible that decreases in SERCA activity or content could elevate cytosolic Ca^{2+} and increase calcineurin activity in both genotypes. A

decrease in SERCA1a and SERCA2a content was expected since glucocorticoids decrease SERCA content in DIA [80], and could also increase cytosolic Ca^{2+} levels and activate calcineurin in the *mdx/Sln^{-/-}* mice. However, SERCA content of either isoform was not altered by DFZ. Although no change in SERCA content suggests that SERCA activity would be unaltered, a measurement of SERCA activity would provide better understanding of SERCA activity and potential differences between genotypes. At this moment, the underlying mechanism for increased calcineurin signaling in *mdx/Sln^{-/-}* SOL is unknown.

Collectively, these data are indicative of SLN not being involved in activating the calcineurin/NFAT pathway, as it was suggested in previous work in our laboratory [81]. It could be that an increase of SLN content in SOL was a product of upregulations of upstream factors such as myocyte enhancer factor 2 (MEF2), which is involved in muscle regeneration and is activated by the NFAT [151, 152]. However, if SLN is playing a role in activating calcineurin, compensatory adaptations in the *mdx/Sln^{-/-}* mice could not be ruled out. Upregulations of other SERCA regulators such as phospholamban (PLN), myoregulin (MLN) and DWORF [153, 154] could be a compensatory mechanism to elevate cytosolic Ca^{2+} and activate calcineurin in the *mdx/Sln^{-/-}* mice. Increased SR leak or changes to Ca^{2+} handling proteins such as the ryanodine receptor or the voltage sensing dihydropyridine receptor, could result in increased Ca^{2+} release and increased cytosolic Ca^{2+} . Additionally, store operated Ca^{2+} entry, through increase Stromal interaction molecule 1 (STIM1) content, are already elevated in *mdx* mice [155] and could have differences in expression in the *mdx/Sln^{-/-}* model. Alterations in other Ca^{2+} handling proteins in addition to SERCA regulators could provide compensatory responses in *mdx/Sln^{-/-}* mice to DFZ treatment which elevate cytosolic Ca^{2+} and activate calcineurin.

The activation of the calcineurin/NFAT pathway is known to elevate utrophin content, whether through the chronic activation of calcineurin [101, 130, 131] or through glucocorticoids [3]. However, despite activation of calcineurin/NFAT pathway in the SOL, utrophin content is unaffected by DFZ in this thesis, regardless of muscle or method of detection. One possible explanation for the lack of change in utrophin, is that overall NFAT translocation was unaffected by DFZ. In this study only NFATc1 was utilized, as its translocation is necessary in the promotion of an oxidative phenotype [31, 93, 156], but other NFAT isoforms could be essential for the upregulation of utrophin and the mitigation of a dystrophic phenotype. The utrophin A promoter has a binding site for NFAT, but it is unknown where this binding site is exclusive to NFATc1. It is plausible that other NFAT isoforms could bind to this region and alter utrophin promotion. NFATc1 to NFATc4 are all sensitive to calcineurin, and together these isoforms work in concert to bring about adaptation and regeneration of muscle, [90, 92, 93, 95, 157]. For example, NFATc2 is essential in the growth of fibres and the loss of NFATc2 results in reduced myofibre number and reduces CSA [158, 159]. SLN overexpression is shown to decrease the ratio of NFATc3-p to total NFATc3, indicating an increase in translocation of NFATc3 to the nucleus [105]. Other isoforms of NFAT were not measured in this study and thus it is unknown to what extent changes in each isoform are playing with respect to utrophin promotion. Although utrophin content is normally associated with type I fibres and myosin heavy chain I promotion is associated with NFATc1, individual knock down of NFAT isoforms 1-4 have shown blunting of the MHCI promoter [160] and thus have the potential to influence utrophin content. Future studies should examine the influence of DFZ on other NFAT isoforms and any alterations of downstream targets, such as utrophin.

This lack of utrophin upregulation is consistent with the unaltered type I and IIA fibre content. It was hypothesized that DFZ treatment would increase calcineurin activity, promoting a slow muscle phenotype (i.e. increase proportion of type I and IIA fibres), and that *mdx/Sln^{-/-}* mice would not have this same promotion. Contrary to this hypothesis, DFZ did not alter the presence of type I and IIA fibres in either muscle. This suggests that calcineurin activity was not sufficient to alter type I and IIA myosin heavy chain content. Unexpectedly, DFZ appeared to altered type IIX fibres in both the SOL and DIA muscles in both genotypes. Although calcineurin is a major regulator of fibre type [84], other fibre type regulators such as thyroid hormone [161], Ca²⁺/calmodulin-dependent kinase (CaMK) [162] and FOXO1, a member of the forkhead transcription factor forkhead box protein O family [163], also regulate fibre type transitions and alterations in these pathways could mitigate fibre type transitions. In the study that showed the calcineurin/NFAT pathway was activated by DFZ *in vivo*, myosin heavy chain distribution was never analyzed in any muscle [3] so it is unknown whether a slow muscle phenotype was promoted by DFZ. Studies that have a chronic activation of calcineurin (for example the *CnA/mdx* mice), show a significant increase in IIA fibres in skeletal muscle [101, 131], while only one study has shown that type I fibres are actually decreased after one week of glucocorticoid treatments in the SOL of *mdx* mice [148]. In that study it was suggested that glucocorticoids tried to return fibre distribution to that of healthy WT tissue. As the SOL is primarily composed of myosin heavy chains I and IIA, this decrease in MHC IIX would be consistent with a return to a normal fibre distribution. Similarly, the increase in IIX fibre content in DIA with DFZ would be consistent with a return to a normal fibre distribution, as the DIA is mainly composed of type IIA and IIX fibres [164].

The calcineurin/NFAT pathway has also been implicated in muscle fiber growth [84, 91]. It was hypothesized that DFZ treatment in *mdx* mice would have increased CSA area compared to VEH controls, and that *mdx/Sln^{-/-}* mice would not have this same increase. In contrast to the hypothesis, CSA was unaltered in both DIA and SOL of both genotypes, illustrating that DFZ had little effect on CSA. It is important to note that CSA is an unreliable measure when assessing treatment effects on dystrophic muscle but rather the variance coefficient of minimal Feret's diameter is a sensitive measure that is used for quantitative measures of muscular dystrophy to assess heterogeneity of fibre size. Unexpectedly, variability in fibre size in the SOL seemed to be elevated with DFZ in *mdx* mice, but a decrease was observed in *mdx/Sln^{-/-}* mice, while the DIA showed no difference between groups. In similar studies, fiber size variability was improved with DFZ treatment [3] but it was measured using the deviation of CSA, instead of the covariance of minimal Feret's diameter, which is more sensitive to improvements in the phenotype from therapeutic interventions [17]. A covariance value over 250 is designated as dystrophic [165] but the average values from all groups are just above this cutoff. Based on the contradictory increase in fibre size variability in *mdx* SOL with DFZ and the lack of effect in DIA, DFZ may not have such a pronounced effect on fibre size variability.

This thesis challenges whether the improvements in the dystrophic phenotype by DFZ are through the calcineurin/NFAT pathway in this time frame, as downstream targets such as utrophin content, type I and IIA fibre content and CSA area were not altered. Improvements in histological features occurred in both *mdx* and *mdx/Sln^{-/-}* SOL and DIA despite activation of this pathway only in the SOL. Consistent with the hypothesis, fibrosis and number of centrally nucleated fibres were reduced in *mdx* mice, but this benefit was also exhibited in *mdx/Sln^{-/-}*

mice, which could indicate these positive effects are through the immunosuppressive effects of glucocorticoids, instead of the activation of the calcineurin/NFAT pathway. . In DMD, repeated cycles of degeneration and regeneration of DMD results in sustained infiltration of immune cells that promotes fibrosis and increased centralized nuclei [166-169].

Glucocorticoids decrease this immune driven response by inhibiting the activity of pro-inflammatory cytokines or upregulating the expression of anti-inflammatory proteins (reviewed in [170]). Possibly DFZ has similar effects in both *mdx* and *mdx/Sln^{-/-}* mice through reducing immune driven damage, which would be independent of SLN expression. DFZ treatment improved the appearance of centralized nuclei in DIA [3], but the effects are less pronounced in the SOL [148], which in this thesis only shows a trending improvement. This may be due to the milder severity of the dystrophic phenotype in limb muscles potentially due to the decreased loading on limb muscles [19, 171, 172], compared with DIA.

Serum CK is a clinical measure of muscle breakdown. It was hypothesized that DFZ would decrease serum CK levels in the *mdx* mice, as glucocorticoids delay muscle breakdown [116, 124, 173]. In mice, CK is highly variable and thus the majority of studies in *mdx* mice concerning glucocorticoid treatment demonstrate no changes or trending decreases in CK levels [124, 174, 175]. However, in this study serum CK levels were increased by DFZ treatment compared to VEH controls in both *mdx* and *mdx/Sln^{-/-}* mice. It is unknown why CK levels were higher following DFZ treatment but duration of the treatment may play a factor. If given a longer duration treatment, serum CK levels could possibly decrease after an initial increase, but this remains to be seen.

Body weight after DFZ treatment also displays contradictory results to the literature. One of the major reported side effects of glucocorticoids in humans is weight gain [116, 175],

yet in this study, although only a trend, DFZ treated animals weighed less than the VEH group. The results here are consistent with a previous study in *mdx* mice, in which animals that were treated for 4 weeks with DFZ gained less weight than controls [124]. The length of treatment is a major difference between the animal studies and many human studies. Human DMD studies often treat patients with low dosage (<10mg/kg body weight) glucocorticoids for at least a year and typically document weight gain after 12 months of treatment [116, 128, 175]. The cause of this decreased body weight cannot be attributed to changes in muscle weight of SOL, DIA and EDL as DFZ did not alter muscle weight, although other muscles may be altered with DFZ. Instead these changes in body weight could be a result of alterations in adiposity and organ weight. Monitoring body composition via computed tomography during the course of treatment would provide better understanding in changes in body compositions that could affect overall weight.

This is the first study that examined DFZ treatment in *mdx* and *mdx/Sln^{-/-}* mice, but other work from our laboratory has examined the *mdx/Sln^{-/-}* mice at a later age (3-6 months). Basal genotype differences were observed in collagen infiltration in the DIA, serum CK, fibre type distribution and NFATc1-p to total NFATc1 ratios in the expected manner as previously shown by Fajardo et al. However, there were several unexpected differences to weight and muscle mass, centralized nuclei, fibre size variability, CSA, calcineurin signaling and utrophin content in comparison to previous examination of this line. *Mdx/Sln^{-/-}* mice were shown to have a blunted calcineurin/NFAT signaling cascade that results in a shift from slow-to-fast muscle phenotype, diminished CSA, increased fibre size variability, higher ratios of NFATc1-p to total NFATc1, and decreased utrophin content in comparison to *mdx* controls [81]. The blunting of the calcineurin/NFAT signaling was associated with a loss of SLN, likely resulting in

decreased cytosolic Ca^{2+} and a worsened muscle phenotype. These earlier observations drove a number of the hypothesis generated based on basal genotype differences, including muscle phenotype (centralized nuclei, collagen infiltration and fibre type distribution) and underlying calcineurin activity.

The most surprising difference between these studies was that *mdx/Sln*^{-/-} mice appeared to have minimal blunting of the calcineurin NFAT system as utrophin content and CSA was unaltered, although a shift from slow-to-fast fibre type distribution was exhibited. A slow-to-fast shift in fibre type was consistent with the hypothesis as the SOL exhibited increases in IIX, IIB and hybrid IIX/IIB fibres, while there were minor increases in hybrid I/IIA and IIA/IIX fibres in the DIA. This shift is consistent with a worsened pathology as type II fibres are more susceptible to damage in DMD [176], yet utrophin content and CSA was unaltered between genotypes, which could be suggestive of limited blunting of the calcineurin/NFAT system.

Interestingly and in complete contradiction to the previous study of *mdx/Sln*^{-/-} mice, centralized nuclei are not different compared to *mdx* mice in the SOL and are increased in the DIA. The increase in centralized nuclei observed in *mdx/Sln*^{-/-} DIA may be due to their age and regenerative capacity. At this time point, regeneration is ongoing and thus the appearance of centrally nucleated fibres is expected. The elevation of regenerating fibres could indicate increases in muscle breakdown, which would be consistent with a worsened pathology. In contrast, a lack of centralized nuclei in the older age group may be indicative of a failure of regeneration. It is unlikely that satellite cell pools have been exhausted at this time point, as pools remain relatively unchanged despite the progression of DMD [177, 178]. It is plausible that there is some impairment in regeneration at this time point that has not yet developed in the younger *mdx/Sln*^{-/-} mice.

Finally, body and muscle weight between the *mdx* and *mdx/Sln^{-/-}* was unexpectedly different compared to what was known in the older age group [81]. Interestingly, *mdx/Sln^{-/-}* mice were consistently larger than *mdx* mice through the treatment protocol (Appendix S1.1), though weight gain over the week was not different between genotypes. These differences in body weight between *mdx* and *mdx/Sln^{-/-}* could partly be due to larger muscle masses in *mdx/Sln^{-/-}* mice as both DIA and SOL (but not EDL) masses were greater compared to *mdx* mice. Other components of body composition, such as adiposity and muscle edema, could also influence differences in body weight between genotypes and should be investigated in future studies.

One factor that could explain these differences in pathology and anthropometrics is the age that the mice were studied at. Here, 4-5 week old mice were studied whereas in the previous study of *mdx/Sln^{-/-}* [81], mice were examined at 3-6 months of age. The age of mice for this thesis was chosen as they would be aged similarly to those used by St. Pierre and colleagues which showed that DFZ increased utrophin content through the calcineurin/NFAT pathway [122]. Although *mdx* mice have a milder phenotype in limb muscles [142], they undergo bouts of degeneration and regeneration between 3-7 weeks of age [20, 42] that is similar to human DMD patients. This chosen age puts the animals in this window of degeneration and regeneration that would allow for the effect of glucocorticoid steroids to be more correlative to human DMD. At 3-6 months of age, *mdx* mice are within a plateau period where muscle regeneration is able to mitigate disease progression [43, 164]. This thesis challenges whether improvements in the dystrophic phenotype by glucocorticoid treatments are through the calcineurin/NFAT pathway when treatment protocols are short. Given longer treatment protocols downstream targets of the calcineurin/NFAT pathway, such as utrophin,

may be improved. In addition, this study shows that SLN may not be involved in the beneficial effects of DFZ, as minimal differences between *mdx* and *mdx/Sln*^{-/-} mice were observed. However, this study provides *in vivo* evidence that DFZ does stimulate calcineurin signaling and that glucocorticoids increase SLN protein content.

This thesis challenges whether improvements in the dystrophic phenotype by glucocorticoid treatments are through the calcineurin/NFAT pathway when treatment protocols are short. Given longer treatment protocols downstream targets of the calcineurin/NFAT pathway, such as utrophin, may be improved. In addition, this study shows that SLN may not be involved in the beneficial effects of DFZ, as minimal differences between *mdx* and *mdx/Sln*^{-/-} mice were observed. However, this study provides *in vivo* evidence that DFZ does stimulate calcineurin signaling and that glucocorticoids increase SLN protein content.

In summary, although SLN content is elevated in the SOL of *mdx* mice after DFZ treatment and the calcineurin/NFAT pathway is activated, utrophin content was not altered. Despite the histological improvements, calcineurin signaling was not stimulated by DFZ in the DIA. Based on this thesis, SLN may not play a role in the positive effects of DFZ treatment.

Future Directions

In the future, I believe there is much to be done in investigating the role of SERCA regulatory proteins in the progression of DMD. Identifying the underlying mechanisms for SLN upregulation after glucocorticoid treatment may provide better understanding of the role of SLN in disease treatment. Despite a measurement of SERCA content, SERCA activity was not measured in this study, and therefore it is unknown whether SERCA uptake is further

impaired by the increased SLN content after DFZ treatment. In unpublished data from Fajardo et al., maximal SERCA activity is not different between *mdx* and *mdx/Sln^{-/-}* mice [4]. A measure of SERCA activity and Ca²⁺ uptake would provide better understanding of SERCA function and Ca²⁺ levels in the dystrophic muscle after treatment. Techniques already implement in this laboratory could be utilized in future studies [81, 140]. Along the same line, a major limitation of this thesis is the lack of intracellular Ca²⁺ measurement that would provide sufficient evidence to show that SLN can increase cytosolic Ca²⁺ that would then activate calcineurin and downstream signaling. It is assumed that an upregulation of SLN and corresponding inhibition of SERCA would elevate cytosolic Ca²⁺ that would then activate calcineurin. Intracellular measures of Ca²⁺ have been performed and quantified previously in *mdx* isolated single fibres using Indo-1, a Ca²⁺-fluorescent dye that is able to assess both resting Ca²⁺ and Ca²⁺ dynamics during depolarization [179].

This thesis also defines calcineurin activity solely through NFATc1 translocation, but other NFAT isoforms, namely NFATc2-c4 are sensitive to calcineurin [90, 92, 93, 158]. NFATc1 was chosen for its promotion of an oxidative phenotype [90, 96, 97], yet *Sln^{OE}* mice which have a shift to an oxidative phenotype, have an increase NFATc3 translocation [105]. NFATc3 is involved with myoblast differentiation in synergy with STIM1 [180] and is responsive to over expression of SLN [105]. Other isoforms of NFAT may also affect muscle phenotype. NFATc2, for example, is involved with myoblast fusion and muscle growth; ablation of it results in decrease CSA and muscle fusion [158]. It was suggested that NFATc2 and NFATc3 may aim to preserve muscle mass as part of a stress-response mechanism [181]. Given that, translocation of other NFAT isoforms may better identify differences between treatment effects in *mdx* and *mdx/Sln^{-/-}* mice. Future studies should examine the effect of *Sln*-

ablation in all NFAT isoforms, as they direct different aspects of muscle growth, development and adaptation.

Finally, given the limited effect of DFZ in activating the calcineurin/NFAT pathway, treatment durations should be lengthened to fully identify if DFZ can stimulate this pathway and increase utrophin content. As described earlier, treatment with glucocorticoids in human DMD patients is much longer [116, 175], thus 7 days of DFZ treatment may not be sufficient to fully activate calcineurin/NFAT signaling. St. Pierre et al., utilized a varying lengths of treatments (1-4 weeks), where animals were given DFZ or a VEH once every other day [3]. After one week, histological benefits (centralized nuclei and fibre size variability), while increases utrophin A mRNA took approximately 8 days [3]. Time-release pellets of DFZ or prednisolone, a water soluble form of prednisone, could be used for longer durations in place of injections.

Conclusions

The results obtained from this thesis provide further evidence that DFZ stimulates calcineurin activity in *mdx* mice. This thesis compared the treatment effects of DFZ in both *mdx* and *mdx/Sln^{-/-}* mice, as DFZ is shown to increase calcineurin activity which has been shown to mitigate the dystrophic phenotype through the promotion of utrophin [3]. Glucocorticoids have been shown to increase SLN content [80] and *mdx* mice already have an intrinsic upregulation of SLN [2] potentially functioning to activate the calcineurin/NFAT pathway. Given that *mdx/Sln^{-/-}* mice that already have blunted calcineurin/NFAT signaling, it

was hypothesized that *mdx/Slm*^{-/-} treated mice would not show the same improvements as the treated *mdx* mice.

This study demonstrates that DFZ improves some of the histological features of the dystrophic phenotype, namely centralized nuclei and collagen infiltration. The hypothesized fast-to-slow fibre type transition and decrease in fibre size variability by DFZ was not observed in either muscle examined. DFZ did stimulate calcineurin activity in both *mdx* and *mdx/Slm*^{-/-} mice but downstream utrophin content was not altered. SERCA content was not altered in either genotype by the treatment, but potential elevations in cytosolic Ca²⁺ could be a result of increased SLN content by DFZ in the SOL. At this point, the data does not support the view that SLN is involved with the positive effects of DFZ treatment, as both *mdx* and *mdx/Slm*^{-/-} mice have improvements in the dystrophic phenotype and activation of the calcineurin/NFAT cascade. Given that the treatment protocol was for a short duration, the positive effects seen here may be a result of an immunosuppressive effect of DFZ. Given more time, improvements in the calcineurin/NFAT pathway and other adaptive responses could be observed.

References

1. Berchtold, M.W., H. Brinkmeier, and M. Muntener, *Calcium ion in skeletal muscle: its crucial role for muscle function, plasticity, and disease*. *Physiol Rev*, 2000. **80**(3): p. 1215-65.
2. Schneider, J.S., et al., *Increased sarcolipin expression and decreased sarco(endo)plasmic reticulum Ca²⁺ uptake in skeletal muscles of mouse models of Duchenne muscular dystrophy*. *J Muscle Res Cell Motil*, 2013. **34**(5-6): p. 349-56.
3. St-Pierre, S.J., et al., *Glucocorticoid treatment alleviates dystrophic myofiber pathology by activation of the calcineurin/NF-AT pathway*. *Faseb j*, 2004. **18**(15): p. 1937-9.
4. Fajardo, V.A., et al., *Sarcolipin deletion in mdx mice impairs calcineurin signalling and worsens dystrophic pathology*. 2017: *Human Molecular Genetics*. p. 18.
5. Emery, A.E.H., *The muscular dystrophies*. *The Lancet*, 2002. **359**(9307): p. 687-695.
6. Hoffman, E.P., R.H. Brown, Jr., and L.M. Kunkel, *Dystrophin: the protein product of the Duchenne muscular dystrophy locus*. *Cell*, 1987. **51**(6): p. 919-28.
7. Emery, A., *Duchenne muscular dystrophy or Meryon's disease*. *The Lancet*, 2001. **357**(9267): p. 1529.
8. Eagle, M., et al., *Survival in Duchenne muscular dystrophy: improvements in life expectancy since 1967 and the impact of home nocturnal ventilation*. *Neuromuscul Disord*, 2002. **12**(10): p. 926-9.
9. Spurney, C.F., *Cardiomyopathy of Duchenne muscular dystrophy: current understanding and future directions*. *Muscle Nerve*, 2011. **44**(1): p. 8-19.
10. Ray, P.N., et al., *Cloning of the breakpoint of an X;21 translocation associated with Duchenne muscular dystrophy*. *Nature*, 1985. **318**(6047): p. 672-5.
11. Cooper, S.T. and S.I. Head, *Membrane Injury and Repair in the Muscular Dystrophies*. *Neuroscientist*, 2015. **21**(6): p. 653-68.
12. Allen, D.G. and N.P. Whitehead, *Duchenne muscular dystrophy--what causes the increased membrane permeability in skeletal muscle?* *Int J Biochem Cell Biol*, 2011. **43**(3): p. 290-4.
13. Ervasti, J.M., *Dystrophin, its interactions with other proteins, and implications for muscular dystrophy*. *Biochimica et Biophysica Acta (BBA) - Molecular Basis of Disease*, 2007. **1772**(2): p. 108-117.
14. Petrof, B.J., et al., *Dystrophin protects the sarcolemma from stresses developed during muscle contraction*. *Proc Natl Acad Sci U S A*, 1993. **90**(8): p. 3710-4.
15. Glass, D.J., *Signaling pathways perturbing muscle mass*. *Curr Opin Clin Nutr Metab Care*, 2010. **13**.
16. Bulfield, G., Siller, WG., Wight, PAL., Moore, K., *X chromosome-linked muscular dystrophy (mdx) in the mouse*. *Proc. Nati. Acad. Sci. USA*, 1983. **81**(February): p. 1189-1192.
17. Briguët, A., et al., *Histological parameters for the quantitative assessment of muscular dystrophy in the mdx-mouse*. *Neuromuscul Disord*, 2004. **14**(10): p. 675-82.
18. Marshall, P.A., P.E. Williams, and G. Goldspink, *Accumulation of collagen and altered fiber-type ratios as indicators of abnormal muscle gene expression in the mdx dystrophic mouse*. *Muscle Nerve*, 1989. **12**(7): p. 528-37.
19. Bell, C.D. and P.E. Conen, *Histopathological changes in Duchenne muscular dystrophy*. *J Neurol Sci*, 1968. **7**(3): p. 529-44.

20. Carnwath, J.W. and D.M. Shotton, *Muscular dystrophy in the mdx mouse: histopathology of the soleus and extensor digitorum longus muscles*. J Neurol Sci, 1987. **80**(1): p. 39-54.
21. Torres, L.F. and L.W. Duchen, *The mutant mdx: inherited myopathy in the mouse. Morphological studies of nerves, muscles and end-plates*. Brain, 1987. **110 (Pt 2)**: p. 269-99.
22. Deconinck, N., et al., *Consequences of the combined deficiency in dystrophin and utrophin on the mechanical properties and myosin composition of some limb and respiratory muscles of the mouse*. Neuromuscul Disord, 1998. **8**(6): p. 362-70.
23. McDonald, A.A., et al., *Disease course in mdx:utrophin+/- mice: comparison of three mouse models of Duchenne muscular dystrophy*. Physiol Rep, 2015. **3**(4).
24. Tinsley, J., et al., *Expression of full-length utrophin prevents muscular dystrophy in mdx mice*. Nat Med, 1998. **4**(12): p. 1441-4.
25. Campanelli, J.T., et al., *A role for dystrophin-associated glycoproteins and utrophin in agrin-induced AChR clustering*. Cell, 1994. **77**(5): p. 663-74.
26. Gramolini, A.O., J. Wu, and B.J. Jasmin, *Regulation and functional significance of utrophin expression at the mammalian neuromuscular synapse*. Microsc Res Tech, 2000. **49**(1): p. 90-100.
27. Takemitsu, M., et al., *Dystrophin-related protein in the fetal and denervated skeletal muscles of normal and mdx mice*. Biochem Biophys Res Commun, 1991. **180**(3): p. 1179-86.
28. Helliwell, T.R., et al., *The dystrophin-related protein, utrophin, is expressed on the sarcolemma of regenerating human skeletal muscle fibres in dystrophies and inflammatory myopathies*. Neuromuscul Disord, 1992. **2**(3): p. 177-84.
29. Fardeau, M., et al., *[Presence of dystrophine-like protein at the neuromuscular junction in Duchenne muscular dystrophy and in "mdx" mutant mice]*. C R Acad Sci III, 1990. **311**(5): p. 197-204.
30. Blake, D.J., J.M. Tinsley, and K.E. Davies, *Utrophin: a structural and functional comparison to dystrophin*. Brain Pathol, 1996. **6**(1): p. 37-47.
31. Chakkalakal, J.V., et al., *Expression of utrophin A mRNA correlates with the oxidative capacity of skeletal muscle fiber types and is regulated by calcineurin/NFAT signaling*. Proc Natl Acad Sci U S A, 2003. **100**(13): p. 7791-6.
32. Pasquini, F., et al., *The effect of glucocorticoids on the accumulation of utrophin by cultured normal and dystrophic human skeletal muscle satellite cells*. Neuromuscul Disord, 1995. **5**(2): p. 105-14.
33. Passaquin, A.C., P. Lhote, and U.T. Ruegg, *Calcium influx inhibition by steroids and analogs in C2C12 skeletal muscle cells*. Br J Pharmacol, 1998. **124**(8): p. 1751-9.
34. Karpati, G., et al., *Localization and quantitation of the chromosome 6-encoded dystrophin-related protein in normal and pathological human muscle*. J Neuropathol Exp Neurol, 1993. **52**(2): p. 119-28.
35. Tinsley, J.M., et al., *Amelioration of the dystrophic phenotype of mdx mice using a truncated utrophin transgene*. Nature, 1996. **384**(6607): p. 349-53.
36. Jasmin, B.J., et al., *Multiple regulatory events controlling the expression and localization of utrophin in skeletal muscle fibers: insights into a therapeutic strategy for Duchenne muscular dystrophy*. J Physiol Paris, 2002. **96**(1-2): p. 31-42.

37. Matsumura, K., et al., *Association of dystrophin-related protein with dystrophin-associated proteins in mdx mouse muscle*. Nature, 1992. **360**(6404): p. 588-91.
38. Balaban, B., et al., *Corticosteroid treatment and functional improvement in Duchenne muscular dystrophy: long-term effect*. Am J Phys Med Rehabil, 2005. **84**(11): p. 843-50.
39. DiMario, J., et al., *Fibroblast Growth Factor in the Extracellular Matrix of Dystrophic (mdx) Mouse Muscle*. Science, 1989. **244**(4905): p. 688-690.
40. Head, S.I., *Branched fibres in old dystrophic mdx muscle are associated with mechanical weakening of the sarcolemma, abnormal Ca²⁺ transients and a breakdown of Ca²⁺ homeostasis during fatigue*. Exp Physiol, 2010. **95**(5): p. 641-56.
41. Williams, M.S. and J. Kwon, *T cell receptor stimulation, reactive oxygen species, and cell signaling*. Free Radic Biol Med, 2004. **37**(8): p. 1144-51.
42. Coulton, G.R., et al., *The mdx mouse skeletal muscle myopathy: I. A histological, morphometric and biochemical investigation*. Neuropathol Appl Neurobiol, 1988. **14**(1): p. 53-70.
43. Coirault, C., et al., *Severe muscle dysfunction precedes collagen tissue proliferation in mdx mouse diaphragm*. J Appl Physiol (1985), 2003. **94**(5): p. 1744-50.
44. Lynch, G.S., et al., *Contractile properties of diaphragm muscle segments from old mdx and old transgenic mdx mice*. Am J Physiol, 1997. **272**(6 Pt 1): p. C2063-8.
45. Chamberlain, J.S., et al., *Dystrophin-deficient mdx mice display a reduced life span and are susceptible to spontaneous rhabdomyosarcoma*. Faseb j, 2007. **21**(9): p. 2195-204.
46. Whitehead, N.P., E.W. Yeung, and D.G. Allen, *Muscle damage in mdx (dystrophic) mice: role of calcium and reactive oxygen species*. Clin Exp Pharmacol Physiol, 2006. **33**(7): p. 657-62.
47. Culligan, K. and K. Ohlendieck, *Abnormal Calcium Handling in Muscular Dystrophy*. Basic Appl Myol, 2002. **12**(4): p. 147-157.
48. Allen, D.G., et al., *Calcium and the damage pathways in muscular dystrophy*. Can J Physiol Pharmacol, 2010. **88**(2): p. 83-91.
49. Alderton, J.M. and R.A. Steinhardt, *How Calcium Influx through Calcium Leak Channels Is Responsible for the Elevated Levels of Calcium-dependent Proteolysis in Dystrophic Myotubes*. Trends in Cardiovascular Medicine, 2000. **10**(6): p. 268-272.
50. Turner, P.R., et al., *Increased protein degradation results from elevated free calcium levels found in muscle from mdx mice*. Nature, 1988. **335**(6192): p. 735-8.
51. Robert, V., et al., *Alteration in calcium handling at the subcellular level in mdx myotubes*. J Biol Chem, 2001. **276**(7): p. 4647-51.
52. Bonuccelli, G., et al., *Proteasome inhibitor (MG-132) treatment of mdx mice rescues the expression and membrane localization of dystrophin and dystrophin-associated proteins*. Am J Pathol, 2003. **163**(4): p. 1663-75.
53. Sandri, M., et al., *Caspase 3 expression correlates with skeletal muscle apoptosis in Duchenne and facioscapulo human muscular dystrophy. A potential target for pharmacological treatment?* J Neuropathol Exp Neurol, 2001. **60**(3): p. 302-12.
54. Badalamente, M.A. and A. Stracher, *Delay of muscle degeneration and necrosis in mdx mice by calpain inhibition*. Muscle Nerve, 2000. **23**(1): p. 106-11.
55. Toyoshima, C., et al., *Crystal structures of the calcium pump and sarcolipin in the Mg²⁺-bound E1 state*. Nature, 2013. **495**(7440): p. 260-4.

56. Tupling, A.R., et al., *HSP70 binds to the fast-twitch skeletal muscle sarco(endo)plasmic reticulum Ca²⁺-ATPase (SERCA1a) and prevents thermal inactivation*. J Biol Chem, 2004. **279**(50): p. 52382-9.
57. Asahi, M., et al., *Regulation of sarco(endo)plasmic reticulum Ca²⁺ adenosine triphosphatase by phospholamban and sarcolipin: implication for cardiac hypertrophy and failure*. Trends Cardiovasc Med, 2003. **13**(4): p. 152-7.
58. Wu, X. and D.M. Bers, *Sarcoplasmic Reticulum and Nuclear Envelope Are One Highly Interconnected Ca²⁺Store Throughout Cardiac Myocyte*. Circulation Research, 2006. **99**(3): p. 283-291.
59. Fajardo, V.A., et al., *Co-expression of SERCA isoforms, phospholamban and sarcolipin in human skeletal muscle fibers*. PLoS One, 2013. **8**(12): p. e84304.
60. Lafoux, A., et al., *Diaphragm tension reduced in dystrophic mice by an oxidant, hypochlorous acid*. Can J Physiol Pharmacol, 2010. **88**(2): p. 130-40.
61. Dremina, E.S., et al., *Oxidation and inactivation of SERCA by selective reaction of cysteine residues with amino acid peroxides*. Chem Res Toxicol, 2007. **20**(10): p. 1462-9.
62. Divet, A. and C. Huchet-Cadiou, *Sarcoplasmic reticulum function in slow- and fast-twitch skeletal muscles from mdx mice*. Pflugers Arch, 2002. **444**(5): p. 634-43.
63. Kargacin, M.E. and G.J. Kargacin, *The sarcoplasmic reticulum calcium pump is functionally altered in dystrophic muscle*. Biochim Biophys Acta, 1996. **1290**(1): p. 4-8.
64. Mazala, D.A., et al., *SERCA1 overexpression minimizes skeletal muscle damage in dystrophic mouse models*. Am J Physiol Cell Physiol, 2015. **308**(9): p. C699-709.
65. Goonasekera, S.A., et al., *Mitigation of muscular dystrophy in mice by SERCA overexpression in skeletal muscle*. J Clin Invest, 2011. **121**(3): p. 1044-52.
66. Gehrig, S.M., et al., *Hsp72 preserves muscle function and slows progression of severe muscular dystrophy*. Nature, 2012. **484**(7394): p. 394-8.
67. Dremina, E.S., V.S. Sharov, and C. Schoneich, *Heat-shock proteins attenuate SERCA inactivation by the anti-apoptotic protein Bcl-2: possible implications for the ER Ca²⁺-mediated apoptosis*. Biochem J, 2012. **444**(1): p. 127-39.
68. Smith, W.S., et al., *Sarcolipin uncouples hydrolysis of ATP from accumulation of Ca²⁺ by the Ca²⁺-ATPase of skeletal-muscle sarcoplasmic reticulum*. Biochemical Journal, 2002. **361**(2): p. 277-286.
69. MacLennan, D., et al., *The Mechanism of Muscle Contraction*. 1972.
70. Shaikh, S.A., S.K. Sahoo, and M. Periasamy, *Phospholamban and sarcolipin: Are they functionally redundant or distinct regulators of the Sarco(Endo)Plasmic Reticulum Calcium ATPase?* J Mol Cell Cardiol, 2016. **91**: p. 81-91.
71. Periasamy, M. and A. Kalyanasundaram, *SERCA pump isoforms: their role in calcium transport and disease*. Muscle Nerve, 2007. **35**(4): p. 430-42.
72. Gorski, P.A., et al., *Sarco(endo)plasmic reticulum calcium ATPase (SERCA) inhibition by sarcolipin is encoded in its luminal tail*. J Biol Chem, 2013. **288**(12): p. 8456-67.
73. Wawrzynow, A., et al., *Sarcolipin, the "proteolipid" of skeletal muscle sarcoplasmic reticulum, is a unique, amphipathic, 31-residue peptide*. Arch Biochem Biophys, 1992. **298**(2): p. 620-3.
74. Bal, N.C., et al., *Sarcolipin is a newly identified regulator of muscle-based thermogenesis in mammals*. Nat Med, 2012. **18**(10): p. 1575-9.

75. Tupling, A.R., et al., *Enhanced Ca²⁺ transport and muscle relaxation in skeletal muscle from sarcolipin-null mice*. *Am J Physiol Cell Physiol*, 2011. **301**: p. C841-C849.
76. Bombardier, E., et al., *Ablation of sarcolipin decreases the energy requirements for Ca²⁺ transport by sarco(endo)plasmic reticulum Ca²⁺-ATPases in resting skeletal muscle*. *FEBS Lett*, 2013. **587**(11): p. 1687-92.
77. Fajardo, V.A., et al., *Phospholamban overexpression in mice causes a centronuclear myopathy-like phenotype*. *Disease Models and Mechanisms*, 2015.
78. Ottenheijm, C.A.C., et al., *Sarcoplasmic reticulum calcium uptake and speed of relaxation are depressed in nebulin-free skeletal muscle*. *Faseb j*, 2008. **22**(8): p. 2912-9.
79. Nakagawa, O., et al., *Centronuclear myopathy in mice lacking a novel muscle-specific protein kinase transcriptionally regulated by MEF2*. *Genes Dev*, 2005. **19**(17): p. 2066-77.
80. Gayan-Ramirez, G., et al., *Corticosteroids decrease mRNA levels of SERCA pumps, whereas they increase sarcolipin mRNA in the rat diaphragm*. *J Physiol*, 2000. **524 Pt 2**: p. 387-97.
81. Fajardo, V.A., *The Role of Phospholamban and Sarcolipin in Skeletal Muscle Disease in Kinesiology*. 2015, University of Waterloo: Waterloo, Ontario, Canada p. 198.
82. Dolmetsch, R.E., et al., *Differential activation of transcription factors induced by Ca²⁺ response amplitude and duration*. *Nature*, 1997. **386**(6627): p. 855-8.
83. Flanagan, W.M., et al., *Nuclear association of a T-cell transcription factor blocked by FK-506 and cyclosporin A*. *Nature*, 1991. **352**(6338): p. 803-7.
84. Chin, E.R., et al., *A calcineurin-dependent transcriptional pathway controls skeletal muscle fiber type*. *Genes Dev*, 1998. **12**(16): p. 2499-509.
85. Stemmer, P.M. and C.B. Klee, *Dual calcium ion regulation of calcineurin by calmodulin and calcineurin B*. *Biochemistry*, 1994. **33**(22): p. 6859-66.
86. Klee, C.B., T.H. Crouch, and M.H. Krinks, *Calcineurin: a calcium- and calmodulin-binding protein of the nervous system*. *Proc Natl Acad Sci U S A*, 1979. **76**(12): p. 6270-3.
87. Steinbach, W.J., et al., *Harnessing calcineurin as a novel anti-infective agent against invasive fungal infections*. *Nat Rev Micro*, 2007. **5**(6): p. 418-430.
88. Yu, S.J., Y.L. Chang, and Y.L. Chen, *Calcineurin signaling: lessons from Candida species*. *FEMS Yeast Res*, 2015. **15**(4): p. fov016.
89. Horsley, V. and G.K. Pavlath, *NFAT: ubiquitous regulator of cell differentiation and adaptation*. *J Cell Biol*, 2002. **156**(5): p. 771-4.
90. Olson, E.N. and R.S. Williams, *Calcineurin Signalling and Muscle Remodeling*. *Cell* 2000. **101**: p. 689-692.
91. Dunn, S.E., E.R. Chin, and R.N. Michel, *Matching of calcineurin activity to upstream effectors is critical for skeletal muscle fiber growth*. *J Cell Biol*, 2000. **151**(3): p. 663-72.
92. Musaro, A., et al., *IGF-1 induces skeletal myocyte hypertrophy through calcineurin in association with GATA-2 and NF-ATc1*. *Nature*, 1999. **400**(6744): p. 581-5.
93. Ehlers, M.L., B. Celona, and B.L. Black, *NFATc1 controls skeletal muscle fiber type and is a negative regulator of MyoD activity*. *Cell Rep*, 2014. **8**(6): p. 1639-48.

94. Clipstone, N.A. and G.R. Crabtree, *Identification of calcineurin as a key signalling enzyme in T-lymphocyte activation*. Nature, 1992. **357**(6380): p. 695-7.
95. Olson, E.N. and R.S. Williams, *Remodeling Muscles with Calcineurin*. BioEssays, 2000. **22**: p. 510-519.
96. Serrano, A.L., et al., *Calcineurin controls nerve activity-dependent specification of slow skeletal muscle fibers but not muscle growth*. Proc Natl Acad Sci U S A, 2001. **98**(23): p. 13108-13.
97. Schiaffino, S. and C. Reggiani, *Fiber types in mammalian skeletal muscles*. Physiol Rev, 2011. **91**(4): p. 1447-531.
98. Shen, T., et al., *Regulation of the nuclear export of the transcription factor NFATc1 by protein kinases after slow fibre type electrical stimulation of adult mouse skeletal muscle fibres*. J Physiol, 2007. **579**(Pt 2): p. 535-51.
99. Liu, W., et al., *Calcineurin-NFAT Signaling and Neurotrophins Control Transformation of Myosin Heavy Chain Isoforms in Rat Soleus Muscle in Response to Aerobic Treadmill Training*. J Sports Sci Med, 2014. **13**(4): p. 934-44.
100. Tothova, J., et al., *NFATc1 nucleocytoplasmic shuttling is controlled by nerve activity in skeletal muscle*. J Cell Sci, 2006. **119**(Pt 8): p. 1604-11.
101. Chakkalakal, J.V., et al., *Stimulation of calcineurin signaling attenuates the dystrophic pathology in mdx mice*. Hum Mol Genet, 2004. **13**(4): p. 379-88.
102. Chin, E., *Intracellular Calcium Signaling in Skeletal Muscle: Decoding a Complex message*. Exerc. Sport Sci. Rev., 2010. **38**(2): p. 76-85.
103. Fajardo, V.A., et al., *Sarcolipin deletion exacerbates soleus muscle atrophy and weakness in phospholamban overexpressing mice*. PLoS One, 2017. **12**(3): p. e0173708.
104. Fajardo, V.A., et al., *Effects of sarcolipin deletion on skeletal muscle adaptive responses to functional overload and unload*. Am J Physiol Cell Physiol, 2017: p. ajpcell.00291.2016.
105. Maurya, S.K., et al., *Sarcolipin Is a Key Determinant of the Basal Metabolic Rate, and Its Overexpression Enhances Energy Expenditure and Resistance against Diet-induced Obesity*. J Biol Chem, 2015. **290**(17): p. 10840-9.
106. Eagle, M., et al., *Managing Duchenne muscular dystrophy--the additive effect of spinal surgery and home nocturnal ventilation in improving survival*. Neuromuscul Disord, 2007. **17**(6): p. 470-5.
107. Robinson-Hamm, J.N. and C.A. Gersbach, *Gene therapies that restore dystrophin expression for the treatment of Duchenne muscular dystrophy*. Human Genetics, 2016. **135**(9): p. 1029-1040.
108. Ousterout, D.G., et al., *Multiplex CRISPR/Cas9-Based Genome Editing for Correction of Dystrophin Mutations that Cause Duchenne Muscular Dystrophy*. Nat Commun, 2015. **6**: p. 6244.
109. Long, C., et al., *Prevention of muscular dystrophy in mice by CRISPR/Cas9-mediated editing of germline DNA*. Science, 2014. **345**(6201): p. 1184-8.
110. Bushby, K., et al., *Report on the 124th ENMC International Workshop. Treatment of Duchenne muscular dystrophy; defining the gold standards of management in the use of corticosteroids. 2-4 April 2004, Naarden, The Netherlands*. Neuromuscul Disord, 2004. **14**(8-9): p. 526-34.

111. Oakley, R.H. and J.A. Cidlowski, *The Biology of the Glucocorticoid Receptor: New Signaling Mechanisms in Health and Disease*. J Allergy Clin Immunol, 2013. **132**(5): p. 1033-44.
112. Braun, T.P. and D.L. Marks, *The regulation of muscle mass by endogenous glucocorticoids*. Frontiers in Physiology, 2015. **6**(12).
113. Dittmar, K.D., et al., *The role of DnaJ-like proteins in glucocorticoid receptor.hsp90 heterocomplex assembly by the reconstituted hsp90.p60.hsp70 foldosome complex*. J Biol Chem, 1998. **273**(13): p. 7358-66.
114. Dittmar, K.D., et al., *Folding of the glucocorticoid receptor by the heat shock protein (hsp) 90-based chaperone machinery. The role of p23 is to stabilize receptor.hsp90 heterocomplexes formed by hsp90.p60.hsp70*. J Biol Chem, 1997. **272**(34): p. 21213-20.
115. Smoak, K.A. and J.A. Cidlowski, *Mechanisms of glucocorticoid receptor signaling during inflammation*. Mechanisms of Ageing and Development, 2004. **125**(10): p. 697-706.
116. Drachman, D.B., K.V. Toyka, and E. Myer, *Prednisone in Duchenne muscular dystrophy*. Lancet, 1974. **2**(7894): p. 1409-12.
117. DeSilva, S., et al., *Prednisone treatment in Duchenne muscular dystrophy. Long-term benefit*. Arch Neurol, 1987. **44**(8): p. 818-22.
118. Manzur, A.Y., et al., *Glucocorticoid corticosteroids for Duchenne muscular dystrophy*. Cochrane Database Syst Rev, 2004(2): p. Cd003725.
119. Matthews, E., et al., *Corticosteroids for the treatment of Duchenne muscular dystrophy*. Cochrane Database Syst Rev, 2016(5): p. Cd003725.
120. Kim, S., et al., *Corticosteroid Treatments in Males With Duchenne Muscular Dystrophy: Treatment Duration and Time to Loss of Ambulation*. J Child Neurol, 2015. **30**(10): p. 1275-80.
121. Angelini, C., *The role of corticosteroids in muscular dystrophy: a critical appraisal*. Muscle Nerve, 2007. **36**.
122. Mesa, L.E., et al., *Steroids in duchenne muscular dystrophy — Deflazacort trial*. Neuromuscular Disorders, 1991. **1**(4): p. 261-266.
123. Archer, J.D., C.C. Vargas, and J.E. Anderson, *Persistent and improved functional gain in mdx dystrophic mice after treatment with L-arginine and deflazacort*. Faseb j, 2006. **20**(6): p. 738-40.
124. Anderson, J.E., M. Weber, and C. Vargas, *Deflazacort increases laminin expression and myogenic repair, and induces early persistent functional gain in mdx mouse muscular dystrophy*. Cell Transplant, 2000. **9**(4): p. 551-64.
125. Nayak, S. and B. Acharjya, *DEFLAZACORT VERSUS OTHER GLUCOCORTICOIDS: A COMPARISON*. Indian J Dermatol, 2008. **53**(4): p. 167-70.
126. Mc, A.L., et al., *The Canadian experience with long term deflazacort treatment in Duchenne muscular dystrophy*. Acta Myol, 2012. **31**(1): p. 16-20.
127. Houde, S., et al., *Deflazacort use in Duchenne muscular dystrophy: an 8-year follow-up*. Pediatr Neurol, 2008. **38**(3): p. 200-6.
128. Wong, B.L., et al., *Long-Term Outcome of Interdisciplinary Management of Patients with Duchenne Muscular Dystrophy Receiving Daily Glucocorticoid Treatment*. The Journal of Pediatrics, 2017. **182**: p. 296-303.e1.

129. Courdier-Fruh, I., et al., *Glucocorticoid-mediated regulation of utrophin levels in human muscle fibers*. Neuromuscul Disord, 2002. **12 Suppl 1**: p. S95-104.
130. Stupka, N., et al., *Activated calcineurin ameliorates contraction-induced injury to skeletal muscles of mdx dystrophic mice*. J Physiol, 2006. **575**(Pt 2): p. 645-56.
131. Stupka, N., et al., *Stimulation of calcineurin Aalpha activity attenuates muscle pathophysiology in mdx dystrophic mice*. Am J Physiol Regul Integr Comp Physiol, 2008. **294**(3): p. R983-92.
132. Chakkalakal, J.V., et al., *Targeted inhibition of Ca²⁺ /calmodulin signaling exacerbates the dystrophic phenotype in mdx mouse muscle*. Hum Mol Genet, 2006. **15**(9): p. 1423-35.
133. Stupka, N., et al., *The calcineurin signal transduction pathway is essential for successful muscle regeneration in mdx dystrophic mice*. Acta Neuropathologica, 2004. **107**(4): p. 299-310.
134. Morrison-Nozik, A., et al., *Glucocorticoids enhance muscle endurance and ameliorate Duchenne muscular dystrophy through a defined metabolic program*. 2015. **112**(49): p. E6780-9.
135. Bello, L., et al., *Prednisone/prednisolone and deflazacort regimens in the CINRG Duchenne Natural History Study*. Neurology, 2015. **85**(12): p. 1048-55.
136. Hasselgren, P.O., *Glucocorticoids and muscle catabolism*. Curr Opin Clin Nutr Metab Care, 1999. **2**(3): p. 201-5.
137. Hasselgren, P.O., et al., *Corticosteroids and muscle wasting: role of transcription factors, nuclear cofactors, and hyperacetylation*. Curr Opin Clin Nutr Metab Care, 2010. **13**(4): p. 423-8.
138. Schakman, O., et al., *Mechanisms of muscle atrophy induced by glucocorticoids*. Horm Res, 2009. **72**.
139. Schakman, O., et al., *Glucocorticoid-induced skeletal muscle atrophy*. The International Journal of Biochemistry & Cell Biology, 2013. **45**(10): p. 2163-2172.
140. Bombardier, E., *The Role of Sarcolipin in Calcium Handling and Obesity*, in *Kinesiology*. 2010, University of Waterloo: Waterloo. p. 165.
141. Vangheluwe, P., et al., *Sarcolipin and phospholamban mRNA and protein expression in cardiac and skeletal muscle of different species*. Biochem J, 2005. **389**(Pt 1): p. 151-9.
142. Stedman, H.H., et al., *The mdx mouse diaphragm reproduces the degenerative changes of Duchenne muscular dystrophy*. Nature, 1991. **352**(6335): p. 536-539.
143. Lavis, L.D., *Histochemistry: Live and in Color*. Journal of Histochemistry and Cytochemistry, 2011. **59**(2): p. 139-145.
144. Bloemberg, D. and J. Quadrilatero, *Rapid determination of myosin heavy chain expression in rat, mouse, and human skeletal muscle using multicolor immunofluorescence analysis*. PLoS One, 2012. **7**(4): p. e35273.
145. Banks, G.B., et al., *Functional capacity of dystrophins carrying deletions in the N-terminal actin-binding domain*. Hum Mol Genet, 2007. **16**(17): p. 2105-13.
146. Szasz, G., W. Gruber, and E. Bernt, *Creatine kinase in serum: I. Determination of optimum reaction conditions*. Clin Chem, 1976. **22**(5): p. 650-6.
147. Tsytsykova, A.V. and A.E. Goldfeld, *Nuclear Factor of Activated T Cells Transcription Factor Nfatp Controls Superantigen-Induced Lethal Shock*. J Exp Med, 2000. **192**(4): p. 581-6.

148. Fisher, I., et al., *Prednisolone-induced changes in dystrophic skeletal muscle*. *Faseb j*, 2005. **19**(7): p. 834-6.
149. Stupka, N., et al., *Differential calcineurin signalling activity and regeneration efficacy in diaphragm and limb muscles of dystrophic mdx mice*. *Neuromuscul Disord*, 2006. **16**(5): p. 337-46.
150. Vandebrouck, C., et al., *The effect of methylprednisolone on intracellular calcium of normal and dystrophic human skeletal muscle cells*. *Neurosci Lett*, 1999. **269**(2): p. 110-4.
151. Naya, F. and E.N. Olson, *MEF2 transcriptional target for signalling pathway controlling skeletal muscle growth and differentiation*. *Current Opinion in Cell Biology*, 1999(11): p. 683-688.
152. Liu, N., et al., *Requirement of MEF2A, C, and D for skeletal muscle regeneration*. *Proc Natl Acad Sci U S A*, 2014. **111**(11): p. 4109-14.
153. Anderson, D.M., et al., *A micropeptide encoded by a putative long noncoding RNA regulates muscle performance*. *Cell*, 2015. **160**(4): p. 595-606.
154. Nelson, B.R., et al., *A peptide encoded by a transcript annotated as long noncoding RNA enhances SERCA activity in muscle*. *Science*, 2016. **351**(6270): p. 271-5.
155. Onopiuk, M., et al., *Store-operated calcium entry contributes to abnormal Ca²⁺ signalling in dystrophic mdx mouse myoblasts*. *Archives of Biochemistry and Biophysics*, 2015. **569**: p. 1-9.
156. McCullagh, K.J.A., et al., *NFAT is a nerve activity sensor in skeletal muscle and controls activity-dependent myosin switching*. *Proc Natl Acad Sci U S A*, 2004. **101**(29): p. 10590-5.
157. Crabtree, G.R. and E.N. Olson, *NFAT signaling: choreographing the social lives of cells*. *Cell*, 2002. **109 Suppl**: p. S67-79.
158. Horsley, V., et al., *Regulation of the growth of multinucleated muscle cells by an NFATC2-dependent pathway*. *J Cell Biol*, 2001. **153**(2): p. 329-38.
159. Daou, N., et al., *A new role for the calcineurin/NFAT pathway in neonatal myosin heavy chain expression via the NFATc2/MyoD complex during mouse myogenesis*. *Development*, 2013. **140**(24): p. 4914-25.
160. Calabria, E., et al., *NFAT isoforms control activity-dependent muscle fiber type specification*. *Proc Natl Acad Sci U S A*, 2009. **106**(32): p. 13335-40.
161. Zhang, D., et al., *Thyroid hormone regulates muscle fiber type conversion via miR-133a1*. *J Cell Biol*, 2014. **207**(6): p. 753-66.
162. Mu, X., et al., *Roles of the calcineurin and CaMK signaling pathways in fast-to-slow fiber type transformation of cultured adult mouse skeletal muscle fibers*. *Physiol Genomics*, 2007. **30**(3): p. 300-12.
163. Xu, M., et al., *FoxO1: a novel insight into its molecular mechanisms in the regulation of skeletal muscle differentiation and fiber type specification*. *Oncotarget*, 2017. **8**(6): p. 10662-10674.
164. Petrof, B.J., et al., *Adaptations in myosin heavy chain expression and contractile function in dystrophic mouse diaphragm*. *Am J Physiol*, 1993. **265**(3 Pt 1): p. C834-41.
165. Dubowitz, V., et al., *Muscle Biopsy: A Practical Approach*. Fourth Edition ed. 2013, England: Oxford: Saunders Elsevier. 572.
166. Villalta, S.A., A.S. Rosenberg, and J.A. Bluestone, *The immune system in Duchenne muscular dystrophy: Friend or foe*. *Rare Dis*, 2015. **3**(1): p. e1010966.

167. Kharraz, Y., et al., *Understanding the process of fibrosis in Duchenne muscular dystrophy*. Biomed Res Int, 2014. **2014**: p. 965631.
168. Hussein, M.R., et al., *The effects of glucocorticoid therapy on the inflammatory and Dendritic cells in muscular dystrophies*. International Journal of Experimental Pathology, 2006. **87**(6): p. 451-461.
169. Vidal, B., et al., *Fibrinogen drives dystrophic muscle fibrosis via a TGFbeta/alternative macrophage activation pathway*. Genes & development, 2008. **22**.
170. Oppong, E. and A.C.B. Cato, *Effects of Glucocorticoids in the Immune System*, in *Glucocorticoid Signaling: From Molecules to Mice to Man*, J.-C. Wang and C. Harris, Editors. 2015, Springer New York: New York, NY. p. 217-233.
171. Dupont-Versteegden, E.E. and R.J. McCarter, *Differential expression of muscular dystrophy in diaphragm versus hindlimb muscles of mdx mice*. Muscle Nerve, 1992. **15**(10): p. 1105-10.
172. Lang, J.M., K.A. Esser, and E.E. Dupont-Versteegden, *Altered activity of signaling pathways in diaphragm and tibialis anterior muscle of dystrophic mice*. Exp Biol Med (Maywood), 2004. **229**(6): p. 503-11.
173. Takagi, A., et al., *[Effect of long-term administration of prednisolone on serum creatine kinase and muscle pathology of mdx mouse]*. Rinsho Shinkeigaku, 1998. **38**(8): p. 724-8.
174. Spurney, C.F., et al., *PRECLINICAL DRUG TRIALS IN THE mdx MOUSE: ASSESSMENT OF RELIABLE AND SENSITIVE OUTCOME MEASURES*. Muscle Nerve, 2009. **39**(5): p. 591-602.
175. Bonifati, M.D., et al., *A multicenter, double-blind, randomized trial of deflazacort versus prednisone in Duchenne muscular dystrophy*. Muscle Nerve, 2000. **23**(9): p. 1344-7.
176. Gehrig, S.M., et al., *Making Fast-Twitch Dystrophic Muscles Bigger Protects Them from Contraction Injury and Attenuates the Dystrophic Pathology*. American Journal of Pathology, 2010. **176**(1).
177. Kottlors, M. and J. Kirschner, *Elevated satellite cell number in Duchenne muscular dystrophy*. Cell Tissue Res, 2010. **340**(3): p. 541-8.
178. Reimann, J., A. Irintchev, and A. Wernig, *Regenerative capacity and the number of satellite cells in soleus muscles of normal and mdx mice*. Neuromuscul Disord, 2000. **10**(4-5): p. 276-82.
179. Collet, C., et al., *Intracellular calcium signals measured with indo-1 in isolated skeletal muscle fibres from control and mdx mice*. J Physiol, 1999. **520 Pt 2**: p. 417-29.
180. Phuong, T.T., et al., *Positive feedback control between STIM1 and NFATc3 is required for C2C12 myoblast differentiation*. Biochem Biophys Res Commun, 2013. **430**(2): p. 722-8.
181. Zhang, Y. and K.B. Storey, *Expression of nuclear factor of activated T cells (NFAT) and downstream muscle-specific proteins in ground squirrel skeletal and heart muscle during hibernation*. Mol Cell Biochem, 2016. **412**(1-2): p. 27-40.

Appendices

Appendix A: Supplementary Material for Thesis

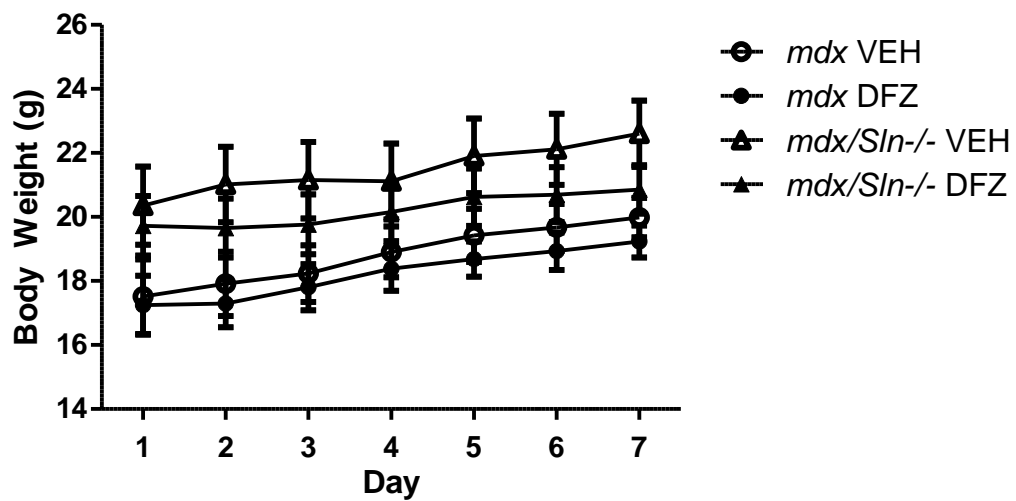


Figure S1.1: Body weight monitoring during injection protocol. A main effect of genotype indicates that *mdx/Sln^{-/-}* mice are heavier than *mdx* mice throughout the treatment protocol ($p < 0.05$, $mdx < mdx/Sln^{-/-}$). All values are presented as mean \pm standard error (n=8-10 per group).

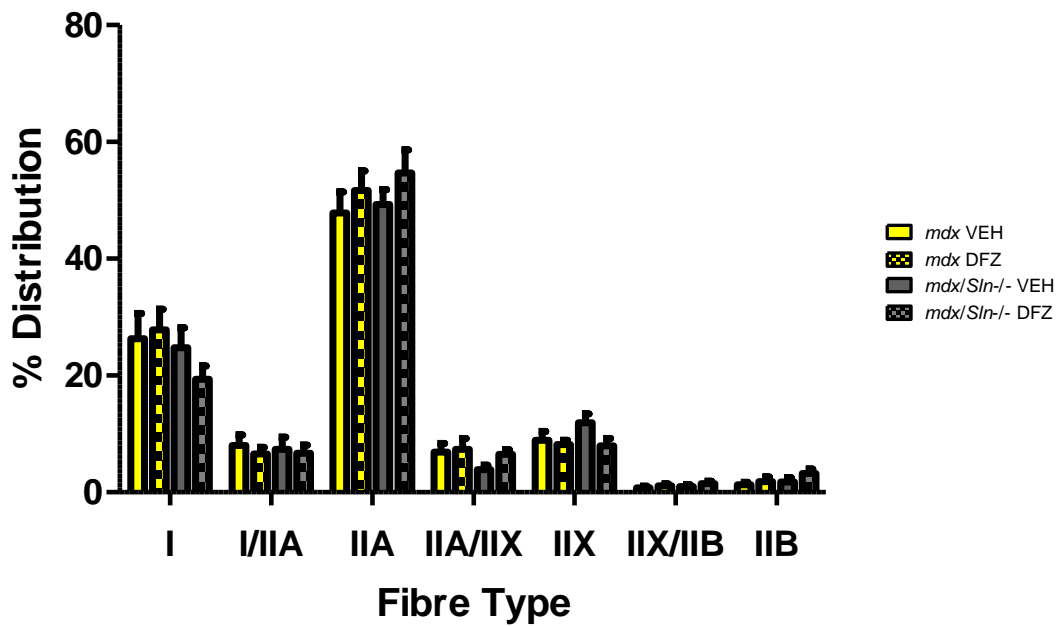


Figure S1.2: Distribution of all fibre types in SOL of *mdx* and *mdx/Sln*^{-/-} after treatment protocol. A trend of genotype was observed in IIX/IIB fibres ($p=0.069$, $mdx < mdx/Sln^{-/-}$). All values are displayed as mean \pm SE (n=8-9 per group).

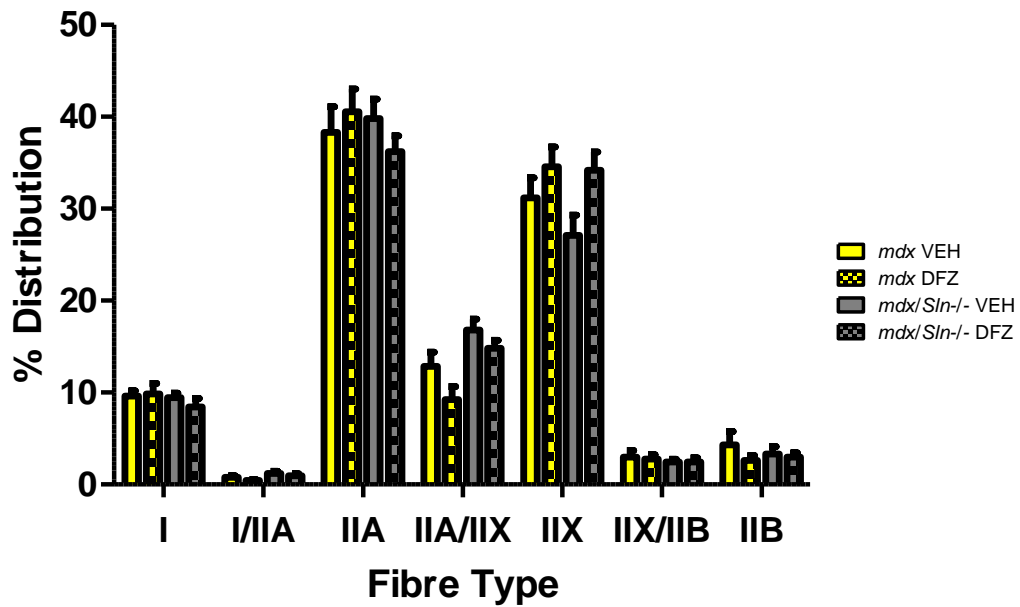
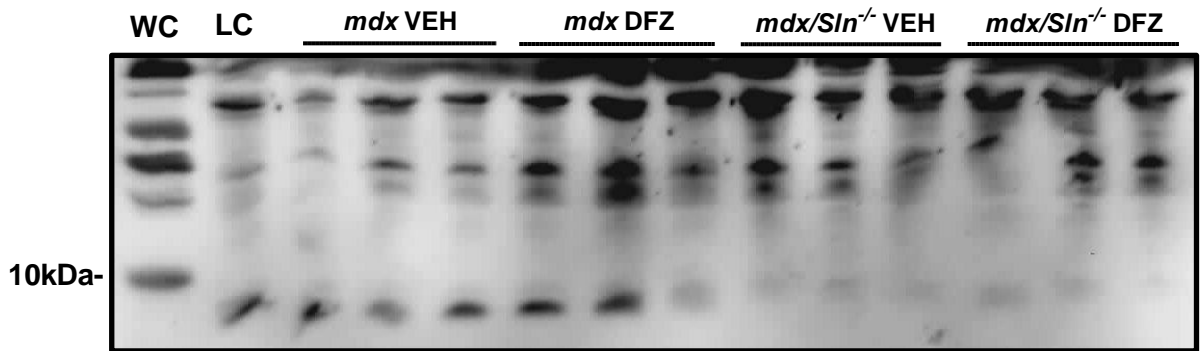


Figure S1.3 Distribution of all fibre types in DIA of *mdx* and *mdx/Sln*^{-/-} after treatment protocol. A main effect of genotype in I/IIA and IIA/IIX fibres ($p < 0.05$, $mdx < mdx/Sln^{-/-}$) was observed. Main effect of treatment was observed in IIA/IIX fibres ($p < 0.05$, $VEH < DFZ$). All values are displayed as mean \pm SE (n=8-9 per group).

A



B

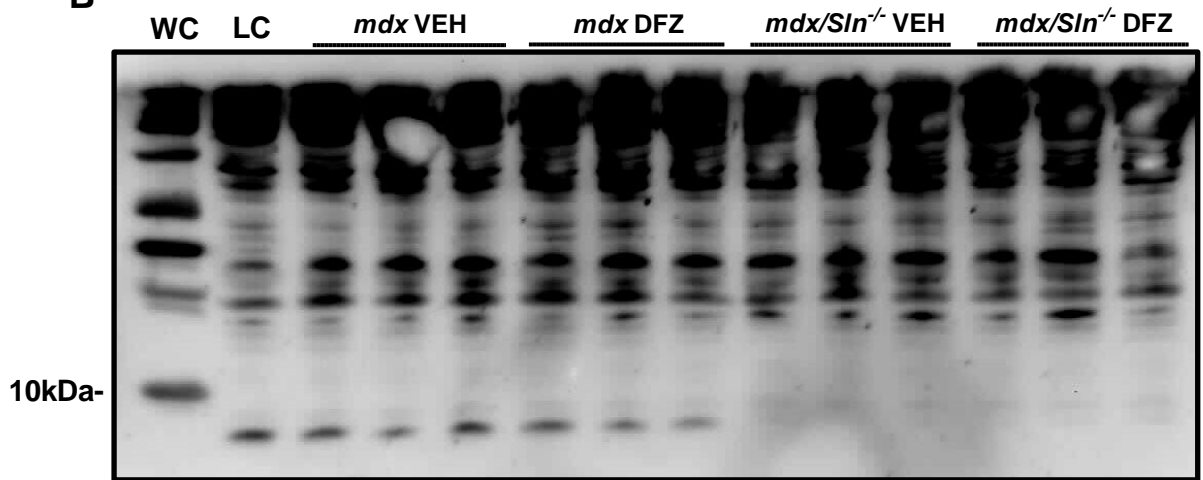
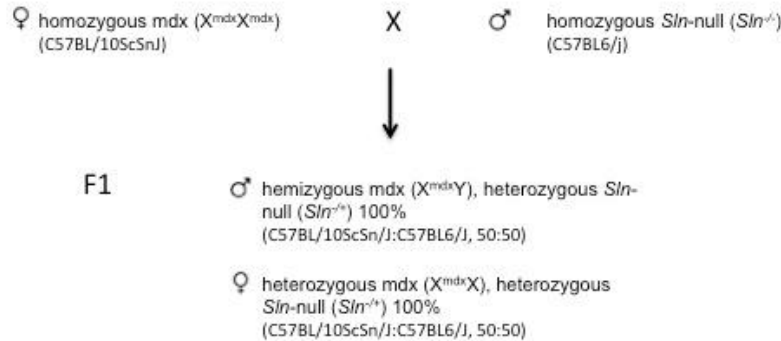


Figure S1.4: Full western blot of SLN content in SOL and DIA from *mdx* and *mdx/Sln^{-/-}* mice after DFZ or VEH treatment. (A) SOL (B) DIA.

Appendix B: Breeding Strategy and Genotyping Protocol for *mdx* and *mdx/Sln*^{-/-}

Generation of *mdx* and *mdx/Sln*^{-/-} mice adapted from [81]

To generate our experimental animals for our *mdx/Sln*^{-/-} and *mdx/Sln*^{+/+} (*mdx*) colonies we first crossed homozygous female *mdx* animals from Jackson Laboratories with a male homozygous *Sln*^{-/-} mouse.

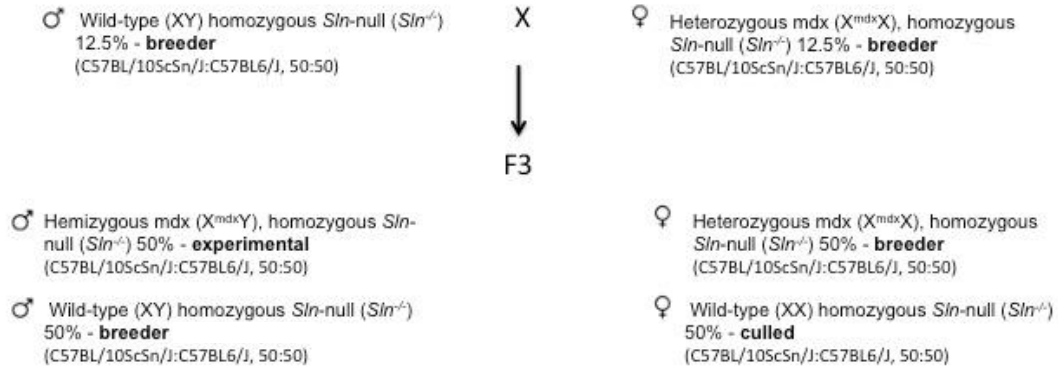


From these animals, an F1 offspring that are either female hemizygous *mdx* or male heterozygous *mdx* were obtained. All F1 offspring were heterozygous for *Sln* ($Sln^{+/-}$). Next, we crossed F1 offspring, from separate breeding pairs, to obtain our F2 generation.

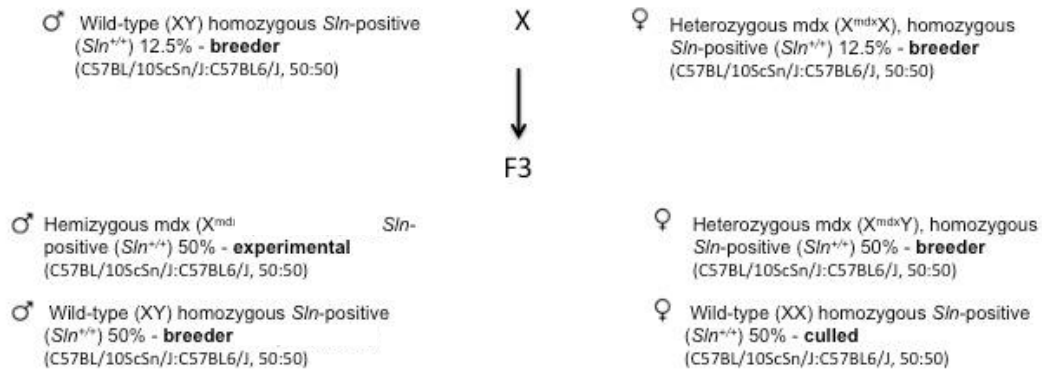


F2 offspring had a variety of genotypes including our experimental animals, *mdx* and *mdx/Sln*^{-/-}. To adhere to the guidelines outlined by the Canadian Council of Animal Care and the University of Waterloo Animal Care Committee to reduce the amount of animals culled; two separate subset colonies were created to generate the experimental animals. These

colonies independently gave rise to *mdx* mice and *mdx/Sln^{-/-}* mice. ***mdx/Sln^{-/-}***: For this subset colony a WT (*dystrophin* positive) male mice from F2 were bred with heterozygous *mdx* females from F2. Both the sires and dams were homozygous for *Sln^{-/-}*. This yielded our experimental *mdx/Sln^{-/-}* used in this study.



mdx: For this subset colony a WT (*dystrophin* positive) male mice from F2 were bred with heterozygous *mdx* females from F2. Both sires and dams were homozygous for *Sln^{+/+}*. This yielded our experimental *mdx/Sln^{+/+}* used in this study.



Note: Because crosses were bred from previous generations, the strain is a 50:50 mix of C57BL/10Scn:C57BL6/J). To prevent genetic drift, the *mdx* and *mdx/Sln^{-/-}* subset colonies should be limited to 3 additional generations.

High DNA Extraction Protocol

Buffers:

Mouse Ear-notch/Tail DNA Isolation Buffer

0.5% SDS

0.1M NaCl

0.05M Tris base (pH 8.0)

2-4mM EDTA

Set final pH to 8.0.

8M Potassium Acetate

157.02g in 200mL dH₂O (autoclaved water)

1. Add Proteinase K (Sigma-Aldrich) to mouse ear-notch/tail DNA Isolation Buffer (see recipe below) at a concentration of 1.0 mg/ml and mix.
2. Add 200ul of solution to each Eppendorf tube with sample (ear notch/tail clip). Place tubes in a conical tube.
3. Immediately place tubes in a water bath set to 63°C. Let tissue digest overnight.
4. Add 37.5ul of 8M potassium acetate to each tube.
5. Add 500ul of chloroform to each tube. Vortex for 5-10 mins.
6. Spin 5-8mins at 9,000 g.
7. Pipetter aqueous top layer in a new Eppendorf tube. There should be approximately 200ul.
8. Add 2 volumes (if you get 200ul from step 7 then you add 400ul) of 100% ethanol at room temperature. Mix by inverting.
9. Spin at 14000 rpm for 20min at 4°C.
10. Remove the supernatant and air dry for 2-3 mins.
11. Add 30 ul of Autoclaved Water.
12. Dilute to 20ng/ul concentration with autoclaved water after determining concentration in a Nanodropper 2000

Table S2.1: Forward and reverse primers for *mdx* mice detection

Primer Name	Sequence
Common Forward (DL1577)	5'GCG CGA AAC TCA AAT ATG CGT GTT AGT GT-3'
WT Forward (DL1509) 134 bp	5'-GAT ACG CTG CTT TAA TGC CTT TAG TCA CTC AGA TAG TTG AAG CCA TTT TG-3'
<i>Mdx</i> Reverse (DL1573) 117 bp	5'-CGG CCT GTC ACT CAG ATA GTT GAA GCC ATT TTA-3'

Genotype Protocol

All mice were ear notched at 3 weeks of age and the DNA was extracted using the protocol described above. PCR was performed to amplify the DNA of interest. 40ng of DNA was added to Taq DNA polymerase mix (EP0402, Thermo Scientific Fermentas, Canada) containing Taq Buffer with $(\text{NH}_4)_2\text{SO}_4$ buffer (diluted to 1X), 4mM MgCl_2 , 200 μM dNTP (R0192, Thermo Scientific Fermentas), 0.625 units of Taq DNA polymerase, and 0.66 μM of the appropriate forward and reverse primers (listed below). Samples were then placed in a thermal cycler (MJ MINI, Bio- Rad Canada) and underwent their respective PCR reactions (protocol below). The primers used in this reaction were based from a competitive PCR reaction that uses the common forward primer established by Shin et al (listed below). The amplified products were then separated on a 3% agarose gel (in 1X TBE) containing 0.01% ethidium bromide (Bioshop, Canada) for 80 min at 100V. The gel is then imaged using a bio-imaging system (Syngene, Frederick, MD).

Table S2.2: PCR cycle for *mdx* mice.

	Temperature ($^{\circ}\text{C}$)	Time	Number of cycles
<i>mdx</i>			
1. Denaturation	94	5 min	1
2. Denaturation	94	30 sec	
3. Annealing	60	30 sec	34 cycles (go to step
4. Extension	72	30 sec	2 34x)
5. Final Extension	72	3 min	1
6. Hold	4	∞	Hold until electrophoresis

Appendix C: Western Blotting Protocols

Table 3.1: Western blotting protocol for all protein

Target Protein	Antibody Info	Total Protein Load	Run	Primary	Secondary	Detection
CnA	Sigma Aldrich C1956 Monoclonal Mouse	10µg DIA 10µg SOL	15 mins @100V 60 mins @ 120v	1:1000 5% milk in TBST overnight 4°C	1:2000	Femto 30 sec exposure
NFAT-p	Pierce Antibodies PA5-38301 Polyclonal Rabbit	20µg DIA 20µg SOL	15mins @100V, 60 mins @ 120V	1:2000 signal enhancer overnight 4°C	1:2000	femto 1 min exposure
NFAT	Pierce Antibodies MA3-024 Monoclonal Mouse	Strip and reprobe NFAT-p membrane		1:2000 5% milk overnight at 4°C	1:5000	Luminata 1 min exposure
SLN	Lampire Biological Laboratories Proprietary Polyclonal Rabbit	5µg DIA 12.5µg SOL	100V for 80mins	1:100 5% BSA overnight at 4°C	1:2000	DIA- Luminata 30s exposure SOL- Luminata 10s exposure
SERCA1a	Generously Donated from Dr. MacLennan, University of Toronto Mouse	100ng	100V for 15mins, 120V for 60 mins	1:10000 5% milk 1hr at RT	1:20000	Luminata 10s exposure
SERCA2a	Pierce Antibodies 2A7-A1 Monoclonal Mouse	4µg DIA	100V for 15mins, 120V for 60mins	1:2000 5% milk 1hr at RT	1:10000	Femto 30s exposure

Pan-Actin	Sigma Aldrich A2066 Polyclonal Rabbit	Strip and Reprobe SERCA1a membrane		1:10000 5% milk 1hr at RT	1:2000	ECL 10 sec exposure
Utrophin	BD Biosciences 610896 Polyclonal Mouse	40µg	60V for 20 minutes, 100V for 120mins	1:500 5% milk overnight at 4°C	1:2000	Femto 10sec exposure